Geology, geochemistry and tectonic settings of molybdenum deposits in Southwest China: A review

Yong-Fei Yang, Pin Wang

PII: S0169-1368(16)30631-X
DOI: doi:10.1016/j.oregeorev.2016.10.017
Reference: OREGEO 1980

To appear in: *Ore Geology Reviews*

Received date: 30 November 2015
Revised date: 17 October 2016
Accepted date: 18 October 2016

Please cite this article as: Yang, Yong-Fei, Wang, Pin, Geology, geochemistry and tectonic settings of molybdenum deposits in Southwest China: A review, *Ore Geology Reviews* (2016), doi:10.1016/j.oregeorev.2016.10.017

Geology, geochemistry and tectonic settings of molybdenum deposits in Southwest China: A review

Yong-Fei Yang[a,b*], Pin Wang[b,c]

[a] *Chengdu Center, China Geological Survey, Chengdu 610081, China*

[b] *Key Laboratory of Orogen and Crust Evolution, Peking University, Beijing 100871, China*

[c] *Key Laboratory of Mineralogy and Metallogeny, Guangzhou Institute of Geochemistry, CAS, Guangzhou 510640, China*

[*] Corresponding author; email: yyf6811@163.com

Abstract

Southwest (SW) China hosts more than 26 Mo (Mo-only, Mo-dominated and Mo-bearing) deposits with a total reserve of >2.5 Mt Mo metal. The region has become one of the most important Mo mineral provinces in China. These Mo deposit are usually fault-controlled, and are located mainly in: (1) Lhasa Terrane, characterized by widely distributed Yanshanian–Himalayan igneous rocks; (2) Qiangtang Terrane, composed by Proterozoic and Early-Paleozoic crystalline basement and Devonian to Jurassic cover rocks; (3) East Kunlun Terrane, comprising Precambrian metamorphic rocks intruded by Paleozoic and Mesozoic granitoid plutons; (4) West Kunlun Terrane, characterized by Precambrian metamorphic

basement, Paleozoic metasedimentary rocks, and Early-Paleozoic and Carboniferous–Triassic arc-type plutons; and (5) Yidun arc, composed by Middle and Upper Triassic volcanic–sedimentary successions. The Mo mineralization styles are dominated by porphyry-type, but also contain porphyry-skarn, skarn and porphyry-quartz vein types. Orebodies are vein-type or lensoidal, and are hosted by a variety of metamorphic, volcanic, granitic and sedimentary rocks of different ages. Fluid-rock interactions are exemplified by alteration zonation, which usually grades from an innermost potassic alteration zone, via a silicic / sericite alteration zone, to an outermost propylitic alteration zone. The initial high-temperature ore-forming fluids are magmatic in origin, and contain CO_2-bearing fluid inclusions. The initial ore-forming fluids would have then evolved to low-temperature, low-pressure, low-salinity and CO_2-poor (with meteoric water input) at the late alteration / mineralization stage. Causative granitoids for these Mo deposits have relatively high SiO_2, K_2O and Al_2O_3, and low TiO_2 and MgO, showing a metaluminous to peraluminous high-K calc-alkaline to shoshonitic affinity. These granitoids exhibit significant depletions in Ba, Nb, Ta, P and Ti, and enrichments in Rb, Th, U and K. It is suggested that they were originated from partial melting of a lower rejuvenated crust, as evidenced by their Sr-Nd-Pb isotopic signatures. The Mo deposits in East Kunlun and West Kunlun were formed in the Triassic (ca. 258 – 214 Ma), related to the Paleo-Tethys Ocean subduction and the subsequent continental collision. Major Mo mineralization in the Qiangtang and Lhasa terranes mainly occurred during the syn-collisional compression to post-collisional extension transition of the Qiangtang–Lhasa (ca. 43 – 35 Ma) and India–Asia (ca. 30 – 14 Ma) collisions, respectively. The Late-Cretaceous Mo mineralization (ca. 88 – 73 Ma) in the Yidun arc was formed during the late- or post-

Lhasa–Qiangtang collision setting, or the intraplate extension led by the post-Himalayan escape tectonics. The wide range of molybdenite Re contents in these major SW Chinese Mo deposits indicate remarkable differences in metal, fluid sources and ages.

***Keywords*:** Southwest China; Molybdenum deposit; Ore geology; Geochemistry; Tectonic setting

1. Introduction

China has the largest molybdenum reserve in the world, with the majority being concentrated in the Qinling–Dabie Orogenic Belt (Li et al., 2007a; Chen et al., 2016a), the eastern part of the Central Asian Orogenic Belt (NE China; Chen et al., 2016b), South China Block (Zhong et al., 2016) and Southwest (SW) China.

The East Qinling–Dabie is the most important Mo belt in the world, with 8.43 Mt of proven Mo metal reserves (Li et al., 2007a; Mao et al., 2011). The Mo deposits in East Qinling–Dabie are mainly associated with Mesozoic porphyry or porphyry-skarn systems formed in a post-subduction collision regime (Chen and Li, 2009; Chen et al., 2000, 2007a, 2009, 2016a; Li et al., 2007a, 2012a, 2013a; Mao et al., 2008, 2010, 2011; Mi et al., 2015; Yang et al., 2016a), showing different geological and geochemical features from those in the subduction-related magmatic arc settings such as West Cordillera, North America (Pirajno, 2009; Wang et al., 2014a; Mi et al., 2015; Yang et al., 2016a). Therefore, Chen and Fu (1992) and Chen et al. (2000, 2004, 2007, 2009) proposed a tectonic model for collisional orogeny, petrogenesis, metallogenesis and fluid flow (referred to as the CMF; Pirajno, 2009, 2013).

The NE China lies in the eastern sector of the Central Asian Orogenic Belt (CAOB), accommodating multistage magmatism, crustal growth and mineralization. 69 Mo-only or Mo-dominated and 9 Cu-Mo deposits have been discovered in NE China, with a total resource of 10.5 Mt Mo metal (Chen et al., 2016b; and references therein). The majority of the deposits are porphyry (including breccia pipes) type, followed by the skarn and quartz vein types, formed during Paleozoic and Mesozoic tectono-magmatic events (Chen et al., 2016b; and references therein).

The South China block (SCB) consists of the Yangtze Craton and HuananOrogen, sutured by the Jiang–Shao Fault (Zhong et al., 2016). The SCB hosts at least 46 Mo deposits (including Mo-only, Mo-dominated and Mo-bearing) with a total resource of ~1.8 Mt Mo metal and accounting for ~10% of the total Mo resources of China (Zhong et al., 2016; and references therein). These Mo deposits are predominantly porphyries, skarns and combinations thereof, formed in a long time span from the Early-Paleozoic to Late-Mesozoic (Zhong et al., 2016; and references therein).

The SW China is mainly composed of the Tibetan Plateau and its surrounding region (Fig. 1), and contains one of the youngest and best known continental collision orogenic belt (Himalaya Orogen; Yin and Harrison, 2000). Two world-famous metallogenic belts have been recognized in SW China: (1) the Gangdese porphyry Cu belt (ca. 19.7 − 11.5 Ma) (Hou et al., 2009; Qu et al., 2007) in southern Tibet (Rui et al., 2003, 2004; Qu et al., 2003, 2009; Hou et al., 2009); (2) Sanjiang Tethyan polymetallic metallogenic belt (Deng et al., 2014; Hou et al., 2007a), including the Yulong porphyry Cu belt in eastern Tibet (Hou and Cook, 2009; Hou et al., 2006a; Rui et al., 1984; Zaw et al., 2007). Recent years, some important Mo deposits were

discovered in SW China (Fig 1), such as the Sharang (Zhao et al., 2014) and Mingze (Fan et al., 2011) porphyry Mo deposits in Lhasa Terrane; the Narigongma (Yang et al., 2014a) and Lurige (Hao et al., 2013) porphyry Mo-Cu deposit in Qiangtang Terrane; the Lalinzaohuo porphyry Mo deposit in East Kunlun Terrane (Wang et al., 2013); the Kayizi porphyry Mo deposit in West Kunlun Terrane (Liu et al., 2010a); and the Xiuwacu (Wang et al., 2015) and Tongchanggou (Yang et al., 2016c) deposits in Yidun arc. These Mo deposits, with a total Mo metal reserve of >2.5 Mt (Table 1), make SW China one of the most Mo productive and prospective regions in China.

In this paper, we describe and summarize the principal geological, age and geochemical features of the major Mo deposits (including Mo-only, Mo-dominated and Mo-bearing deposits) in SW China, and discuss the spatial–temporal distribution and tectonic settings of Mo mineralization, on the basis of an extensive compilation of published and unpublished Mo geological data.

2. Tectonic framework and evolution

2.1. Tectonic framework

Southwest China encompasses the region bounded by the Tarim Basin and Qaidam Basin in the north, by the Longmenshan Fault in the northeast and by the Ailaoshan–Red River suture zone in the east (Fig. 1). From south to north, SW China comprises the northern part of the Himalaya Orogen, the Lhasa Terrane, the Qiangtang Terrane, the Songpan-Ganzi-Hoh Xil Terrane and the Kunlun Terrane, with terrane boundaries marked by the Indus–Yarlung,

Bangong–Nujiang, Jinshajiang and Ayimaqin–Kunlun–Mutztagh sutures (Fig.1B).

The Himalaya Orogen was formed by the India–Asia collision from the end Cretaceous to Eocene (Mo et al., 2008). The orogen comprises the Lesser Himalayan Metasedimentary (LHM) and Higher Himalayan Metasedimentary (HHM) series and the Tethyan Himalayan Sequences (THS), with boundaries that include the Main Boundary Thrust (MBT), Main Central Thrust (MCT) and South Tibet Detachment System (STDS) (Fig. 1B). Most parts of the THS are located in China, and comprise Paleozoic–Cenozoic sedimentary sequences deposited on the Indian passive continental margin (Li et al., 2015a). The THS sedimentary sequences are characterized by deep-water, distal-margin shale, chert and turbidites in the northern part, and shallow-water carbonates and shelf to coastal clastic sediments in the southern part (Wang et al., 2016). Early Paleozoic granites and Miocene leucogranites are exposed in a series of metamorphic domes within the northern THS (Wang et al., 2016). The Tethyan Himalayan fold–thrust system developed in this belt during Eocene–Oligocene (Li et al., 2015a).

The Lhasa Terrane extends more than 2000 km E-W and 200–300 km N-S. A N-S shortening of >180 km may have occurred in the Lhasa Terrane led by its collision with the Qiangtang Terrane in the Jurassic–Late Cretaceous (Allègre et al., 1984; Dewey et al., 1988; Murphy et al., 1997; Pierce and Mei, 1988). The Lhasa Terrane is mainly composed of the mid-Proterozoic and Early Cambrian crystalline basement and the overlying Ordovician, Carboniferous and Triassic shallow-sea clastic rocks (Yin et al., 1988). Lower–Middle Cretaceous marine carbonate rocks are widespread, but Upper Cretaceous sedimentary rocks are confined along the Bangong–Nujiang suture zone (Hou et al., 2009). Mesozoic magmatism in the Lhasa Terrane forms the widely distributed Gangdese arc granitoid batholiths (ca. 130 –

70 Ma) (Schärer et al., 1984), suggesting northward subduction of the Neo-Tethys in the Late Cretaceous (Allègre et al., 1984; Harrison et al., 1992). Cenozoic magmatism in the Lhasa Terrane is represented by the voluminous Linzizong arc volcanic succession (ca. 66 – 40 Ma) (Allègre et al., 1984), Paleocene peraluminous granites (Dong et al., 2006a) and the Eocene gabbroids and granitoids (Dong et al., 2005; Mo et al., 2005).

The Qiangtang Terrane is composed dominantly of metamorphic rocks, Upper Paleozoic shallow marine strata and Jurassic–Cretaceous marine carbonates with terrestrial clastic interbeds (Hou et al., 2003). The western segment of this terrane is characterized by high-pressure metamorphic rocks and contains Late Paleozoic marine strata, whereas the eastern segment contains Triassic–Jurassic shallow-marine carbonates and arc volcano-sedimentary sequences (Hou et al., 2003).

The Songpan–Ganzi–Hoh Xil Terrane was likely formed during the shortening and closure of the Songpan–Ganzi basin (a branch of the Paleo-Tethys Ocean) (Burchfiel et al., 1995). Due to the India–Asia continental collision since the Paleocene, the ocean basin was subducted southward beneath the Qiangtang Terrane along the Jinshajiang suture (Yin and Harrison, 2000). The terrane contains very thick (>3000m) Triassic marine sedimentary sequence which is crosscut by numerous thrust faults (Burchfiel et al., 1995). In the southern end of the terrane, the Late Triassic Yidun arc was developed by the W-dipping subduction of the Paleozoic Songpan–Ganzi–Litang ocean basin (Hou et al., 2001).

The Kunlun Terrane was formed by the Late-Triassic to Early-Jurassic collision between the Qaidam and Qiangtang terranes (Roger et al., 2003; Wang, 2004; Xiao et al., 2001), and can be divided into West Kunlun and East Kunlun by Altyn Fault (Fig. 1B).

2.2. Tectonic evolution

Prior to the India–Asia collision, the formation and evolution of the SW China are related intrinsically to those of the Tethyan Ocean (Pan et al., 2012). During the Late Paleozoic, the Kunlun tectonics were affected by both the N-dipping Paleo-Tethyan Ocean subduction and the W-dipping Jinshajiang Ocean subduction (Pan et al., 2012). In the Early–Middle Triassic, the final closure of the Paleo-Tethyan Ocean along the Kunlun and Jinshajiang sutures may have occurred. The northern Gondwana margin may have still been an active continental margin, and the bipolar subduction of the Bangong–Nujiang Tethyan Ocean (Neo-Tethyan Ocean) continued (Mo and Pan, 2006; Pan et al., 2012). In the Late Triassic, continental collision occurred in Kunlun in the north; the Yarlung Zangbo back-arc oceanic basin (Neo-Tethyan Ocean) developed, and the Gangdese separated from Indian plate (Mo and Pan, 2006; Pan et al., 2012). During Early–Middle Jurassic, the initial northward subduction of the Yarlung Zangbo oceanic basin occurred by means of low-angle subduction. From the Late Jurassic to the Late Cretaceous, continued northward subduction of the Yarlung Zangbo Ocean lead the formation of the Gangdese magmatic arc (Allègre et al., 1984; Harrison et al., 1992; Mo and Pan, 2006; Pan et al., 2012; Yin and Harrison, 2000). The final closure of the Bangong–Nujiang Neo-Tethyan Ocean occurred in the Late Cretaceous (Pan et al., 2004; Yin and Harrison, 2000).

The India–Asia collision occurred at the end Cretaceous to Eocene (Mo et al., 2008) may have led to compression in the Himalaya–Gangdese, and formed the strike-slip thrusts in the Sanjiang–Bayan Har and Qinling–Qilian–Kunlun areas (Pan et al., 2012). In the Early Miocene, the strong intracontinental convergence resulted in the formation of the Main Central Thrust (MCT) and the Southern Tibet Detachment System (Burchfiel et al., 1992). During the Middle

to Late Miocene, the Main Boundary Thrust (MBT) may have formed, and the Tibetan Plateau uplifting may have extended further into the Qaidam basin, Altyn Tagh, Qilianshan, eastern Longmenshan, and western Qinling, forming the archetype of the present-day Tibetan Plateau (Pan et al., 2012).

3. Types and spatial distribution of the Mo deposits in SW China

More than 26 Mo deposits have been discovered in SW China (Fig. 1), and they can be grouped into four major types (Chen et al., 2007b), i.e. porphyry, skarn, porphyry-skarn and porphyry-quartz vein types, dominated by porphyry type which contains more than 90% Mo reserves (Table 1).

Five Mo-mineralization belts are present in SW China, namely the Lhasa, Qiangtang, East Kunlun and West Kunlun terranes, and the Yidun arc.

3.1. Lhasa Terrane

The Mo deposits in the Lhasa terrane are mainly located in the eastern Gangdese magmatic belt (Fig. 1B), which also hosts the Gangdese porphyry Cu belt, the largest Cu metallogenic belt in China (Hou et al., 2009; Li et al., 2006).

In the eastern Gangdese magmatic belt, major sedimentary strata are Cretaceous to Tertiary (Pan et al., 2012; Yin and Harrison, 2000), and Jurassic–Cenozoic igneous rocks are widespread. The Cenozoic porphyry stocks, intruding the Gangdese granitoid batholiths and

the sedimentary wallrocks, are closely related to the porphyry-(skarn) Cu-Mo mineralization. Most of these porphyry stocks were developed along the E-trending thrust zone or the intersections of the N-trending normal faults and the E-trending thrust faults, suggesting structural constraints on the localization of felsic intrusions and related Cu-Mo mineralization (Hou and Cook, 2009; Hou et al., 2006a, b, c, 2009).

One giant Cu-Mo deposit, five large Cu-Mo and Mo deposits, and some medium to small Cu-Mo deposits were discovered in the Lhasa Terrane (Fig. 1). These include the Qulong porphyry Cu-Mo deposit, the Jiama porphyry-skarn Cu-Mo deposit, the Sharang and Mingze porphyry Mo deposits, the Tangbula and Bangpu porphyry Mo-Cu deposits, the Tinggong and Lakange porphyry Cu-Mo deposits, and the Nuri skarn Cu-W-Mo deposit (Table 1).

3.2. Qiangtang Terrane

The Yulong porphyry Cu-Mo and Narigongma porphyry Mo-Cu belts are located in the eastern part of the Qiangtang Terrane. It is bounded by the Bangong-Nujiang suture to the south and the Jinshajiang suture to the north (Fig. 1B; Hou et al., 2003; Yang et al., 2014a).

The eastern Qiangtang Terrane comprises a poorly exposed Proterozoic to Early Paleozoic folded crystalline basement (upper-greenschist and lower-amphibolite facies metamorphosed) and the widespread Lower to Middle Ordovician meta-turbidites and carbonates, Permian-Lower Triassic (ca. 275 – 248 Ma) arc volcanics, Upper Triassic (ca. 225 – 205 Ma) arc magmatic rocks, Uppermost Triassic volcaniclastics, Jurassic sedimentary rocks, as well as Cretaceous to Neogene clastic rocks (Hou et al., 2003; Yang et al., 2014a).

A series of NW-trending thrust faults (Yushu-Nangqian thrust belt) were developed in the Narigongma porphyry Mo-Cu belt (Xu et al., 2016), and the NNW-trending Jinshajiang strike-slip fault system is spatially associated with the Yulong porphyry Cu-Mo belt (Fig. 1; Chen, 1996; Chen et al., 1997, 2007a; Hou et al., 2003). These faults have controlled the distribution of the Eocene–Oligocene Mo-(Cu) mineralized granite porphyry intrusions. The Lurige and Narigongma porphyry Mo-Cu deposits are located in the Narigongma porphyry Mo-Cu belt; and the Yulong, Zhanaga, Mangzong, Duoxiasongduo and Malasongduo Cu-Mo deposits developed in the Yulong porphyry Cu-Mo belt (Fig. 1).

3.3. East Kunlun Terrane

The nearly E–W-trending East Kunlun Terrane was formed by the closure of the Paleo-Tethys Ocean at the end of Triassic, which was followed by the Jurassic–Early Cretaceous continental collision, and consequently intracontinental deformations (Zheng et al., 2016).

The East Kunlun Terrane can be divided into the Northern Belt (NKB), Central Belt (CKB) and Southern Belt (SKB), with the belt boundaries being the North, Central and South East Kunlun faults (He et al., 2015; Jiang et al., 1992; Zheng et al., 2016). The NKB is dominated by Ordovician meta-clastic rocks and pillow lava (Wang et al., 2012a), which are intruded by Early Paleozoic granitoids (Gao et al., 2011; Li et al., 2013b) and unconformably overlain by Devonian sandstone and conglomerate. The CKB is characterized by widespread Precambrian metamorphic rocks comprising the Proterozoic Jinshuikou and Binggou groups, and the Ordovician to Silurian Tanjianshan Formation clastic sedimentary rocks, and the

Upper Devonian to Triassic rocks (He et al., 2015). Numerous Paleozoic and Mesozoic granitoids were documented in the CKB (Liu et al., 2012; Meng et al., 2015). The SKB mainly consists of the Precambrian rocks of the Kuhai Wanbaogou Group, and the cover sequences consisting mainly of the Lower Paleozoic volcanics–sediments, Carboniferous-Middle Triassic marine sediments, and the Upper Triassic–Jurassic terrestrial sediments (Jiang et al., 1992). A small number of Late Paleozoic and Mesozoic granitic plutons were documented to have intruded the covers of the SKB (Liu et al., 2005).

The belt contains the Aikengdelesite porphyry Mo-Cu deposit, the Lalingzaohuo porphyry-skarn Mo deposit, and the Ketinghaer and Yazigou porphyry Cu-Mo deposits (Fig. 1).

3.4. West Kunlun Terrane

The West Kunlun terrane subdivided into a northern and southern unit by the Oytag–Kudi–Qimanyute suture, which is accepted to be the Early Paleozoic suture of the Proto-Tethys Ocean (Jiang et al., 2002; Mattern and Schneider, 2000). The northern unit is composed of Precambrian metamorphic basement, Paleozoic metasedimentary rocks, and Ordovician–Silurian and Triassic arc-type plutons; and the southern unit maily consists of the metamorphic basement complex and massive Caledonian and Hercynian intrusive rocks (Cowgill et al., 2003; Schwab et al., 2004). The south-dipping West Kunlun thrust belts, delimited by the Tiklik and Tam Karaul thrusts, probably initiated in the Early Eocene, in response to India–Asia collision (Cao et al., 2013; Yin et al., 2002), and were likely reactivated in the Early Miocene (Jiang et al., 2013; Wang et al., 2003).

Only a few porphyry or porphyry-skarn Mo deposits were indentified in the West Kunlun Terrane, i.e., the Kayizi porphyry Mo deposit and the Xiaotong porphyry-skarn Mo deposit (Fig. 1).

3.5. Yidun arc

The Yidun arc lies to the east of the Jinshajiang Suture, to the west of the Ganzi–Litang Suture and to the northwest of South China Block, extending for more than 500 km from north to south (Fig. 1B). It was formed by the westward subduction of the Ganzi–Litang Ocean crust in Triassic (Hou and Zhou, 2001).

The Yidun arc is largely composed of Middle and Upper Triassic flysch and mafic–felsic volcanics (Hou and Zhou, 2001; Wang et al., 2014c, d). These Triassic volcanics show geochemical affinities with continental arc volcanics (Hou et al., 2003; Mo et al., 2001). These volcanic–sedimentary successions in the southern Yidun Arc are intruded by numerous granitoids. The Late Triassic (peak at 215 Ma) arc-related quartz diorite porphyry, quartz monzonite porphyry, and granitic porphyry occur as NW-trending stocks and dikes (Yang et al., 2016b) are closely related to the porphyry Cu mineralization, such as the Pulang Cu deposit (Li et al., 2011).

The NNE–SSW-oriented Late-Cretaceous granite porphyry intrusions are associated with the porphyry (–skarn) Cu–Mo metallogenic system, forming the Mo mineralization in Xiuwacu, Relin, Hongshan, and Tongchanggou (Yang et al., 2015, 2016b, c).

4. Major Mo metallogenic epochs in SW China

Table 2 summarizes the isotopic age data for the major Mo deposits in SW China. It is clear that the molybdenite Re-Os and zircon U-Pb ages for these major Mo deposit are nearly coeval (Table 2; Fig. 2), which is typical for porphyry-skarn Mo systems worldwide (Sillitoe, 2010). The Mo mineralization ages in SW China can be grouped into three episodes (Fig. 2): Late Permian–Triassic (ca. 258 – 214 Ma), Late Cretaceous (ca. 88 – 73 Ma) and Cenozoic (ca. 63 – 14 Ma).

The Cenozoic episode is the most important Mo mineralization event in SW China, and had formed at least 16 of the 26 major Mo deposits (Table 2; Fig. 2). The two giant Mo deposits (Qulong and Narigongma) were formed in this event, together with all Mo deposits in the Qiangtang Terrane (ca. 63 – 35 Ma (mainly ca. 40 – 35 Ma), or about 60 Ma after the final Bangong–Nujiang Neotethys closure at ca. 99 Ma; Mo and Pan, 2006; Yin and Nie, 1996). Except for the Shangrang deposit (ca. 52 Ma), other Mo deposits in the Lhasa Terrane were formed in the Miocene (ca. 30 – 14 Ma), or about 30 Ma after the final closure of the Yarlung Zangbo Ocean (ca. 65 – 50 Ma; Mo and Pan, 2006; Yin and Nie, 1996).

Late Cretaceous Mo mineralization was mainly developed in the southern Yidun arc. The Xiuwacu, Relin, Hongshan and Tongchanggou deposits were formed at ca. 75.5 – 88.3 Ma, and the ore-related porphyries at ca. 73.4 – 87.4 Ma (Table 2; Fig. 2).

At least four Late Permian–Triassic Mo deposits were discovered in the Kunlun Terrane, i.e., the Aikengdelesite (ca. 248 Ma) and Lalingzaohuo (ca. 214 – 243 Ma) porphyry-skarn Mo deposits and the Yazigou porphyry Cu-Mo deposit (ca. 217 – 227 Ma) in the East Kunlun Terrane, together with the Kayizi porphyry Mo deposit (ca. 250 – 258 Ma) in the West Kunlun

Terrane. Molybdenum exploration in the Kunlun Terrane remains largely poorly developed, and the discovery of the Late Permian–Triassic mineralization suggests good Mo prospectivity in this terrane.

5. Geology of the Mo deposits

5.1. Host rocks

The Mo deposits in SW China are hosted by a wide variety of rock types of difference ages (Table 1), implying that the Mo mineralization was host rock independent.

The host lithology for the Mo deposits in the Lhasa and Qiangtang terranes are mainly Permian–Cretaceous volcanic and sedimentary rocks (Table 1). In the Qulong Cu-Mo deposit, the ore-related monzogranite porphyry intruded the Lower–Middle Jurassic Yeba Formation, which consists of felsic lava, volcaniclastic rocks and interbedded limestone, sandstone and slate (Fig. 3; Yang et al., 2009a; Xiao et al., 2012), with a zircon U-Pb age of 174.4 ± 1.7 Ma for the rhyolite (Dong et al., 2006b). The causative intrusions of the Sharang Mo deposit was emplaced into the Upper Permian Mengla Formation siliceous clastics and carbonates (Fig. 4; Zhao et al., 2014). The Narigongma Mo-Cu deposit is hosted by the Middle–Upper Permian basalt, basaltic andesite, and minor andesite, interbedded with sandstone, slate, and muddy limestone (Fig. 5; Yang et al., 2014a). The Yulong Cu-Mo deposit is hosted by the Upper Triassic Wangka and Jiapila formations slate, sandy shale, limestone and marble (Liang et al., 2008). It is exceptional that the ore-hosting rock units for the Tinggong and Bangpu deposits are mainly volcanic tuffs, tuffaceous sandstone and tuff breccia of the Eocene Pana Formation

and the Paleocene Dianzhong Formation (Chen et al., 2014; Wang et al., 2012b, c).

The ore-hosting rocks of the Mo deposits in Yidun arc are mainly Upper Triassic volcanic–sedimentary successions, e.g., the Xiuwacu Mo-W deposit is hosted by the Lamaya Formation sandstone and slate (Wang et al., 2015), whilst the Tongchanggou deposit is hosted by the Permian Heinishao Formation basalt and volcanic breccia interbeds, and the Triassic Beiya Formation limestone and marble (Yang et al., 2016c).

The ore-hosting rocks for the major Mo deposits in the East Kunlun and West Kunlun terranes are mainly Paleo- and Meso-Proterozoic metamorphic basement rocks, Cambrian-Ordovician volcanics and ore-related granitoids (Table 1). The Lalingzaohuo Mo deposit is hosted by the Paleo-Proterozoic Baishahe Formation biotite-bearing plagioclase gneiss, migmatite, siltstone and dolomite marble (Fig. 8; Chen et al., 2013). The Yazigou Cu-Mo deposit is hosted by the Cambrian–Ordovician Tanjianshan Group andesite, basalt and marble, as well as Triassic tuff, andesite and rhyolite (He et al., 2009). The Kayizi Mo deposit is hosted by Meso-Proterozoic Sangzhutage Formation slate, quartz schist, tuff, limestone, and marble (Fig. 9; Liu et al., 2010a).

5.2. Ore-forming intrusions

The Mo deposits in the SW China are generally associated with intermediate–felsic small intrusions, which usually occur as elliptical, elongated and irregular stocks. The lithologies of the mineralization-related intrusions are composed of granite porphyry, granodiorite porphyry, monzogranite porphyry, K-feldspar granite porphyry, syenogranite porphyry and alkali-feldspar granite porphyry (Table 1).

These mineralization-related intrusions of the Mo deposits in SW China are generally characterized by multiple-stage magmatic activity. The mineralization-related complex in the Sharang Mo deposit is composed of the mineralized granite, porphyritic granite, granite porphyry, fine-grained granite porphyry (Fig. 4; Zhao et al., 2014). In the Narigongma Mo-Cu deposit, the biotite granite porphyry (43.3 Ma) and fine-grained granite porphyry (43.6 Ma) are related to the Mo-Cu mineralization (Fig. 5; Yang et al., 2014a). The mineralization-related intrusions in the Yulong deposit formed a steeply dipping multiphase stock with ages ranging from 42 to 35 Ma (Fig. 6; Hou et al., 2003). Similar multiphase magmatism was also recognized in the Jiama, Tangbula, Zhanaga, Mangzong, Malasongduo, Xiuwacu and Lalingzhaohuo deposits.

In the Qulong (Fig. 3; Yang et al., 2009a), Mingze (Fan et al., 2011), Nuri (Chen et al., 2015) deposits, although multiphase magmatism was developed in a short time (<10Ma), but just one of these intrusions was related to Mo mineralization. In other Mo deposits, the mineralization-related intrusion was formed by one magmatic phase, such as the granodiorite porphyry in the Tongchnaggou Mo-Cu deposit in the Yidun arc (Fig. 7; Yang et al., 2016c); the granodiorites in the Kayizi and Xiaotong Mo deposits in the West Kunlun Terrane (Liu et al., 2010a, b).

5.3. Structures

W- and NW–NNW-trending thrust faults are common in SW China (Fig. 1). These faults were usually accompanied by voluminous eruption and intrusion of intermediate–felsic magma. Most Mo deposits and related magmatic rocks are time-space associated with these regional W-

and NW–NNW-trending faults and their subsidiary structures. The Mo deposits in the Lhasa Terrane are controlled by the W-trending Indus–Yarlung Zangbo thrust fault and the NW-trending Jiali fault. The Mo deposits in the Qiangtang Terrane are controlled by the NW-trending fold-thrust system and the NNW-trending Jinshajiang strike-slip fault system. The Mo deposits in the Kunlun orogenic belt are distributed along the W-trending Ayimaqin–Kunlun–Mutztagh thrust zone (Fig. 1B).

In the abovementioned deposits, the structures had facilitated the emplacement of porphyries and hydrothermal mineralization. In the Narigongma Mo-Cu deposit, a NW-trending fault and a NE-trending fault were identified (Fig. 5; Yang et al., 2014a). The NW- and NE-trending faults in the Tongchanggou Mo-Cu deposit have controlled the distribution of the ore-forming granodiorite porphyry (Fig. 7; Yang et al., 2016c). In the Kayizi Mo deposit, the ore-associated granodiorite was emplaced in the intersection between a NW-trending and a N-trending fault (Liu et al., 2010a).

5.4. Orebody occurrence

The orebodies are mainly lensoidal or vein-type, and usually occur in ore-related porphyries and/or around the intrusive contact between the porphyries and wallrocks. The spatial relationships between orebodies and porphyries include two types: (1) orebodies completely occur inside the causative porphyries, as in the Sharang Mo (Fig. 4; Zhao et al., 2014), Tinggong (Chen et al., 2014) and Lakange Cu-Mo (Leng et al., 2015) deposits; and (2) orebodies occur also in the intrusive contact zones or wallrocks, e.g., the Qulong Cu-Mo (Fig. 3), Jiama Cu-Mo, Narigongma Mo-Cu (Fig. 5), Yulong Cu-Mo (Fig. 6), Tongchanggou Mo-Cu

(Fig. 7), and Lalingzaohuo Mo (Fig. 8) deposits.

5.5. Metal assemblage and geochemistry

Except for several Mo-only deposits (e.g., Kayizi, Xiaotong, Lalingzaohuo and Sharang), the Mo deposits in SW China contain economic endowments of other metals. The Mo-Cu metal assemblage are represented by the Narigongma and Lurige deposits in the Qiangtang Terrane, the Bangpu, Mingze and Tangbula deposits in the Lhasa Terrane, and the Aikengdelesite deposit in Eastern Kunlun, and the Tongchnaggou deposit in the Yidun arc. The Cu-Mo deposits are the Qulong, Lakangge, Tinggong deposits in the Lhasa Terrane, the Yazigou deposit in Eastern Kunlun and these Cu-Mo deposits in the Qiangtang Terrane. All the Jiama (Cu + Mo + Pb + Zn), Nuri (Cu + W + Mo) and Xiuwacu (Mo + W) deposits are polymetallic.

The most important factor controlling the metal assemblage is suggested to be the causative porphyries, from which the metals may have been predominantly derived (Sillitoe, 2010; Richard, 2011). The Cu-Mo deposits in SW China are mostly associated with felsic–intermediate I-type granitoids, such as granodiorite, monzogranite and diorite, which contain a more important contribution from the mantle, whilst the W-Mo deposits are commonly related to S-type or A-type granites, esp. biotite granites. For instance, the Qulong and Yulong Cu-dominated deposits are related to monzogranite porphyries; while the Xiuwacu Mo-W mineralization is related to biotite monzogranite porphyry and alkali-feldspar granite (Table 1).

Ore minerals from the various major Mo deposits in SW China include mainly

molybdenite, chalcopyrite, galena and sphalerite. Compared with Mo-dominated deposits in SW China, Cu–Mo deposits contain a higher proportion of chalcopyrite, while skarn deposits contain a higher proportion of galena and magnetite.

5.6. Wallrock alteration

Extensive wallrock alteration was documented in all the major Mo deposits in SW China, with alteration styles including potassic, silicic, phyllic, propylitic, and argillic-. Typical alteration zonation includes an outward transition from potassic, via silicic / sericite, to the outermost propylitic alteration, from planar infiltration metasomatism to linear injection metasomatism, and from alkali metasomatism to acid leaching (Chen et al., 2007b; Hu, 2002; Khashgerel et al., 2006).

According to Chen et al. (2007b), Chen and Li (2009), Pirajno and Zhou (2015), two wallrock alteration assemblages are proposed for the porphyry metallogenic system: (1) anhydrous alteration caused by low H_2O activity fluids with high K/Na, F/Cl and CO_2/H_2O ratios, developed in the intra-continental setting (including syn- to post-collisional and intra-continental or backarc rifts settings); (2) hydrous alteration caused by high H_2O activity fluids with relatively low K/Na, F/Cl and CO_2/H_2O ratios, formed in the subduction-related setting. The former is characterized by K-feldspar, quartz, epidote, fluorite and carbonate, and minor garnet and diopside;, whereas the latter is featured by strong biotite, sericite, chlorite, albite, hornblende, and serpentine. The anhydrous alteration is identified in the Yulong (Liang et al., 2009a) and Narigongma (Yang et al., 2014a) deposits in the Qiangtang Terrane, along with extensive K-feldspar alteration. The hydrous alteration developed in the Aikengdelesite

(Yang et al., 2014b) deposit in East Kunlun.

The Mo mineralization in the Narigongma Mo-Cu deposit took place during the potassic alteration stage and was almost completed by the beginning of the phyllic alteration; while the Cu mineralization began during the biotite alteration stage, and mainly formed during the phyllic stage (Yang et al., 2014a). On the contrary, Cu mineralization in the Qulong Cu-Mo deposit was closely associated with potassic alteration; and molybdenum mineralization is formed during transition between the potassic and feldspar-destructive (phyllic ± argillic) alteration, which is slightly later than Cu mineralization (Yang et al., 2009a). The factors that caused the above-mentioned difference between the Narigongma and Qulong deposits, however, are not yet clear and need further research.

6. Descriptions of representative Mo deposits

6.1. Qulong porphyry Cu-Mo deposit

The Qulong porphyry Cu-Mo deposit is located in southern Lhasa Terrane (29°36′ – 29°40′ N, 91°33′ – 91°37′E), about 50 km east of Lhasa city (Fig. 1). Two main lithologic units occur in the district: (1) a middle Jurassic volcano-sedimentary sequence consisting of felsic lava, volcaniclastic rocks and interbedded limestone, sandstone and slate, and (2) a Miocene multiphase intrusion, mainly consists of medium- to fine-grained granodiorite–monzogranite (Fig. 3; Yang et al., 2009a; Hou et al., 2009).

The dominant mineralized intrusion is the monzogranite porphyry stock (<1.0 km^2), which intruded older intrusive phases of the Miocene multiphase intrusion (Fig. 3). The porphyry contains 25 – 30 vol.% phenocrysts, which comprise ~15 vol.% plagioclase, 5–7

vol.% quartz, K-feldspar (3–5 vol.%) and biotite (3 vol.%). The groundmass is quartzo-feldspathic, and displays a fine-grained aplitic texture at shallow levels. Accessory minerals include magnetite, zircon, titanite, apatite and rutile.

The Cu-Mo orebody is mainly lensoidal (2000 m long and 1500 m wide). This deposit contains about 10.6 Mt Cu metal @ 0.5%, and 0.51 Mt Mo metal @ 0.03%. Three major mineralization styles were recognized (Hou et al., 2009): (1) pyrite + chalcopyrite + molybdenite + bornite veinlets inside the porphyry intrusion, forming a pipe-like body with high-grade Cu ore pockets; (2) fine quartz-molybdenite veinlets and chalcopyrite + bornite + sphalerite + galena stockwork, which is usually associated with the fluorite + quartz + sericite alteration assemblage; (3) supergene mineralization dominated by malachite, covellite and minor chalcocite near the surface.

Major alteration styles developed at Qulong include K-silicate, quartz-sericite, argillic, and propylitic alteration (Yang et al., 2009a). The K-silicate alteration can only be observed in the deeper part of the porphyry stock, and is featured by secondary biotite, K-feldspar and anhydrite. The K-silicate alteration is closely related to the Cu and Mo mineralization. Quartz-sericite alteration is mainly developed inside the porphyry stock, and contains granular quartz, fine-grained scaly sericite and irregular granular pyrite. Structurally-controlled argillic alteration, dominated by kaolinite group minerals and quartz, locally occurs as patches in the altered stock, and mainly overprints the quartz-sericite alteration halo. A propylitic (chlorite + epidote + calcite) alteration zone was well-developed in the Yeba Formation and pre-mineralization granodiorite-monzogranite.

The multiphase granitic intrusion at Qulong was dated to be ca. 18 − 14 Ma (Hou et al.,

2004; Wang et al., 2006; Yang, 2008), of which the causative monzogranite porphyry was zircon U-Pb dated to be 17.6 ± 0.76 Ma (Hou et al., 2004). The mineralization was molybdenite Re-Os dated to be 15.69 ± 1.98 Ma – 16.85 ± 0.19Ma (Hou et al., 2009; Li et al., 2005a; Meng et al., 2003; Wang et al., 2006).

6.2. Sharang porphyry Mo deposit

The Sharang porphyry Mo deposit is located in the northeastern part of the Lhasa Terrane (30°10′N, 92°40′E). The deposit is mainly hosted by granite porphyry at the southern margin of the Sharang pluton (Fig. 4) emplaced in the Upper Permian Mengla Formation. Syn-mineralization Etrending thrust faults (with 40°–50° dip angle) and post-mineralization N-trending faults are the main structures at Sharang. A tectonic breccia occurs in the footwall of the post-mineralization fault plane, which contains meta-sedimentary clasts in a matrix of quartz and calcite.

Three magmatic phases were identified at Sharang (Zhao et al., 2014): (1) pre-mineralization quartz monzonite (zircon U-Pb: 53.1 ± 0.6 Ma); (2) syn-mineralization granite, granite porphyry, porphyritic granite, fine-grained granite porphyry, which were zircon U-Pb dated to be 52.9 ± 0.5 Ma, 52.9 ± 0.4 Ma–52.6 ± 0.5 Ma, 52.3 ± 0.4 Ma and 51.6 ± 0.4 Ma, respectively; and (3) post-mineralization dykes of granodiorite porphyry, dacite porphyry and lamprophyre. The granite porphyry is massive and porphyritic, containing phenocrysts of K-feldspar, plagioclase and quartz in the groundmass of quartz, plagioclase, K-feldspar and minor biotite. The quartz phenocrysts are skeletal, “quartz-eye” texture and miarolitic cavities.

Several lenticular to tabular ore shells are distributed in the granite porphyry. The Sharang deposit contains an estimated reserve of ca. 100 Mt ore @ 0.061% Mo. Four Mo mineralization types were identified (Zhao et al., 2014): (1) ribbon-textured quartz + molybdenite (± pyrite) veins with symmetrical mineral distribution, are the most economic ore type, in which the molybdenite grain size and vein thickness decrease from top to bottom, and the molybdenite occurs in some places as brecciated vein-filling minerals at the center with deformed vein walls; (2) quartz + molybdenite stockwork in the granite porphyry; (3) quartz + molybdenite ± pyrite ± anhydrite veins with different alteration halos, and with spotted or radial molybdenite distributed as clusters in the vein; (4) disseminated molybdenite in the matrix of magmatic and hydrothermal breccias.

Almost all rock types in the Sharang complex are altered. The alteration zones comprise potassic, quartz-sericite-pyrite, argillic and propylitic zones. Molybdenite is commonly associated with the potassic and quartz-sericite-pyrite alteration zones. Three main hypogene and one epigenetic alteration-mineralization stages were recognized at Sharang (Zhao et al., 2014): (1) early mineralization stage characterized by K-silicate alteration and local occurrence of magnetite veins, biotite ± quartz ± anhydrite ± epidote ± chlorite veins, K-feldspar ± biotite ± magnetite ± quartz veins, minor K-feldspar + quartz + molybdenite veins and stockwork quartz–molybdenite veins; (2) main mineralization stage contains all four major molybdenite mineralization styles, with major metallic minerals include molybdenite, and rare chalcopyrite, pyrite and scheelite. Non-metallic minerals comprise quartz, K-feldspar, kaolinite, muscovite, sericite, illite, anhydrite, gypsum, tourmaline and garnet; (3) the late mineralization stage is featured by carbonate veins with quartz + pyrite +

sericite alteration halos. Ore mineral assemblage contains coarse-grained pyrite, sphalerite and galena, and major gangue minerals include quartz, gypsum, sericite, muscovite, kaolinite, illite, magnetite, calcite and fluorite; (4) the epigenetic stage, with limonite, molybdenite and ferrimolybdite occurring on the surface of granite porphyry.

The molybdenite Re-Os ages of the deposit are 51.37 ± 0.75 Ma – 52.69 ± 0.77Ma (Tang et al., 2009a; Zhao et al., 2014), consistent with the magmatic ages of the ore-forming granites.

6.3. Narigongma porphyry Mo-Cu deposit

The Narigongma porphyry Mo-Cu deposit (33°31′N, 94°46′E) is located in the northern part of the Qiangtang Terrane, about 185 km northwest of Zaduo county, Qinghai (Fig. 1).

Two main geologic units are present at Narigongma (Fig. 5): (1) Middle–Upper Permian volcanic–sedimentary rocks; and (2) Eocene intrusive rocks comprise mineralization-related biotite granite porphyry, fine-grained granite porphyry, and post-mineralization quartz diorite porphyry. The NW-trending Middle–Upper Permian volcanic–sedimentary sequence comprises basalt, basaltic andesite and minor andesite interbedded with sandstone, slate and muddy limestone. The NE-trending biotite granite porphyry dikes contain 20 – 35 vol.% phenocrysts (plagioclase + K-feldspar + quartz + biotite + (minor) hornblende) The fine-grained granite porphyry generally crops out as NE-striking dikes (Fig. 5). Phenocrysts in the fine-grained granite porphyry include mainly K-feldspar, biotite, quartz, and minor plagioclase. The groundmass of the fine-grained granite porphyry is quartzo-feldspathic, with accessory zircon, titanite and apatite. The NE-trending post-mineralization quartz diorite

porphyry dikes are the youngest intrusions at Narigongma and are characterized by their well-preserved magmatic texture and original gray color. Phenocrysts in the quartz diorite porphyry dikes range from 0.2 to 0.6 cm in size, and consist mainly of plagioclase (15 – 20 vol.%), and minor quartz (5 vol.%) and K-feldspar (3 vol.%).

A NW-trending and a NE-trending fault were identified at Narigongma (Fig. 5). The NW-trending (ENE-dipping) fault is just ~100 m long at the surface, and occurs along the margin of the biotite granite porphyry. The presence of disseminated molybdenite and pyrite on this fault plane indicates that earlier movements of the fault pre-dated the mineralization (Yang et al., 2014a). The NE-trending (NW-dipping) fault is an extensional structure (Fig. 5). It extends for approximately 1 km at the surface, and controlled the biotite granite porphyry emplacement.

Molybdenum-Cu mineralization at Narigongma mainly occurs in the biotite granite porphyry, and the Mo-Cu orebodies are mainly lensoidal in shape, ca. 100 – 900 m long and ca. 30 – 170 m wide. The deposit contains ca. 0.675 Mt Mo metal @ 0.079%, and 0.252 Mt Cu metal @ 0.33% (Wang et al., 2008). Molybdenum mineralization occurs in quartz + molybdenite ± K-feldspar veins. Molybdenite is typically lamellar–columnar.

Hydrothermal alteration styles at Narigongma include (Yang et al., 2014a): (1) potassic alteration, shown by the formation of biotite, K-feldspar and abundant quartz; (2) phyllic alteration, pervasively or as halo along pyrite-bearing veins, with mineral assemblage of sericite, quartz, pyrite and calcite; (3) propylitic alteration, which is strongly developed, with epidote, chlorite and calcite as the major hydrothermal minerals; (4) argillic alteration, structural-controlled and occurred as a N- to NE-trending belt, and is characterized by

pervasive replacement of feldspar by clay minerals.

The mineralization-related biotite granite porphyry and fine-grained granite porphyry yielded zircon U-Pb ages of ca. 41.5 – 43.4 Ma and 43.6 ± 0.5 Ma (Table 2; Hao et al., 2012; Song et al., 2012; Yang et al., 2008, 2014a), respectively, and the molybdenite Re-Os ages of the deposit are ca. 40.8 – 43.1 Ma (Hao et al., 2012; Wang et al., 2008).

6.4. Yulong porphyry-skarn Cu-Mo deposit

The Yulong porphyry-skarn Cu-Mo deposit, the largest Cu-Mo deposit in YPCB, is located in the eastern part of the Qiangtang terrane (Hou et al., 2007b; Liang et al., 2009a). The exposed Upper Triassic Wangka and Jiapila formations shale and limestone were metamorphosed to hornfels and marble. The Eocene Yulong felsic porphyry and breccia, a complex multiphase intrusion (ca. 55 − 38 Ma), host the porphyry-related Cu-Mo orebodies (Hou et al., 2003).

The Yulong deposit consists of a Cu-Mo pipe-like orebody hosted in a porphyry stock surrounded by a high-grade Cu-Au zone (Fig. 6; Hou et al., 2007b). The pipe-like ore body is steeply dipping, 1000 m long and 600 m wide, with a down-dip extension of 500 m. The high-grade Cu-Au zone is gently dipping, about 200 – 300 m wide and 20 – 100 m thick, thinning outward from the stock.

According Tang and Luo (1995) to Liang et al. (2009a), five alteration / mineralization stages were developed at Yulong, i.e., (from oldest to youngest) (1) potassic alteration stage, which produced secondary K-feldspar, biotite, albite, and magnetite and in the relatively barren porphyry intrusion; (2) K-silicate alteration stage, which developed within the upper

portion of the Yulong porphyry intrusion and is characterized by the formation of secondary quartz, K-feldspar and biotite associated with quartz-sulfide (chalcopyrite + bornite + pyrite)-magnetite mineralization; (3) quartz-sericite alteration stage, which formed fine replacement grains of quartz and sericite, together with abundant quartz-sulfide-sericite veinlets; (4) propylitic alteration stage, which formed chlorite, epidote, albite, pyrite and carbonate minerals; (5) argillic to advanced argillic alteration stage, which formed hydro-mica, montmorillonite, kaolinite, halloysite, and vuggy quartz associated with chalcocite, covellite, and molybdenite mineralization, and occurs mainly in the intrusive contact zone and in the surrounding Late Triassic sedimentary strata.

The mineralization-related monzogranite porphyry yielded zircon U-Pb ages of ca. 38.9 – 43.8 Ma (Table 2; Guo et al., 2006; Jiang et al., 2006; Liang et al., 2006, 2008; Wang et al., 2009). The molybdenite Re-Os ages of the Yulong deposit are ca. 39.7 – 41.3 Ma (Hou et al., 2006a; Tang et al., 2009b).

6.5. Tongchanggou porphyry-skarn Mo-Cu deposit

The Tongchanggou Mo-Cu deposit is located in the southern margin of the Yidun arc. Exposed strata at Tongchanggou consist of Permian basalt interbedded with volcanic breccia and Triassic limestone and marble (Li et al., 2012b; Yang et al., 2016c). A granodiorite porphyry stock exposed in the intersection of a NW-trending fault and a N-trending fault (Fig. 7a). Subsequently, a concealed granodiorite batholith has been discovered at depth beneath the deposit through drilling (Fig. 7b).

Three types of orebodies were developed in the Tongchanggou deposit, including

skarn-type, disseminated or stockwork porphyry and veined orebodies (Li et al., 2012b; Yang et al., 2016c). The porphyry-type Mo-Cu mineralization is mainly hosted in the outcropped granodiorite porphyry (Fig. 7a). The skarn-type Mo-Cu mineralization generally occurs along the contact zone between the Triassic limestone and Permian basalt, and mostly in the limestone, away from the concealed granodiorite porphyry (Fig. 7b). The veined orebodies mainly developed along interlayered contact and faults around the granodiorite.

Ore textures are dominated by disseminated, veinlets and stockworks. Ore minerals occur in the form of granular aggregates with molybdenite, chalcopyrite, pyrrhotite, pyrite and magnetite. Non-metallic minerals include garnet, diopside, tremolite, quartz, dolomite, K-feldspar, biotite, sericite and calcite. Major mineralization-related alteration styles include skarn, potassic, silicic and propylitic alterations (Yang et al., 2016c).

Wang et al. (2014c) obtained LA-ICP-MS zircon U-Pb ages of 87.4 Ma and 86.3 Ma for the biotite monzogranite. Yang et al. (2016c) reported LA-ICP-MS zircon U-Pb ages of 85 ± 0.4 Ma and 84 ± 0.4 Ma for the concealed granodiorite. These ages correspond to the molybdenite Re-Os ages of 82.3 – 88.3 Ma (Li et al., 2012b; Yang et al., 2016c), indicating that the mineralization system was formed in the Late Cretaceous.

6.6. Lalingzaohuo porphyry-skarn Mo deposit

The Lalingzaohuo porphyry-skarn Mo deposit is located in the central part of the East Kunlun Terrane (Fig. 1). Major lithostratigraphic units at Lalingzaohuo include the Paleo-Proterozoic Baishahe Formation biotite-bearing plagioclase gneiss, migmatite, siltstone and marble (Fig. 8; Chen et al., 2013). NW- and NE-trending faults were developed in the

deposit, and had controlled the granite emplacement.

The Middle–Late Triassic granitic stocks and the Early Cretaceous K-feldspar granite are two major types of intrusions (Fig. 8), of which the Middle Triassic granodiorite porphyry was suggested to be Mo mineralization-related (Chen et al., 2013; Wang et al., 2013). The granodiorite porphyry contains about 40 vol.% phenocrysts, which consist of plagioclase (30 vol.%), quartz (9%) and biotite (1%). The groundmass comprises K-feldspar, plagioclase, quartz and biotite, with accessory zircon, titanite, monazite and rutile. In the porphyry stock, dioritic and mafic-ultramafic enclaves were documented (Chen et al., 2013; Wang et al., 2013).

Four Mo orebodies are mainly hosted in the granodiorite porphyry and its intrusive contact with the Baishahe Formation (Fig. 8). The NW- or NE-trending orebodies (ca. 200 – 900 m long) are lenticular or vein-shape (Fig. 8), with Mo grades of 0.05% – 0.09%. Major metallic minerals include molybdenite, pyrite, chalcopyrite (uneconomic) and minor magnetite, and major gangue minerals are garnet, actinolite, epidote, quartz, feldspar, sericite, chlorite and calcite. Molybdenite occurs as spots and flakes, sparse disseminations in the altered granite porphyry and skarn, and as fine-grained aggregates or radial coarse-grained aggregates disseminated in hydrothermal stockworks. Various ore textures were observed, such as flaky, replacement remnant and embayment, idiomorphic to hypidiomorphic grain, phenocryst, and cataclastic. Ore structures include disseminations, veins, veinlets, stockworks and breccias. Hydrothermal alteration styles at Lalingzaohuo include skarn, potassic, silicic, sericite, propylitic and argillic alterations.

The ore-associated granodiorite porphyry yielded a zircon U-Pb age of 242.6 ± 3.4 Ma

(Table 2; Chen et al., 2013). The molybdenite Re-Os ages of the deposit fall into two clusters of ca. 235.7 – 240.6 Ma and ca. 214.1 Ma – 223.9 Ma (Wang et al., 2013).

7. Geochemistry of causative intrusions

7.1. Major and trace element

The mineralization-related granitoids of the major Mo deposits in SW China exhibit similar major element compositions (Fig. 9). They have high SiO_2 (53.04 – 77.61%), Al_2O_3 (11.55 – 18.00%), $K_2O + Na_2O$ (6.15 – 11.34%) and K_2O/Na_2O (0.32 – 18.0), which mainly belong to the high-K calc alkaline to the shoshonitic series (Fig. 9A). They are characterized by low TiO_2 (0.01 – 1.27%) and MgO (0.01 – 2.96%), and their A/CNK and A/NK are 0.59 – 1.85 and 1.05 – 1.94, respectively, showing a metaluminous to peraluminous affinity (Fig. 9B). It is noted that, the Late Permian–Triassic (Lalingzaohuo and Kayizi), Late Cretaceous (Xiuwacu, Relin, Hongshan and Tongchnaggou) and Eocene (Sharang, Narigongma, Yulong, Duoxiasongduo, Malasongduo and Mangzong) causative intrusions have higher K_2O/Na_2O values (0.80 – 2.42, 0.65 – 9.32 and 0.82 – 18.0) than the Miocene causative intrusions (Qulong, Jiama, Tinggong, Bangpu; K_2O/Na_2O = 0.43 – 1.62) (Appendices A to C).

In the Lhasa Terrane, the Eocene mineralization-related granite porphyry in the Sharang Mo deposit have higher ∑REE (143 – 232 ppm), but lower δEu (0.48 – 0.98), $(La/Yb)_N$ (13.39 – 17.12) and Sr/Y (7.49 – 23.8) than those of the Miocene mineralization-related granitoids from other Mo-(Cu) deposits (∑REE = 79.2 – 175, δEu = 0.71 – 1.00, $(La/Yb)_N$ = 21.07 – 71.59, Sr/Y = 26.21 – 140.82). These geochemical features indicate that the Miocene intrusions may have originated from a thicker crust (Appendices A to C).

These Late-Permian–Triassic mineralization-related granitoids in the East Kunlun and West Kunlun terranes, and the Eocene mineralization-related granitoids in the Qiangtang Terrane exhibit similar trace element compositions. These rocks contain ∑REE of 112 − 394 ppm, δEu of 0.55 – 0.99 and $(La/Yb)_N$ of 9.72 – 50.86. They also contain relatively high Sr (269 – 504 ppm), low Y (7.9 – 29 ppm) and high Sr/Y ratios (2.33 – 80.24).

In the Yidun arc, the mineralization-related granitoids were formed in the Late Cretaceous (Table 2). The mineralization-related granitoids of the Xiuwacu Mo-W deposit have low ∑REE values of 49.8 to 263 ppm, and lowest Sr/Y ratios of 0.25 – 15.29. Their δEu and $(La/Yb)_N$ values are 0.03 – 0.59 and 1.43 – 38.72, respectively. The mineralization-related granitoids from the other deposits in the Yidun arc yield ∑REE values of 129 − 356 ppm, δEu of 0.57 – 0.97 and $(La/Yb)_N$ of 11.92 – 49.72, with higher Sr/Y ratios (11.68 − 72.03) (Appendices A to C).

All data reported for the Lhasa, West Kunlun, East Kunlun and Qiangtang terranes are enriched in LREE (light rare earth elements), depleted in HREE (heavy rare earth elements), and show a steep negative slope of the REE pattern with no or slightly negative Eu anomaly (Fig. 10A, C, E). They exhibit strong peaks in Rb, Th, U and K, and troughs in Ba, Nb, Ta, P and Ti in the primitive mantle-normalized spider diagram (Fig. 10B, D, F). The granitoids in the Yidun arc show strong to medium Eu depletion, and their MREE (middle rare earth elements) are more deleted than the LREEs and HREEs (Fig. 10G). They are more enriched in Rb, Th, U and K, and more deleted in Ba, P and Ti, than other Mo mineralization-related granitoids in SW China (Fig. 10H).

7.2. Isotope systematics

The mineralization-related intrusions in the Lhasa, Qiangtang, West Kunlun and East Kunlun terranes have various $^{87}Sr/^{86}Sr$ ratios varying from 0.70535 to 0.70857, with $(^{87}Sr/^{86}Sr)i$ of 0.70499 – 0.70720; and their εNd(t) range from −6.18 to 0.60. These mineralization-related intrusions in the Yidun arc have higher $(^{87}Sr/^{86}Sr)i$ of 0.70625 – 0.71010, and lower εNd(t) of −8.0 to −4.2. The Sr-Nd features indicate that all these intrusions may have been derived from partial melting of a lower rejuvenated crust. The lower $(^{87}Sr/^{86}Sr)i$ and higher εNd(t) suggest that some mantle materials were mixed in to the source of the mineralization-related intrusions in the Lhasa, Qiangtang, West Kunlun and East Kunlun terranes.

The $^{206}Pb/^{204}Pb$, $^{207}Pb/^{204}Pb$, and $^{208}Pb/^{204}Pb$ values of these mineralization-related intrusions in the Lhasa, Qiangtang, West Kunlun and East Kunlun terranes are 18.408 – 18.995, 15.567 – 15.733, and 38.609 – 39.153, respectively (Table 3). The mineralization-related intrusions in the Yidun arc yielded relatively high $^{206}Pb/^{204}Pb$ of 18.675 – 19.730, $^{207}Pb/^{204}Pb$ of 15.625 – 16.650, and $^{208}Pb/^{204}Pb$ of 39.114 – 40.065. In the $^{207}Pb/^{204}Pb$ vs. $^{206}Pb/^{204}Pb$ diagram, these intrusions are plotted between the evolutionary lines of the upper crust and the orogen or above the evolutionary line of the upper crust (Fig. 11A). In the $^{208}Pb/^{204}Pb$ vs. $^{206}Pb/^{204}Pb$ diagram, these data points plot near the evolutionary curve of the orogen Fig. 11B). Besides, these mineralization-related intrusions show a decrease in Pb isotope ratios with decreasing ages (Fig. 11A and B).

8. Geochemistry of the Mo deposits

8.1. Fluid inclusions

To discriminate the genesis of hydrothermal mineral systems, Chen et al. (2007b, 2009) suggested a compositional classification of fluid inclusions (FIs), i.e., aqueous FIs or H_2O-NaCl solution (W-type), the daughter mineral- or solid-bearing FIs (S-type), carbonic-aqueous FIs or CO_2-H_2O system (C-type), and pure carbonic FIs (PC-type). This classification of FIs has been widely applied to the Mo metallogenic studies in China. The published FI types, homogenization temperatures, salinities and estimated trapping pressures for the major Mo deposits in SW China were listed in Table 4. Three FI types were recognized, i.e., H_2O-NaCl solution (W-type), the daughter mineral-bearing FIs (S-type), and carbonic-aqueous FIs (C-type). W-type FIs comprise the WL- (liquid-rich) and WV- (vapor-rich) subtypes.

These Mo deposits in SW China, except for the Lalingzaohuo and Xiuwacu deposits, contain W-type and S-type FIs with high homogenization temperatures (up to 590 °C), which are characteristics of magmatic fluids (Chen et al., 2007b). The high-salinity, high-density S-type FIs usually coexisted with the low-salinity, low-density WV-subtype FIs in a same mineralization stage (Hou et al., 2009; Luo et al., 2012; Nan et al., 2005; Yang et al., 2005, 2009a; Zhou et al., 2011a), which is attributed to fluid immiscibility or fluid boiling (Chen et al., 2007b; Chen and Li, 2009; Sillitoe, 2010). Daughter minerals of the S-type FIs in these Cu-Mo deposits are characterized by the presence of halite, chalcopyrite, barite, carbonate and ilmenite (e.g., Yulong, Qulong and Tinggong; Hou et al., 2007b, 2009; Yang et al., 2005, 2009a). S-type

FIs in these Mo-Cu deposits contain daughter minerals of halite, sylvite, hematite, chalcopyrite, pyrite (e.g., Bangpu; Zhao et al., 2015a, b) and molybdenite (e.g., Narigongma; Nan et al., 2005). The presence of daughter hematite and barite suggests oxidized ore-forming fluids for Mo-(Cu) mineralization.

C-type inclusions were widely reported in the Nuri (Chen et al., 2010), Yulong (Hou et al., 2007b), Xiuwacu (Wang et al., 2015), Hongshan (Li et al., 2013c), Relin (Wan et al., 2012) and Lalingzaohuo (Ma et al., 2014) deposits. Moreover, CO_2 was reported in the WV-subtype FIs from the Tinggong (Yang et al., 2005), Bangpu (Luo et al., 2012), Jiama (Zhou et al., 2011a) and Narigongma deposits (Nan et al., 2005), which is too low to form a single phase. The CO_2-rich or CO_2-bearing magmatic-hydrothermal system is widely shared by the intracontinental Mo deposits in China (Chen and Li, 2009; Chen et al., 2007b; Deng et al., 2011, 2013; Li et al., 2012a; Pirajno, 2013; Pirajno and Zhou, 2015; Shi et al., 2009; Wang et al., 2014a; Wu et al., 2014; Xiang et al., 2013; Yang et al., 2009, 2012, 2013a,b).

Nearly all Mo deposits in SW China are characterized by the wide range of homogenization temperatures, salinities and densities (Table 4). The marked decrease of homogenization temperatures from the early to late mineralization stages demonstrate a cooling process, possibly resulted from the input of low-temperature meteoric water. The estimated minimum FI trapping pressures are 10 – 140 MPa, corresponding to 1 – 5 km deep. The pressures in each deposit have shown a decrease in the ore-forming process, which have been frequently reported for porphyry mineral systems, such as the Mo deposits in the Qinling–Dabie Orogen (Li et al., 2007a), NE China (Chen et al., 2016b; and references therein) and South China block (Zhong et al., 2016; and references therein).

8.2. Hydrogen and oxygen isotopes

The $\delta^{18}O$ and δD signatures of three Mo deposits in SW China were summarized in Table 5 and illustrated in Figure 12.

The published $\delta^{18}O_{mineral}$ values range 1.8 – 15.3‰, yielding calculated $\delta^{18}O_{H2O}$ values between −5.6‰ and 12.9‰; and the δD_{H2O} values are between −158‰ and −29‰ (Table 5). Most of the data obtained from the mineralization-stage minerals plot in or adjacent to the box of primary magmatic water (Fig. 12), indicating that the fluids were predominantly magma-derived.

Hou et al. (2007) obtained the $\delta^{18}O$ and δD composition of the K-silicate alteration, the quartz-sericite alteration and the advanced argillic alteration (Fig. 12), suggesting that the ore-fluid source may have gradually shifted from magmatic to meteoric.

8.3. Sulfur and lead isotopes

The $\delta^{34}S$ values of sulfides from the Mo deposits in SW China were listed in Table 6 and illustrated in Figure 13.

These sulfides from the Qulong, Jiama, Bangpu and Tongchanggou deposits yielded $\delta^{34}S$ values of −6.3‰ to 3.8‰, mainly in the range of −4.0‰ to 2.0‰ (peak value is about 0‰). These $\delta^{34}S$ values are similar to those of the granitoids (Hoefs, 2009) and porphyry Mo deposits worldwide, such as the Climax-type Mo deposit (0.8 – 6.8‰) (Carten et al., 1993), and are typical of magmatic-hydrothermal systems (0 ± 5‰, Ohmoto and Rye, 1979; Hoefs, 2009). The anhydrite at Qulong yielded higher $\delta^{34}S$ values of 12.5 − 14.4‰, also similar to that of sulfates in the magmatic-hydrothermal systems worldwide (Ohmoto and Rye, 1979). Hence, the $\delta^{34}S$

isotope compositions support that the sulfides and sulfates in these Mo deposit were magmatic-hydrothermal in origin.

Sulfides from the Narigongma, Xiuwacu, and Hongshan deposits yield $\delta^{34}S$ values of 2.1‰ to 8.0‰ (peak at about 5.0‰), higher than those of the Qulong, Jiama, Bangpu and Tongchanggou deposits. It is noted that the $\delta^{34}S$ values of molybdenite are lower than those of pyrite, and some $\delta^{34}S$ values of pyrite are lower than those of chalcopyrite (Table 6). This indicates that the sulfur isotope fractionation did not reach equilibrium in these deposits (Li et al., 2015b; Wang et al., 2015).

Available lead isotope compositions of sulfides from the Mo deposits in SW China are listed in Table 7. The $^{206}Pb/^{204}Pb$, $^{207}Pb/^{204}Pb$, and $^{208}Pb/^{204}Pb$ values of sulfides are 18.014 – 19.280, 15.480 – 15.930, and 37.816 – 40.880, respectively, which are consistent with those of the mineralization-related granitic intrusions, also suggesting a magmatic-hydrothermal origin.

8.3. Molybdenite Re concentrations

Stein et al. (2001) proposed that molybdenites from the deposits that involve melting of mafic or ultramafic rocks as part of their genesis, may be expected to have overall higher Re concentrations. In contrast, molybdenite from the deposits (whose origin is related to intermediate crustal rocks or organic-poor sedimentary sequences) would contain lower Re concentration. Mao et al. (1999) concluded that the Re contents in molybdenite decrease gradually from hundreds to several ppm from a mantle source, via a mantle-crustal mixed source to a crustal source. Chen et al. (2016b) considered that the Re content of molybdenite can be used as a tracer of the sources of metals and ore-related intrusion, the degree of magma

fractionation, the redox conditions of the magma-fluid system, and thus of the genetic types of porphyry Mo systems.

The Re contents in the molybdenite from the Mo deposits in SW China range from 0.37 – 1218 ppm (Appendix D). A negative correlation between the ages and Re contents was observed (Fig. 14). The molybdenite from Yazigou Cu-Mo deposit (227 – 217 Ma) in EKB, Kayizi Mo deposit (258 – 254 Ma) in WKB contain minimum Re contents of 0.37 – 3.61 ppm, 4.09 – 15.13 ppm; followed by the Late Cretaceous Mo deposits in the Yidun arc, the Eocene Sharang deposit in the Lhasa Terrane and the Narigongma deposit in the Qiangtang Terrane, and then by the Eocene Yulong Cu-Mo deposit in the Qiangtang Terrane and the Miocene Mo deposits in the Lhasa Terrane, with maximum Re content up to 1218 ppm.

In the Qiangtang Terrane, the molybdenite from the Eocene Narigongma Mo-Cu deposit contains obvious lower Re contents (35.49 – 75.01 ppm) than those from the Eocene Yulong Cu-Mo deposit (66.91 – 664.5 ppm). In the -Late-Cretaceous Mo mineralization belt (Yidun arc), the molybdenite Re contents increase from the Xiuwacu Mo-W deposit, to Tongchanggou Mo-Cu deposit, and then to Hongshan Cu-Mo deposit (Fig. 14). Furthermore, most molybdenite from the Mo-dominated deposits (Sharang, Mingze and Bangpu) yield lower Re contents (86.30 – 299.8 ppm) than those (255.7 – 1218 ppm) from Cu-Mo deposits (Qulong, Jiama, Tinggong, Lakange and Nuri) in the Lhasa Terrane. This suggests that the molybdenite Re content is positively correlated with the Cu/Mo ratios, and also, possibly a positive correlation with the mantle contribution, which was reported for the Cu-Mo and Mo-Cu deposits in Mongolia and Siberia (Berzina et al., 2005).

To sum up, the molybdenite Re contents of the major Mo deposits in SW China vary

widely, indicating remarkable differences in metal sources and ages.

9. Tectonic settings of the Mo mineralization in SW China

9.1. Late Permian–Triassic Mo mineralization

The Late Permian–Triassic Mo mineralization was only reported in the East Kunlun and West Kunlun terranes. The East Kunlun Terrane has undergone four orogenic cycles of geologic development in Precambrian, Early Paleozoic, Late Paleozoic–Early Mesozoic, and Late Mesozoic–Cenozoic (Ding et al., 2011; Mo et al., 2007). The Late Paleozoic–Early Mesozoic orogenic cycle has recorded the subduction, closure and continental collision of the A'nyemaqen Ocean (Jiang et al., 1992; Mo et al., 2007; Yang et al., 1996), which is thought to be the northern branch of the Paleo-Tethys Ocean (Jiang et al., 1992;). Many previous works consider that the subduction of the A'nyemaqen Ocean may have occurred during the Late Permian to Middle Triassic (Harris et al., 1988), with continental collision occurred in the Late Triassic (Guo et al., 1998; Luo et al., 2002; Mo et al., 2007). Xia et al. (2014) proposed that seafloor subduction may have started at ca. 260 Ma (Late Permian), lasting for 20 Myrs before the Middle Triassic continental collision (240 − 232 Ma). Late Triassic granites in the East Kunlun Terrane contain abundant mafic to ultramafic enclaves, indicating an extensive magmatic underplating and mixing and a Late Triassic post-collisional setting (Pan et al., 2012; Yang et al., 2009b). The Aikengdelesite granite porphyry has a zircon U-Pb age of 248.3 Ma, formed in an oceanic subduction setting. The Lalingzaohuo deposit was formed at ca. 240.6 – 235.7 Ma and ca. 223.9 – 214.1 Ma (Wang et al., 2013), formed in the Middle Triassic

continental collision setting and the Late Triassic post-collisional intracontinental setting, respectively. The Yazigou deposit, with ages of ca. 227 – 217 Ma, was formed in a post-collisional intracontinental setting.

In the West Kunlun Terrane, from the Carboniferous to Triassic, N-dipping subduction may have continually enlarged the Kara-Kunlun accretionary prism, resulting in the development of a Carboniferous–Triassic magmatic arc with calc-alkaline granitic intrusions in the north and calc-alkaline volcanic rocks in the south (Wang, 2004). The subduction system may have finally collided with the northern active margin of the Qiangtang Terrane in the Late Triassic to Early Jurassic (Xiao et al., 2001; Yin and Harrison, 2000), resulting in the final accretion of the Kunlun and Qiangtang terranes. Therefore, the Kayizi Mo deposit in West Kunlun Terrane (ca. 258 – 250 Ma) (Liu et al., 2010a) may have been related to the Paleo-Tethys subduction.

9.2. Late Cretaceous Mo mineralization

The age data for Mo mineralization and ore-related intrusions in the Yidun arc concentrate in ca. 73 – 88 Ma (Table 2), indicating that these deposits were formed during the Late Cretaceous. Two tectonic models were proposed for the Late Cretaceous magmatic-hydrothermal mineral systems in the Yidun arc:

(1) Wang et al. (2014c, d) proposed that the ore-related intrusions in the southern Yidun Terrane were generated under a late- or post-collisional environment related to the Late Cretaceous Lhasa–Qiangtang collision. Decompression induced upwelling and underplating of mantle-derived magmas may have provided the heat necessary for the anatexis of thickened

lower crust. Late Cretaceous magmas of the southern Yidun arc may have been derived from the mixing of lower continental crustal derived melts and minor mantle-derived melts, and modified by the following fractional crystallization. Afterwards, tectonic setting of the eastern Tibetan Plateau may have been controlled first by the Neotethys Ocean subduction and then by the India–Asia collision.

(2) Yang et al. (2016b, c) suggest that the closure of a Neotethyan seaway in SE Tibet and Indochina may have resulted in the collision of the recently amalgamated Lhasa–Qiangtang–Changdu continental block to the west with the Yangtze Block to the east during the Late Cretaceous. The Yidun arc complex may have then become part of a broad, lithospheric-scale shear zone between these obliquely colliding continental masses. Strain partitioning across the oblique collision front and the ensuing escape tectonics may have developed a series of NNW-trending sinistral faults and shear zones in and across the Yidun arc and the SW Yangtze Block. These lithospheric-scale transtensional faulting, developed as a result of collision-induced escape tectonics in SE Tibet, may have triggered asthenospheric upwelling, and in turn caused intraplate extension, magmatism and Mo-mineralization during the Late Cretaceous. The transtensional sinistral faults provided dilational centers for the magma ascent and pluton emplacement in the Yidun arc.

9.3. Cenozoic Mo mineralization

The Cenozoic Mo mineralization (ca. 63 – 14 Ma) mainly occurred in the Lhasa and Qiangtang terranes. From the Late Cretaceous to Cenozoic, two continental collision events occurred in SW China. The Bangong-Nujiang Neo-Tethys Ocean was closed during the Late

Jurassic to the Early Cretaceous (ca. 160 – 100 Ma), giving rise to the Lhasa−Qiangtang collision at ca. 100 Ma (Chen et al., 1997, 2004; Mo and Pan, 2006; Yin and Nie, 1996). Subsequently, the Yarlung Zangbo Tethys Ocean closed from west to east during ca. 66 – 50 Ma, leading to the India–Asia collision (Chen et al., 2004; and references therein). The entire process of this India–Asia collision may have taken about 20 Mys (Mo and Pan, 2006). The continuous intracontinental convergence exerted a strong S–N compression on the Tibet Plateau and its adjacent areas, reactivating the E-trending faults and the strike-slip ramp thrust in the Sanjiang belt. The strong Early-Miocene intracontinental convergence may have formed the Main Central Thrust (MCT) and the Southern Tibet Detachment System (STDS), as well as the vertical extrusion of the High Himalaya (Burchfiel et al., 1992). During the Middle to Late Miocene, the Main Boundary Thrust (MBT) may have formed, and the Tibetan Plateau uplifting may have extended further into the Qaidam basin, Altyn Tagh, Qilianshan, eastern Longmenshan, and western Qinling (Pan et al., 2012). The post-collisional crustal extension and rifting may have formed a series of N-trending normal faults.

The Mo mineralization in the Qiangtang Terrane, which was mainly formed during ca. 40 – 35 Ma, about 60 Ma later than the final closure of the Bangong–Nujiang Neo-Tethyan Ocean. Coincidentally, Mo deposits in the Lhasa Terrane were mainly formed during ca. 30 – 14 Ma, about 30 Ma after the final closure of the Yarlung Zangbo Ocean. Chen et al. (2004) revealed that the metallogenesis of skarn-type gold deposits in China always postdated the final oceanic closure or the beginning of inter-continent collision by ca. 50 Ma. According to the CMF model for collisional orogeny, petrogenesis, metallogenesis and fluid flow (Pirajno, 2009, 2013), Chen et al. (2004) proposed that the large-scale granitic magmatism and

metallogenesis in China may have occurred in a decompression-geothermal rise regime during tectonic transition from collisional compression to extension, instead of post-collisional tectonism. Therefore, we proposed that the Mo deposits in the Qiangtang and Lhasa terranes may have formed in the tectonic transition from collisional compression to extension.

10. Conclusions

1. Five Mo mineralization belts were indentified in SW China, namely the Lhasa, Qiangtang, East Kunlun and West Kunlun terranes and the Yidun arc. The E-, NW-, and NE-trending regional faults and their subsidiary structures are the major ore-controlling structures.

2. Major Mo mineralization episodes in SW China include Late Permian to Late Triassic (ca. 258 – 214 Ma), Late Cretaceous (ca. 88 – 73 Ma) and Cenozoic (ca. 63 – 14 Ma). The Late-Permian–Triassic Mo mineralization in the East Kunlun and West Kunlun terranes may have been related to the Paleo-Tethys Ocean subduction and the subsequent continental collision, whereas the Cenozoic Mo mineralization in the Lhasa and Qiangtang terranes were formed in the tectonic transition from collisional compression to extension. The Late Cretaceous Mo mineralization in the Yidun arc may have formed in a late- or post-collisional setting related to the Lhasa–Qiangtang collision, or the intraplate extension caused by the India-Asia collision-related escape tectonics in SE Tibet.

3. The Mo deposits in SW China fall mainly into the porphyry, porphyry-skarn, skarn and porphyry-quartz vein types, and are hosted by various rock types of different ages. The

orebodies mainly occur in the causative porphyries and/or their intrusive contact, with the development of potassic, silicic, phyllic, propylitic and argillic alteration.

4. The ore-forming materials may have been largely magma-derived, and the hydrothermal fluid source may have gradually changed from magmatic to meteoric, usually with the occurrence of fluid immiscibility or fluid boiling. CO_2-bearing inclusions are widely reported in these Mo deposits.

5. The ore-related intrusions are mainly metaluminous to peraluminous high-K calc-alkaline to shoshonitic, and may have originated from partial melting of a lower rejuvenated crust.

6. The molybdenite Re contents of these Mo deposits in SW China vary widely, indicating remarkable differences in their metal sources and ages.

Acknowledgments

This is a contribution from the research group on Mineral Deposits in Collisional Orogens (IAGOD), and was funded by the Excellent Ph.D. Thesis Program of Beijing (No. 20131000104), the 973-Projects (Nos. 2006CB403508 and 2012CB416602) and the National Natural Science Foundation of China (Nos. 40730421 and 40425006). Constructive comments from the editor and reviewers led to improvements of the manuscript. Cenozoic Geoscience Editing & Consultancy is acknowledged for its scientific and language editing service.

References

Allègre, J., Courtillot, V., Tapponnier, P., Hirn, A., Mattauer, M., Coulon, C., Jaeger, J.J., Achache, J., Schárer, U., Marcoux, J., Burg, J.P., Girardeau, J., Armijo, R., Gariepy, C., Gopel, C., Li, T., Xiao, X.C., Chang, C.F., 1984. Structure and evolution of the Himalayan–Tibet orogenic belt. Nature 307, 17–22.

Berzina, A.N., Sotnikov, V.I., Economou-Eliopoulos, M., Eliopoulos, D.G., 2005. Distribution of rhenium in molybdenite from porphyry Cu–Mo and Mo–Cu deposits of Russia (Siberia) and Mongolia. Ore Geol. Rev. 26, 91–113.

Burchfiel, B.C., Chen, Z., Hodges, K.V., Liu, Y., Royden, L.H., Deng, C., Xu, J., 1992. The south Tibetan detachment system, Himalayan orogen: extension contemporaneous with and parallel to shortening in a collisional mountain belt. Geological Society of America Special Paper 269, 1–41.

Burchfiel, B.C., Zhiliang, C., Yupinc, L., Royden, L.H., 1995. Tectonics of the Longmen Shan and adjacent regions, Central China. Int. Geol. Rev. 37 (8), 661–735.

Cao, K., Bernet, M., Wang, G., van der Beek, P., Wang, A., Zhang, K., Enkelmann, E., 2013. Focused Pliocene–Quaternary exhumation of the Eastern Pamir domes, western China. Earth Planet. Sci. Lett. 363, 16–26.

Carten, R.B., White, W.H., Stein, H.J., 1993. High-grade granite-related molybdenum system: classification and origin. In Kirkham, R.V., Sinclair, W.D., Thope, R.I., Duke, J.M. (eds.) Mineral deposit modeling. Geological Association of Canada Special Paper 40, 521–554.

Chen, Y.J., 1996. Skarn gold deposits in China. Resource Geology, 46(6): 369-376.

Chen, Y.J., Fu, S.G., 1992. Gold Mineralization in West Henan, China. China Seismological Press, Beijing, 234 (in Chinese with English abstract).

Chen, Y.J., Li, N., 2009. Nature of ore-fluids of intercontinental inclusion-related hypothermal deposits and its

difference from those in island arcs. Acta Petrol. Sin. 25(10), 2477–2508 (in Chinese with English abstract)

Chen, Y.J., Qin, S., Li, X., 1997. Mineralization time, space, geodynamic background and metallogenic model of the skarn gold deposits, China. Universitatis Pekinensis, 33(4): 456-466 (in Chinese).

Chen, Y.J., Chen, H.Y., Liu, Y.L., 2000. Progress and records in the study of endogenetic mineralization during collisional orogenesis. Chinese Sci. Bull. 45(1), 1–10 (in Chinese with English abstract).

Chen, Y.J., Chen, H.Y., Zaw, K., Pirajno, F., Zhang, Z.J., 2004. The geodynamic setting of large-scale metallogenesis in mainland China, exemplified by skarn type gold deposits. Earth Sci. Front. (China Univ. Geosci., Beijing) 11(1), 57–83 (in Chinese with English abstract).

Chen, Y.J., Chen, H.Y., Zaw, K., Pirajno, F., Zhang, Z.J., 2007a. Geodynamic settings and tectonic model of skarn gold deposits in China: an overview. Ore Geol. Rev. 31, 139–169.

Chen, Y.J., Ni, P., Fan, H.R., Pirajno, F., Lai, Y., Su, W.C., Zhang, H.. 2007b. Diagnostic fluid inclusions of different types hydrothermal gold deposits. Acta Petrol. Sin. 23(9), 2085–2108 (in Chinese with English abstract)

Chen, Y.J., Zhai, M.G., Jiang, S.Y., 2009. Significant achievements and open issues in study of orogenesis and metallogenesis surrounding the North China continent. Acta Petrol. Sin. 25, 2695–2726 (in Chinese with English abstract).

Chen, L., Qin, K.Z., Li, J.X., Xiao, B., Li, G.M., Zhao, J.X., Fan, X., 2010. Ore-fluids and D-O-S-Hf isotopes of the Nuri Cu-Mo-W deposit in the Gangdese area, southern Tibet. Mineral Deposits 29 (Supp.), 567–568 (in Chinese).

Chen, J., Xie, Z.Y., Li, B., Li, S.P., Tan, X.S., Ren, H., Zhang, Q.M., 2013. Geological and Geochemical characteristics of the ore-bearing intrusions from the Lalingzaohuo Mo polymetallic deposit and its metallogenic significance. Geology and Exploration 49(5), 813–824 (in Chinese with English abstract).

Chen, R., Liu, Y.L., Guo, L.S., Wang, Z.H., Liu, H.F., Xu, K.F., Zhang, J.S., 2014. Geochronology and geochemistry

of the Tinggong porphyry copper ore deposit, Tibet. Acta Geol. Sin. (English Edition) 88(3), 780–800.

Chen, L., Qin, K.Z., Li, G.M., Li, J.X., Xiao, B., Zhao, J.X., Fan, X., 2015. Zircon U-Pb ages, geochemistry, and Sr-Nd-Pb-Hf isotopes of the Nuri intrusive rocks in the Gangdese area, southern Tibet: Constraints on timing, petrogenesis, and tectonic transformation. Lithos 212–215, 379–396.

Chen, Y.J., Wang, P., Li, N., Yang, Y.F., Pirajno, F., 2016a. The collision-type porphyry Mo deposits in Dabie Shan, China. Ore Geol. Rev., http://554.rm.cglhub.com/10.1016/j.oregeorev.2016.03.025.

Chen, Y.J., Zhang, C., Li, N., Yang, Y.F., Deng, K., 2016b. The Mo deposits of Northeast China: A powerful indicator of tectonic settings and associated evolutionary trends. Ore Geol. Rev., http:// 554.rm.cglhub.com /10.1016/ j.oregeorev.2016.04.017.

Cowgill, E., Yin, A., Harrison, T.M., Xiao-Feng, W., 2003. Reconstruction of the Altyn Tagh fault based on U-Pb geochronology: role of back thrusts, mantle sutures, and heterogeneous crustal strength in forming the Tibetan Plateau. J. Geophys. Res.108, 2346. doi: 10.1029/2002JB002080.

Deng, X.H., Yao, J.M., Li, J., Liu, G.F., 2011. Fluid inclusion and Re-Os isotopic constraints on the timing and origin of the Shimengou Mo deposit, Xixia county, Henan province. Acta Petrol. Sin. 27, 1439–1452 (in Chinese with English abstract).

Deng, X.H., Chen, Y.J., Santosh, M., Yao, J.M., 2013. Re-Os geochronology, fluid inclusions and genesis of the 0.85 Ga Tumen molybdenite-fluorite deposit in Eastern Qinling, China: Implications for pre-Mesozoic Mo-enrichment and tectonic setting. Geol. J. 48, 484–497.

Deng, J., Wang, Q.F., Li, G.J., Santosh, M., 2014. Cenozoic tectono-magmatic and metallogenic processes in the Sanjiang region, southwestern China. Earth-Science Reviews 138, 268–299.

Dewey, J.F., Shackelton, R.M., Chang, C., Sun, Y., 1988. The tectonic evolution of the Tibetan Palteau. Philosophical Transactions-Royal Society of London A327, 379–413.

Ding, S., Huang, H., Niu, Y.L., Zhao, Z.D., Yu, X.H., Mo, X.X., 2011. Geochemistry, geochronology and petrogenesis of East Kunlun high Nb−Ta rhyolites. Acta Petrol. Sin. 27, 3603–3614 (in Chinese with English abstract).

Dong, G.C., Mo, X.X., Zhao, Z.D., Guo, T.-Y., Wang, L.L., Chen, T., 2005. Underplating of mantle-derived magma: evidence from gabbro-pyroxenite in the Gangdese magmatic belt. Acta Geol. Sin. 79, 801–808.

Dong, G.C., Mo, X.X., Zhao, Z.D., Wang, L.L., Chen, T., 2006a. Magma mixing of mantle and crust source during India-Eurasian continental collision: evidences from Gangdese magma belt. Acta Petrol. Sin. 22, 835−844 (in Chinese with English abstract).

Dong, Y.H., Xu, J.F., Zeng, Q.G., Mao, G.Z., Li, J., 2006b. Is there a Neo-Tethys' subduction record earlier than arc volcanic rocks in the Sangri group? Acta Petrol. Sin. 22, 661–668 (in Chinese with English Abstract).

Fan, X., Chen, L., Qin, K.Z., Xiao, B., Li, J.X., Li, Q.P., Chen, Y.S., Chen, J.B., Zhao, J.X., Li, G.M., Huang, S.F., Ju, Y.T., 2011. Characteristics of alteration and mineralization and chronology of the Mingze porphyry Mo deposit in the Shannan area of Southern Tibet. Geology and Exploration 47, 89–99 (in Chinese with English abstract).

Gao, X.F., Xiao, P.X., Jia, Q.Z., 2011. Redetermination of the Tanjianshan Group: Geochronological and geochemical evidence of basalts from the margin of the Qaidam basin. Acta Geol. Sin. 85, 1452–1463 (in Chinese with English abstract).

Guo, Z.F., Deng, J.F., Xu, Z.Q., Mo, X.X., Luo, Z.H., 1998. Late Paleozoic–Mesozoic intracontinental orogenic process and intermediate-acidic igneous rocks from the Eastern Kunlun Mountains from Northwestern China. Geoscience, 51–59 (in Chinese with English abstract).

Guo, L.G., Liu, Y.P., Xu, W., Zhang, X.C., Qin, K.Z., Li, T.S., Shi, Y.R., 2006. Constraints to the mineralization age of the Yulong porphyry copper deposit from SHRIMP U-Pb zircon data in Tibet. Acta Petrol. Sinica 21(4), 1009–1016 (in Chinese with English abstract).

Hao, J.H., Chen, J.P., Dong, Q.J., Tian, Y.G., Li, Y.L., Chen, D., 2012. Zircon LA-ICP-MS U-Pb dating for Narigongma porphyry molybdenite-copper deposit in Southern Qinghai Province and its geological implication. Geoscience 26(1), 45–53 (in Chinese with English abstract).

Hao, J.H., Chen, J.P., Dong, Q.J., Wang, T., Luo, Z.Z., Zhang, Y.T., 2013. Early Paleocene diagenetic and metallogenic events of the Lurige porphyry molybdenum-copper deposit in southern Qinhai, China: evidence from zircon LA-ICP-MS U-Pb and molybdenite Re-Os dating. Acta Geol. Sin. 87, 227–239 (in Chinese with English abstract).

Harris, N., Xu, R.H., Lewis, C., Hawkesworth, C., Zhang, Y.Q., 1988. Isotope geochemistry of the 1985 Tibet geotraverse, Lhasa to Golmud. Philosophical Transactions of the Royal Society of London. Proceedings of the Royal Society of London. Series A: Mathematical and Physical Sciences 327, 263–285.

Harrison, T.M., Copeland, P., Kidd, W.S.F., Yin, A., 1992. Raising Tibet. Science 255, 1663–1670.

He, S.Y., Li, D.S., Li, L.L., Qi, L.Y., He, S.F., 2009. Re-Os Age of molybdenite from the Yazigou copper (molybdenum) mineralized area in Eastern Kunlun of Qinghai Province, and its geological significance. Geotectonica et Metallogenia 33(2), 236–242 (in Chinese with English abstract).

He, G.C., Wang, G.Q., Huang, W.T., Zou, Y.Q., Wu, J., Liang, H.Y., Zhang, Y.Q., Allen, C.M., 2014. Zircon LA-ICP-MS U-Pb age of the Zalaga porphyry associated with Cu-Mo mineralization in the Yulong ore belt and its geological implication. Geochimica 43(4), 399–407 (in Chinese with English abstract).

He, D.F., Dong, Y.P., Liu, X.M. Yang, Z., Sun, S.S., Cheng, B., Li, W., 2015. Tectono-thermal events in East Kunlun, Northern Tibetan Plateau: Evidence from zircon U−Pb geochronology, Gondwana Res., doi: 10.1016/j.gr.2015.08.002

Hoefs, J., 2009. Stable isotope geochemistry, 6th edn. Springer, Berlin, p 285.

Hou, Z.Q., Zhou, J.R., 2001. Collision-orogenic processes of the Yidun Arc in the Sanjiang region: record of granites.

Acta Geologica Sinica 75, 484–497 (in Chinese with English abstract).

Hou, Z., Cook, N.J., 2009. Metallogenesis of the Tibetan collisional orogen: A review and introduction to the special issue. Ore Geol. Rev. 36, 2–24.

Hou, Z.Q., Qu, X.M., Huang, W., 2001. Gangdese porphyry copper belt: the second Yulong porphyry copper belt in Tibet. Geology in China 28, 27–29 (in Chinese with English abstract).

Hou, Z.Q., Ma, H.W., Khin, Z., Zhang, Y.Q., Wang, M.J., Wang, Z., Pan, G.T., Tang, R.L., 2003. The Himalayan Yulong porphyry copper belt: product of large-scale strike-slip faulting in eastern Tibet. Econ. Geol. 98, 125–145.

Hou, Z.Q., Gao, Y.F., Qu, X.M., Rui, Z.Y., Mo, X.X., 2004. Origin of adakitic intrusives generated during mid–Miocene east–west extension in southern Tibet. Earth Planet. Sci. Lett. 220(1), 139–155.

Hou, Z.Q., Zeng, P.S., Gao, Y.F., Dong, F.L., 2006a. The Himalayan Cu-Mo-Au mineralization in the eastern Indo-Asian Collision Zone: constraints from Re-Os dating of molybdenite. Minerlium Deposita 41, 33–45.

Hou, Z.Q., Yang, Z.S., Xu,W.Y., Mo, X.X., Ding, L., Gao, Y.F, Dong, F.L., Li, G.M., Qu, X.M., Li, G.M., Zhao, Z.D, Jiang, S.H., Meng, X.J., Li, Z.Q., Qing, K.Z., 2006b. The Tibetan collisional orogenic belt: I Metallogenesis in main-collisional epoch. Mineral Deposits 25, 337–358 (in Chinese with English abstract).

Hou, Z.Q., Qu, X.M., Yang, Z.S., Meng, X.J., Li, Z.Q., Yang, Z.M., Zheng, M.P., Zheng, Y.Y., Nie, F.J., Gao, Y.F., Jiang, S.H., Li, G.M., 2006c. Metallogenesis in the Tibetan collisional orogenic belt: III. Mineralization in the post-collisional extension setting. Mineral Deposits 25, 629–651 (in Chinese with English abstract).

Hou, Z.Q., Zaw, K., Pan, G.T., Mo, X.X., Xu, Q., Hu, Y.Z., Li, X.Z., 2007a. Sanjiang Tethyan metallogenesis in S.W. China: Tectonic setting, metallogenic epochs and deposit types. Ore Geol. Rev. 31, 48–87.

Hou, Z.Q., Xie, Y.L., Xu, W.Y., Li, Y.Q., Zhu, X.K., Zaw, K., Beaudoin, G., Rui, Z.Y., Huang, W., Luobu, C., 2007b. Yulong Deposit, Eastern Tibet: A High-Sulfidation Cu-Au Porphyry Copper Deposit in the Eastern Indo-Asian

Collision Zone. Int. Geol. Rev. 49, 235–258.

Hou, Z.Q., Yang, Z.M., Qu, X.M., Meng, X.J., Li, Z.Q., Beaudoin, G., Rui, Z.Y., Gao, Y.F., Zaw, K., 2009. The Miocene Gangdese porphyry copper belt generated during post-collisional extension in the Tibetan Orogen. Ore Geol. Rev. 36(1–3), 25–51.

Hu SX. 2002. Petrology of metasomatic rocks and implications for ore exploration. Science Press, Beijing, pp 264 (in Chinese)

Jiang, C.F., Feng, B., Yang, J.S., Zhu, Z., Zhao, M., Chai, Y., Shi, X., Hu, J., 1986. An outline of the geology and tectonics of the Kunlun Mts. area. Bulletin Institute of Geology of Chinese Academy of Geological Sciences 15, 70–79.

Jiang, C.F., Yang, J.S., Feng, B.G., Zhu, Z.Z., Zhao, M., Chai, Y.C., Shi, X.D., Wang, H.D., Hu, J.Q., 1992. Opening-Closing Tectonics of Kunlun Mountains. Geological Publishing House, Beijing (224 pp., in Chinese).

Jiang, Y.H., Jiang, S.Y., Ling, H.F., Zhou, X.R., Rui, X.J., Yang, W.Z., 2002. Petrology and geochemistry of shoshonitic plutons from the western Kunlun orogenic belt, northwestern Xinjiang, China: implications for granitoid geneses. Lithos 63, 165–187.

Jiang, Y.H., Jiang, S.Y., Ling, H.F., Dai, B.Z., 2006a. Low-degree melting of a metasomatized lithospheric mantle for the origin of Cenozoic Yulong monzogranite-porphyry, east Tibet: Geochemical and Sr–Nd–Pb–Hf isotopic constraints. Earth Planet. Sci. Lett. 241, 617– 633.

Jiang, X., Li, Z., Li, H., 2013. Uplift of the West Kunlun Range, northern Tibetan Plateau, dominated by brittle thickening of the upper crust. Geology 41, 439–442.

Khashgerel, B.E., Rye, R.O., Hedenquist, J.W., Kavalieris, I., 2006. Geology and reconnaissance stable isotope study of the Oyu Tolgoi porphyry Cu-Au system, South Gobi, Mongolia. Econ. Geol. 101(3), 503–522.

Leng, Q.F., Tang, J.X., Zheng, W.B., Zhang, J.S., Tang, P., Yan, G., Dong, Y., 2015. Re-Os dating of molybdenite

from the Lakange porphyry Cu-Mo deposit in Tibet and its Geological Significance. Geology in China, 42(2): 570–584 (in Chinese with English abstract).

Li, G.M., Liu, B., Qu, W.J., Lin, F.C., She, H.Q., Feng, C.Y., 2005a. The porphyry-skarn ore-forming system in Gangdese metallogenic belt, southern Tibet: Evidence from molybdenite Re-Os age of Porphyry-type copper deposits and skarn-type copper polymetallic deposits. Geotectonica Et Metallogenia, 29(4): 482–490 (in Chinese with English abstract).

Li, G.M., Rui, Z.Y., Wang, G.M., Lin, F.C., Liu, B., She, H.Q., Feng, C.Y., Qu, W.J., 2005b. Molybdenite Re-Os dating of Jiama and Zhibula polymetallic copper deposits in Gangdese metallogenic belt of Tibet and its significance. Mineral Deposits 24(5), 481–489 (in Chinese with English abstract).

Li, G.M., Qin, K.Z., Ding, K.S., Liu, T.B., Li, J.X., Wang, S.H., Jiang, S.Y., and Zhang, X.C., 2006, Geology, Ar-Ar Age and Mineral Assemblage of Eocene Skarn Cu-Au±Mo Deposits in the Southeastern Gangdese Arc, Southern Tibet: Implications for Deep Exploration. Res. Geol. 56, 315–336.

Li N, Chen YJ, Zhang H, Zhao TP, Deng XH, Wang Y, Ni ZY. 2007a. Geological features and tectonic background of molybdenum deposits in East Qinling. Earth Sci. Front. 14(5), 186–198 (in Chinese with English abstract)

Li, J.X., Qing, K.Z., Li, G.M., Yang, L.K., 2007b. K-Ar and $^{40}Ar/^{39}Ar$ age dating of Nimu porphyry copper orefield in Central Gangdese: Constrains on magmatic-hydrothermal evolution and metallogenetic tectonic setting. Acta Petrol. Sin. 23(5), 953–966 (in Chinese with English abstract).

Li, J.K., Li, W.C., Wang, D.H., Lu, Y.X., Yin, G.H., Xue, S.R., 2007c. Re-Os dating for ore-forming event in the late of Yanshan Epoch and research of ore-forming regularity in Zhongdian Arc. Acta Petrol. Sin. 23(10), 2415–2422 (in Chinese with English abstract).

Li, S.J., Sun, F.Y., Feng, C.Y., Liu, Z.H., Zhao, J.W., Li, Y.C., Wang, S., 2008. Geochronological study on Yazigou polymetallic deposit in Eastern Kunlun , Qinhai Province. Acta Geol. Sin. 82(7), 949–955 (in Chinese with

English abstract).

Li, W.C., Zeng, P.S., Hou, Z.Q., White, N.C., 2011. The Pulang porphyry copper deposit and associated felsic intrusions in Yunnan Province, Southwest China. Econ. Geol. 106 (1),79–92.

Li, N., Ulrich, T., Chen, Y.J., Thomsen, T.B., Pease, V., Pirajno, F., 2012a. Fluid evolution of the Yuchiling porphyry Mo deposit, East Qinling, China. Ore Geol. Rev. 48, 442–459.

Li, W.C., Yu, H.J., Yin, G.H., Cao, X.M., Huang, D.Z., Dong, T., 2012b. Re-Os dating of molybdenite from Tongchanggou Mo-polymetallic deposit in northwest Yunnan and its metallogenic environment. Mineral Deposits 31(2), 282–292 (in Chinese with English abstract).

Li, Y.S., Lü, Z.C., Yan, G.S., Zhen, S.M., Du, Z.Z., 2012c. Isotopic characteristics of S, Pb, H and O of Jiama copper-polymetallic ore deposit, Tibet and their significance. Earth Sci. Front. 19(4), 72–81 (in Chinese with English abstract).

Li, N., Chen, Y.J., Pirajno, F., Ni, Z.Y., 2013a. Timing of the Yuchiling giant porphyry Mo system, and implications for ore genesis. Miner. Deposita 48, 505–524.

Li, W., Neubauer, F., Liu, Y.J., Genser, J., Ren, S.M., Han, G.Q., Liang, C.Y., 2013b. Paleozoic evolution of the Qimantagh magmatic arcs, Eastern Kunlun Mountains: constraints from zircon dating of granitoids and modern river sands. J. Asian Earth Sci. 77, 183–202

Li, W.C., Wang, K.Y., Yin, G.H., Qin, D.H., Yu, H.J., Xue, S.R., Wan, D., 2013c. Geochemical characteristics of ore-forming fluids and genesis of Hongshan copper deposit in northwestern Yunnan Province. Acta Petrol. Sin. 29(1), 270– 282 (in Chinese with English abstract).

Li, G.W., Tian, Y.T., Kohn, B.P., Sandiford, M., Xu, Z.Q., Cai, Z.H., 2015a. Cenozoic low temperature cooling history of the Northern Tethyan Himalaya in Zedang, SE Tibet and its implications. Tectonophysics 643, 80–93.

Li, Y.Z., Kong, H.L., Nanka E.W., Li, J.C., Jia, Q.Z., Du, Y.L., Chen, X.Y., Song, Z.B., Zhang, Y.L., Quan, S.C., 2015b. Analysis of matter source and metallogenic setting of metallogenic rock of Narigongma porphyry copper-molybdenum deposit in Qinghai Province. Geological Science and Technology Information 34(1), 1–9 (in Chinese with English abstract).

Liang, H.Y., Sun, W.D., Yu, H.X., Xie, Y.J., Mo, J.H., Zhang, Y.Q., 2006. The age of ore-bearing porphyries in the Yulong copper belt and the formation process of porphyry Cu (Au) deposits. Mineral Deposits 25(Supp.), 415–418 (in Chinese with English abstract).

Liang, H.Y., Mao, J.H., Sun, W.D., Yu, H.X., Zhang, Y.Q., Allen, C.M., 2008. Study on the duration of the ore-forming system of the Yulong giant porphyry copper deposit in the eastern Tibet, China. Acta Petrol. Sin. 24(10), 2352–2358 (in Chinese with English abstract).

Liang, H.Y., Sun, W.D., Su, W.C., Zartman, R.E., 2009a. Porphyry copper-gold mineralization at Yulong, China, promoted by decreasing redox potential during magnetite alteration. Econ. Geol. 104, 587–596.

Liang, H.Y., Mo, J.H., Sun, W.D., Zhang, Y.Q., Zeng, T., Hu, G.Q., Allen, C.M., 2009b. Study on geochemical composition and isotope ages of the Malasongduo porphyry associated with Cu-Mo mineralization. Acta Petrol. Sin. 25(2), 385–392 (in Chinese with English abstract).

Liu, Y.J., Genser, J., Neubauer, F., Jin, W., Ge, X.H., Handler, R., Takasu, A., 2005. 40Ar/39Ar mineral ages from basement rocks in the Eastern Kunlun Mountains, NW China, and their tectonic implications. Tectonophysics 398, 199–224.

Liu, J.P., Wang, H., Li, S.H., Tong, L.X., Ren, G.L., 2010a. Geological and geochemical features and geochronology of the Kayizi porphyry molybdenum deposit in the northern belt of western Kunlun, NW China. Acta Petrol. Sin. 26(10), 3095–3105 (in Chinese with English abstract).

Liu, J.P., Wang, H., Ren, G.L., 2010b. Geological characters and prospecting significance of Xiaotongxiang

molybdenum deposit in Western Kunlun, Xinjiang. Xinjiang Geology 28(1), 38–44 (in Chinese with English abstract).

Liu, B., Ma, C.Q., Zhang, J.Y., Xiong, F.H., Huang, J., Jiang, H.A., 2012. Petrogenesis of Early Devonian intrusive rocks in the east part of Eastern Kunlun Orogen and implication for Early Paleozoic orogenic processes. Acta Petrol. Sin. 28, 1785–1807 (in Chinese with English abstract).

Liu, X.L., Li, W.C., Zhang, N., Yang, F.C., Kang, J., Zhang, B., 2016. Characteristics of sulfur and lead isotopes and tracing of mineral sources in the Tongchanggou porphyry Mo(Cu) deposit at the southern edge of Geza arc belt, Yunnan. Geology in China, 43(1), 209-220(in Chinese with English abstract).

Luo, Z.H., Ke, S., Cao, Y.Q., Deng, J.F., Chen, H.W., 2002. Late Indosinian mantle derived magmatism in the East Kunlun. Geological Bulletin of China 292–297 (in Chinese with English abstract).

Luo, M.C., Mao, J.W., Wang, L.Q., Leng, Q.F., Chen, W., 2012. Fluid Inclusion Evidence for Magmatic-Hydrothermal Evolution in the Bangpu Porphyry Molybdenum-Copper Deposit, Tibet. Acta Geoscientica Sinica 33(4), 471–484 (in Chinese with English abstract).

Ma, S.Q., Li, B., Xu, Y.F., Chen, J., 2014. Characteristics of ore-forming fluid from the Lalingzaohuo porphyry molybdenum deposit in East Kunlun. J. Mineral. Petrol. 34(3), 23–29 (in Chinese with English abstract).

Mao, J.W., Zhang, Z.C., Zhang, Z.H., 1999. Re-Os isotopic dating of molybdenites in the Xiaoliugou W(Mo) deposit in the northern Qilian Mountains and its geological significance. Geochim. Cosmochim. Acta 63(11–12):1815–1818

Mao, J.W., Xie, G.Q., Bierlein, F., Qü, W.J., Du, A.D., Ye, H.S., Pirajno, F., Li, H.M., Guo, B.J., Li, Y.F., Yang, Z.Q., 2008. Tectonic implications from Re-Os dating of Mesozoic molybdenum deposits in East Qinling-Dabie orogenic belt. Geochim. Cosmochim. Acta 72, 4607–4626.

Mao, J.W., Xie, G.Q., Pirajno, F., Ye, H.S., Wang, Y.B., Li, Y.F., Xiang, J.F., Zhao, H.J., 2010. Late Jurassic-Early

Cretaceous granitoid magmatism in Eastern Qinling, central-eastern China: SHRIMP zircon U-Pb ages and tectonic implications. Aust. J. Earth Sci. 57, 51–78.

Mao, J.W., Pirajno, F., Xiang, J.F., Gao, J.J., Ye, H.S., Li, Y.F., Guo, B.J., 2011. Mesozoic molybdenum deposits in the east Qinling–Dabie orogenic belt: Characteristics and tectonic setting. Ore Geol. Rev. 43(1), 264–293

Mattern, F., Schneider, W., 2000. Suturing of the Proto- and Paleo-Tethys oceans in the western Kunlun (Xinjiang, China). J. Asian Earth Sci. 18, 637–650.

Meng, X.J., Hou, Z.Q., Gao, Y.F., Huang, W., Qu, X.M., Qu, W.J., 2003. Re-Os dating for molybdenite from Qulong porphyry copper deposits in Gangdese metallogenic belt, Xizang and its metallogenic significance. Geol. Rev. 49, 660–666 (in Chinese with English abstract).

Meng, X.J., Hou, Z.Q., Li, Z.Q., 2006. Sulfur and lead isotope compositions of the Qulong porphyry copper deposit, Tibet: implications for the sources of plutons and metals in the deposit. Acta Geol. Sin. 80, 554–560 (in Chinese with English abstract).

Meng, J.Y., Yang, L.Q., Lü, L., Gao, X., Li, J.X., Luo, Y.Z., 2013. Re-Os dating of molybdenite from the Hongshan Cu-Mo deposit in Northwest Yunnan and its implications for mineralization. Acta Petrologica Sinica, 29(4) : 1214–1222 (in Chinese with English abstract).

Meng, F.C., Cui, M.H., Wu, X.K., Ren, Y.F., 2015. Heishan mafic−ultramafic rocks in the Qimantag area of Eastern Kunlun, NW China: Remnants of an early Paleozoic incipient island arc. Gondwana Res. 27, 745–759.

Mi, M., Chen, Y.J., Yang, Y.F., Wang, P., Li, F.L., Wan, S.Q., Xu, Y.L., 2015. Geochronology and geochemistry of the giant Qian'echong Mo deposit, Dabie Shan, eastern China: Implications for ore genesis and tectonic setting. Gondwana Res. 27(3), 1217–1235.

Mo, X.X., Pan, G.T., 2006. From the Tethys to the formation of the Qinghai-Tibet Plateau: Constrained by tectono-magmatic events. Earth Sci. Front. 13(6), 43–51 (in Chinese with English abstract).

Mo, X.X., Deng, J.F., Dong, F.L., H., Y.X., Wang, Y., Zhou, S., Yang, W.G., 2001. Volcanic petrotectonic assemblages in Sanjiang Orogenic Belt, SW China and implication for tectonics. Geological Journal of China Universities 7, 121–138 (in Chinese with English abstract).

Mo, X.X., Zhao, Z.D., Deng, J.F., Dong, G.C., Zhou, S., Guo, T.Y., Zhang, S.Q., Wang, L.L., 2003. Response of volcanism to the India−Asian collision. Earth Sci. Front. 10, 135–148 (in Chinese with English abstract).

Mo, X.X., Dong, G.C., Zhao, Z.D., Guo, T.Y., Wang, L.L., Chen, T., 2005. Timing of magma mixing in the Gangdese magmatic belt during the India−Asian collision: zircon SHRIMP U-Pb dating. Acta Geol. Sin. 7, 66–76(in Chinese with English abstract).

Mo, X.X., Luo, Z.H., Deng, J.F., Yu, X.H., Liu, C.D., Chen, H.W., Yuan, W.M., Liu, Y.H., 2007. Granitoids and crustal growth in the East-Kunlun Orogenic Belt. Geological Journal of China Universities 403–414 (in Chinese with English abstract).

Mo, X.X., Niu, Y.L., Dong, G.C., Zhao, Z.D., Hou, Z.Q., Zhou, S., Ke, S., 2008. Contribution of syncollisional felsic magmatism to continental crust growth: a case study of the Paleocene Linzizong Volcanic Succession in southern Tibet. Chem. Geol. 250, 49–67.

Murphy, M.A., Yin, A., Harrison, T.M., Durr, S.B., Chen, Z., Ryerson, F.J., Kidd, W.S.F., Wang, X., Zhou, X., 1997. Significant crustal shorting in south-central Tibet prior to the Indo-Asian collision. Geology 25, 719–722.

Nan, Z.B., Tang, J.X., Li, B.H., Song, S.C., 2005. Fluid inclusion geochemical characteristics of the Narigongma porphyry copper deposit, Zaduo County, Qinghai Province. Xinjiang Geology 23(4), 373–377 (in Chinese with English abstract).

Ohmoto, H., Rye, R.O., 1979. Isotopes of sulfur and carbon. In: Barnes HL (ed) Geochemistry of hydrothermal ore deposits, 2nd edn. Wiley, New York, pp 509–567

Pan, G.T., Wang, L.Q., Li, R.S., Yuan, S.H., Ji, W.H., Yin, F.G., Zhang, W.P., Wang, B.D., 2012. Tectonic evolution

of the Qinghai-Tibet Plateau. J Asian Earth Sci 53, 3–14.

Pan, G.T., Zhu, D.C., Wang, L.Q., Liao, Z.L., Geng, Q.R., Jiang, X.S., 2004. Bangong Lake–Nu River suture zone−the northern boundary of Gondwanaland: evidence from geology and geophysics. Earth Sci. Front. 11, 371–382 (in Chinese with English abstract).

Pierce, J.A., Mei, H., 1988. Volcanic rocks of the 1985 Tibet Geotraverse Lhasa to Golmud. Philosophical Transaction of Royal Society of London A327, 203–213.

Pirajno, F., 2009. Hydrothermal Processes and Mineral Systems. Springer, Berlin, (1250 pp.).

Pirajno, F., 2013. The geology and tectonic settings of China's mineral deposits. Springer, Berlin, (679 pp.).

Pirajno, F., Zhou, T.F., 2015. Intracontinental porphyry and porphyry–skarn mineral systems in eastern China: scrutiny of a special case "made-in-China". Econ. Geol. 110(3), 603–629.

Qin, K.Z., 2012. Thematic Articles "Porphyry Cu-Au-Mo deposits in Tibet and Kazakhstan". Resource Geology 62, 1–3.

Qin, Z.P., Wang, X.W., Duo, J., Tang, X.Q., Zhou, Y., Peng, H.J., 2011. LA-ICP-MS U-Pb zircon age of intermediate-acidic intrusive rocks in Jiama of Tibet and its metallogenic significance. Mineral Deposits 30(2), 339–348 (in Chinese with English abstract).

Qin, Z.P., Wang, X.W., Tang, J.X., Zhou, Y., Tang, X.Q., 2012. Geochemical Characteristics and Significance of the Jiama Adakitic Porphyry, Tibet. J. Jilin University (Earth Science Edition) 42(1), 267–280.

Qu, X.M., Hou, Z.Q., Li, Z.Q., 2003. $^{40}Ar/^{39}Ar$ ages of porphyries from the Gangdese porphyry Cu belt in south Tibet and implication to geodynamic setting. Acta Geologica Sinica 77, 245–252 (in Chinese with English abstract).

Qu, X.M., Hou, Z.Q., Li, Y.G., 2004. Melt components derived from a subducted slab in late orogenic ore-bearing porphyries in the Gangdese copper belt, southern Tibetan Plateau. Lithos 74, 131–148.

Qu, X.M., Hou, Z.Q., Khin Zaw, Li, Y.G., 2007. Characteristics and genesis of Gangdese porphyry copper deposits in the southern Tibetan Plateau: preliminary geochemical and geochronological results. Ore Geol. Rev. 31, 205–223.

Qu, X.M., Hou, Z.Q., Zaw, K., Mo, X.X., Wenyi, X., Hongbo, X., 2009. A large-scale copper ore-forming event accompanying rapid uplift of the southern Tibetan Plateau: Evidence from zircon SHRIMP U-Pb dating and LA ICP-MS analysis. Ore Geol. Rev. 36, 52–64.

Richards, J.P., 2003. Tectono-magmatic precursors for porphyry Cu-(Mo-Au) deposit formation. Econ. Geol. 98(8), 1515–1533.

Richards, J.P., 2011. Magmatic to hydrothermal metal fluxes in convergent and collided margins. Ore Geol. Rev. 40(1), 1–26.

Roger, F., Arnaud, N., Gilder, S., Tapponnier, P., Jolivet, M., Brunel, M., Malavieille, J., Xu, Z., 2003. Geochronological and geochemical constraints on Mesozoic suturing in East Central Tibet. Tectonics 22 (4), 1037. doi:10.1029/2002TC001466.

Rui, Z.Y., Hou, Z.Q., Qu, X.M., Zhang, L.S., Wang, L.S., Liu, Y.L., 2003. Metallogenic epoch of Gangdese porphyry copper belt and uplift of Qinghai‐Tibetan Plateau. Mineral Deposit 22, 224–232 (in Chinese with English abstract).

Rui, Z.Y., Huang, C.K., Qi, G.M., Xu, J., Zhang, M.T., 1984. The Porphyry Cu(-Mo) Deposits in China. Geological Publishing House, Beijing. 350 pp. (in Chinese with English abstract).

Rui, Z.Y., Li, G.M., Zhang, L.S., Wang, L.S., 2004. The response of porphyry copper deposits to important geological events in Tibet. Earth Sci. Front., 11(1): 145–152 (in Chinese with English abstract).

Schärer, E., Xu, R.H., Allègre, C.J., 1984. U−Pb geochronology of the Gangdese (Trans-Himalaya) plutonism in the Lhasa-Xizang region, Tibet. Earth Planet. Sci. Lett. 69, 311–320

Schwab, M., Ratschbacher, L., Siebel, W., McWilliams, M., Minaev, V., Lutkov, V., Chen, F., Stanek, K., Nelson, B., Frisch, W., Wooden, J.L., 2004. Assembly of the Pamirs: age and origin of magmatic belts from the southern Tien Shan to the southern Pamirs and their relation to Tibet. Tectonics 23, C4002. doi: 10.1029/2003TC001583.

She, H.Q., Feng, C.Y., Zhang, D.Q., Pan, G.T., Li, G.M., 2005. Characteristics and metallogenic potential of skarn copper-lead-zinc polymetallic deposits in central eastern Gangdese. Mineral Deposits 25, 508–520 (in Chinese with English abstract).

Sillitoe, R.H., 2010. Porphyry copper systems. Econ. Geol. 105, 3–41.

Stein, H.J., Markey, R.J., Morgan, J.W., Hannah, J.L., Schersten, A., 2001. The remarkable Re-Os chronometer in molybdenite: how and why it works. Terra Nova 13(6), 479–486.

Su, X.L., Zhao, Y.L., Zhao, C., Zhang, X.M., Li, H.H., Liu, G.Y., Song, T.T., 2014. Prospecting thinking and model for the Ketinghaer porphyry copper molybdenum deposit in the East Kunlun Mountains. Geology in China 41(6), 2048–2062 (in Chinese with English abstract).

Sun, S.S., McDonough, W.F., 1989. Chemical and isotopic systematics of oceanic basalts: implication for the mantle composition and process. In: Saunder., A.D., Norry, M.J. (Eds.), Magmatism in the Ocean Basins. Geological Society of London Special Publication 42, 313–345.

Sun, X., Zheng, Y.Y., Wu, S., You, Z.M., Wu, X., Li, M., Zhou, T.C., Dong, J., 2013. Mineralization age and petrogenesis of associated intrusions in the Mingze-Chengba porphyry-skarn Mo-Cu deposit, Gangdese. Acta Petrol. Sin. 29(4) : 1392–1406 (in Chinese with English abstract).

Tang, R.L., Luo, H.S., 1995, The geology of Yulong porphyry copper (molybdenum) ore belt, Xizang (Tibet): Beijing, Geological Publishing House, 320. (in Chinese with English abstract)

Tang, J.X., Chen, Y.C., Wang, D.H., Wang, C.H., Xu, Y.P., Qu, W.J., Huang, W., Huang, Y., 2009a. Re-Os Dating of Molybdenite from the Sharang Porphyry Molybdenum Deposit in Gongbogyamda County , Tibet and Its

Geological Significance. Acta Geol. Sin. 83(5), 698–704 (in Chinese with English abstract).

Tang, J.X., Wang, C.H., Qu, W.J., Du, A.D., Ying, L.J., Gao, Y.M., 2009b. Re-Os isotopic dating of molybdenite from the Yulong porphyry copper-molybdenum deposit in Tibet and its metallogenic significance. Rock and Mineral Analysis 28, 215–218 (in Chinese with English abstract).

Tang, J.X., Wang, D.H., Wang, X.W., Zhong, K.H., Ying, L.J., Zheng, W.B., Li, F.J., Guo, N., Qin, Z.P., Yao, X.F., Li, L., Wang, Y., Tang, X.Q., 2010. Geological features and metallogenic model of the Jiama copper-polymetallic deposit in Tibet. Acta Geoscientica Sinica 31(4), 495–506 (in Chinese with English abstract).

Taylor, H.P., 1974. The application of oxygen and hydrogen isotope studies to problems of hydrothermal alteration and ore deposition. Econ. Geol. 69, 843–883.

Wan, D., Wang, K.Y., Li, W.C., Yin, G.H., Yu, H.J., Xue, S.R., Wei, L.M., 2012. Characteristics of fluid Inclusions of Relin Cu-Mo deposit in Northwestern Yunnan Province. J. Jilin Univ. (Earth Sci. Edit.) 42, 54–63 (in Chinese with English abstract).

Wang, L.L., 2007. The Characteristics of Qulong or-bearing Porphyries and their relation to Cu-Mo mineralization in the Gangdese belt, Tibet. Unpublished Ph.D. Thesis, Chinese University of Geosciences, Beijing, China, 97 pp (in Chinese with English abstract).

Wang, Z.H., 2004. Tectonic evolution of the western Kunlun orogenic belt, western China. J. Asian Earth Sci. 24, 153–161.

Wang, E., Wan, J., Liu, J., 2003. Late Cenozoic geological evolution of the foreland basin bordering the West Kunlun Range in Pulu area: constraints on timing of uplift of northern margin of the Tibetan Plateau. J. Geophys. Res.108, 2401. doi: 10.1029/2002JB001877.

Wang, L.L., Mo, X.X., Li, B., Dong, G.C., Zhao, Z.D., 2006. Geochronology and geochemistry of the ore-bearing porphyry in Qulong Cu(Mo) ore deposit, Tibet. Acta Petrol. Sin. 22(4), 1001–1008 (in Chinese with English

abstract).

Wang, Z.L., Yang, Z.M., Yang, Z.S., Tian, S.H., Liu, Y.C., Ma, Y.Q., Wang, G.R., Qu, W.J., 2008. Narigongma porphyry molybdenite copper deposit, northern extension of Yulong copper belt: evidence from the age of Re-Os isotope. Acta Petrol. Sin. 24(3), 503–510 (in Chinese with English abstract).

Wang, C.H., Tang, J.X., Chen, J.P., Hao, J.H., Gao, Y.M., Liu, Y.W., Fan, T., Zhang, Q.Z., Ying, L.J., Chen, Z.J., 2009. Chronological research of Yulong copper-molybdenum porphyry deposit. Acta Geol. Sin. 83, 1445–1455 (in Chinese with English abstract)

Wang, B.D., Xu, J.F., Chen, J.L., Zhang, X.G., Wang, L.Q., Xia, B.B., 2010. Petrogenesis and geochronology of the ore-bearing porphyritic rocks in Tangbula porphyry molybdenum-copper deposit in the eastern segment of the Gangdese metallogenic belt. Acta Petrol. Sin. 26(6), 1820–1832 (in Chinese with English abstract).

Wang, X.S., Bi, X.W., Leng, C.B., tang, Y.Y., Lan, J.B., Qi, Y.Q., Shen, N.P., 2011. LA-ICP-MS Zircon U-Pb dating of granite porphyry in the Hongshan Cu-polymetallic deposit, Zhongdian, Northwest Yunnan, China and its geological implication. Acta Mineralogica Sinica 31, 315–321 (in Chinese with English abstract).

Wang, B.Z., Luo, Z.H., Pan, T., Song, T.Z., Xiao, P.X., Zhang, Z.Q., 2012a. Petrotectonic assemblages and LA-ICP-MS zircon U-Pb age of Early Paleozoic volcanic rocks in Qimantag area, Tibetan Plateau. Geological Bulletin of China 31, 860–874 (in Chinese with English abstract).

Wang, L.Q., Chen, Y.C., Tang, J.X., Lv, P.R., Luo, M.C., Wang, H., Chen, W., Leng, Q.F., 2012b. LA-ICP-MS Zircon U-Pb Dating of Intermediate-Acidic Intrusive Rocks and Molybdenite Re-Os Dating from the Bangpu Mo (Cu) Deposit, Tibet and its Geological Implication. Acta Geol. Sin. (English Edition), 86(5): 1225–1240.

Wang, Z.H., Liu, Y.L., Liu, H.F., Guo, L.S., Zhang, J.S., Xu, K.F., 2012c. Geochronology and geochemistry of the Bangpu Mo-Cu porphyry ore deposit, Tibet. Ore Geol. Rev. 46, 95–105.

Wang, F.C., Chen, J., Xie, Z.Y., Li, S.P., Tan, S.X., Zhang, Y.B., Wang, T., 2013. Geological features and Re-Os

isotopic dating of the Lalingzaohuo molybdenum polymetallic deposit in East Kunlun. Geology in China 40(4), 1209–1217 (in Chinese with English abstract).

Wang, P., Chen, Y.J., Fu, B., Yang, Y.F., Mi, M., Li, Z.L., 2014a. Fluid inclusion and H-O isotope geochemistry of the Yaochong porphyry Mo deposit in Dabie Shan, China: A case study of porphyry systems in continental collision orogens. Int. J. Earth Sci. 103, 777–797.

Wang, X.X., Zheng, R.C., Yan, G.Q., Huang, Y., 2014b. Re-Os dating of chalcopyrite of Nuri Cu-Mo-W deposit and its significance. Metal Mine 460, 126–129 (in Chinese with English abstract).

Wang, X.S., Bi, X.W., Leng, C.B., Zhong, H., Tang, H.F., Chen, Y.W., Yin, G.H., Huang, D.Z., Zhou, M.F., 2014c. Geochronology and geochemistry of Late Cretaceous igneous intrusions and Mo–Cu–(W) mineralization in the southern Yidun Arc, SW China: Implications for metallogenesis and geodynamic setting. Ore Geol. Rev. 61, 73–95.

Wang, X.S., Hu, R.Z., Bi, X.W., Leng, C.B., Pan, L.C., 2014d. Petrogenesis of Late Cretaceous I-type granites in the southern Yidun Terrane: New constraints on the Late Mesozoic tectonic evolution of the eastern Tibetan Plateau. Lithos 208–209, 202–219.

Wang, X.S., Bi, X.W., Hu, R.Z., Leng, C.B., Yu, H.J., Yin, G.H., 2015. S-Pb isotopic geochemistry of Xiuwacu magmatic hydrothermal Mo-W deposit in Zhongdian area, NW Yunnan: Constrains on the sources of metal. Acta Petrologica Sinica 31(11) , 3171–3188 (in Chinese with English abstract).

Wang, J.G., Wu, F.Y., Garzanti, E., Hu, X.M., Ji, W.Q., Liu, Z.C., Liu, X.C., 2016. Upper Triassic turbidites of the northern Tethyan Himalaya (Langjiexue Group): The terminal of a sediment-routing system sourced in the Gondwanide Orogen. Gondwana Research 34, 84–98.

Wen, Q., Duo, J., Wen, C.Q., Zhang, X.Q., Zhou, X., Huo, Y., Fei, G.C., 2011. Dating of monzonitic granite porphyry in the Bangpu Mo-Cu deposit, Tibet. J. Minera. L. Petrol. 31(2), 48–53 (in Chinese with English

abstract).

Woodhead, J.D., Eggins, S.M., Johnson, R.W., 1998. Magma genesis in the New Britain island arc: further insights into melting and mass transfer processes. J. Petrol. 39(9), 1641–1668.

Wu, J., Liang, H.Y., Mo, J.H., Zhang, Y.Q., Hu, G.Q., 2011. Petrochemistry and zircon LA-ICP-MS U-Pb age of the Mangzong porphyry associated with Cu-Mo mineralization in the Yulong Ore Bel. Geotectonica et Metallogenia 35(2), 300–306 (in Chinese with English abstract).

Wu, W.Z., Xia, B., Zhang, Y.Q., Dong, B.H., Xia, Z.X., 2013. Geochemical characteristics and metallogenic mechanism of the porphyry Cu-Mo deposits in the Yulong Ore Belt, Eastern Tibet: A case study of the Yulong and Duoxiasongduo Porphyries. Geotectonica et Metallogenia 37(3), 440–454 (in Chinese with English abstract).

Wu, Y.S., Wang, P., Yang, Y.F., Xiang, N., Li, N., Zhou, K.F., 2014. Ore geology and fluid inclusion study of the Donggebi giant porphyry Mo deposit, Eastern Tianshan, NW China. Geol. J., doi: 10.1002/gj.2574.

Wu, C.D., Zheng, Y.C., Zhang, S., Fu, Q., Xu, P.Y., 2015. Ar-Ar age of biotite from the Nuri Cu-W-Mo deposit in Tibet, and its geodynamic significance. Acta Geol. Sin. 89(9), 1673–1682 (in Chinese with English abstract).

Xia, B.B., Xia, B., Wang, B.D., Li, J.F., Zhang, X.G., Wang, Y.C., 2010. Formation Time of the Tangbula Porphyry Mo-Cu Deposit: Evidence from SHRIMP Zircon U-Pb Dating of Tangbula Ore-Bearing Porphyries. Geotectonica et Metallogenia 34, 291–297 (in Chinese with English abstract).

Xia, R., Wang, C.M., Deng, J., Carranza, E.J.M., Li, W.L., Qing, M., 2014. Crustal thickening prior to 220 Ma in the East Kunlun Orogenic Belt: insights from the Late Triassic granitoids in the Xiao–Nuomuhong pluton. J. Asian Earth Sci. 93, 193–210.

Xiang, N., Yang, Y.F., Wu, Y.S., Zhou, K.F., 2013. Fluid inclusion study of the Baishan porphyry Mo deposit in the eastern Tianshan ore field, Xinjiang Province. Acta Petrol. Sin. 29, 146–158 (in Chinese with English abstract)

Xiao, W.J., Windley, B.F., Fang, A.M., Zhou, H., Yuan, C., Wang, Z.H., Hao, J., Hou, Q.L., Li, J.L., 2001. Paleozoic-Early Mesozoic accretionary tectonics of the Western Kunlun Range, NW China. Gondwana Res. 4, 826–827.

Xiao, B., Qin, K.Z., Li, G.M., Li, J.X., Xia, D.X., Chen, L., and Zhang, J.X., 2009. S-rich, highly-oxidized ore-bearing magma in the Qulong giant porphyry type Cu-Mo deposit in southern Tibet–Evidence from magmatogenic anhydrite. Acta Geol. Sin. 83, 1860–1868 (in Chinese with English abstract).

Xiao, B., Qin, K.Z., Li, G.M., Li, J.X., Xia, D.X., Chen, L., and Zhao, J.X., 2012, Highly Oxidized Magma and Fluid Evolution of Miocene Qulong Giant Porphyry Cu-Mo Deposit, Southern Tibet, China. Res. Geol. 62, 4–18.

Xiong, F.H., Ma, C.Q., Jiang, H.A., Liu, B., Zhang, J.Y., Zhou, Q., 2013. Petrogenetic and tectonic significance of Permian calc-alkaline lamprophyres, East Kunlun Orogenic Belt, Northern Qinghai–Tibet Plateau. Int. Geol. Rev. 55, 1817–1834.

Xu, Q.L., 2014. Study on metallogenesis of porphyry deposits in Eastern Kunlun orogenic belt, Qinghai Province. Ph.D. Thesis, Jilin University, Jilin, China, 194 pp (in Chinese with English abstract).

Xu, X.W., Cai, X.P., Qu, W.J., Song, B.C., Qin, K.Z., Zhang, B.L., 2006. Later Cretaceous granitic porphyritic Cu-Mo mineralization system in the Hongshan area, Northwestern Yunnan and its significances for tectonics. Acta Geolo. Sin. 80(9), 1422–1433 (in Chinese with English abstract).

Xu, Y., Bi, X.W., Hu, R.Z., Chen, Y.W., Liu, H.Q., Xu, L.L., 2016. Geochronology and geochemistry of Eocene potassic felsic intrusions in the Nangqian basin, eastern Tibet: Tectonic and metallogenic implications. Lithos 246–247, 212–227.

Yang, Z.M., 2008. The Qulong giant porphyry copper deposit in Tibet: magmatism and mineralization. Unpublished Ph.D. Thesis, Chinese Academy of Geological Sciences, Beijing, China, 145 pp (in Chinese with English abstract).

Yang, Z.M., Hou, Z.Q., 2009. Genesis of giant porphyry Cu deposit at Qulong, Tibet: constraints from fluid inclusions and H-O isotopes. Acta Geol. Sin. 83(2), 1838–1859 (in Chinese with English abstract).

Yang, J.S., Robinson, P.T., Jiang, C.F., Xu, Z.Q., 1996. Ophiolites of the Kunlun Mountains, China and their tectonic implications. Tectonophysics 258, 215–231.

Yang, Z.M., Xie, Y.L., Li, G.M., Xu, J.H., Wang, B.H., 2005. Study of fluid inclusions from Tinggong porphyry copper deposit in Gangdese belt, Tibet. Mineral deposits, 24(6): 584–594 (in Chinese with English abstract).

Yang, Z.M., Hou, Z.Q., Yang, Z.S., Wang, S.X., Wang, G.R., Tian, S.H., Wen, D.Y., Wang, Z.L., Liu, Y.C., 2008. Genesis of porphyries and tectonic controls on the Narigongma porphyry Mo(-Cu) deposit, southern Qinghai. Acta Petrol. Sin. 24(3), 489–502 (in Chinese with English abstract).

Yang, Z.M., Hou, Z.Q., White, N.C., Chang, Z.S., Li, Z.Q., Song, Y., 2009a. Geology of the postcollisional porphyry copper-molybdenum deposit at Qulong, Tibet. Ore Geol. Rev. 36, 133–159 (this issue).

Yang, Y.F., Li, N., Ni, Z.Y., 2009c. Fluid inclusion study of the Jinduicheng porphyry Mo deposit, Hua County, Shaanxi Province. Acta Petrol. Sin. 25, 2983–2994 (in Chinese with English abstract)

Yang, J.S., Shi, R.D., Wu, C.L., Wang, X.B., Robinson, P., 2009b. Dur'ngoi ophiolite in East Kunlun, Northeast Tibetan plateau: evidence for paleo-Tethyan suture in Northwest China. J. Earth Sci. 20, 303–331.

Yang, Y.F., Li, N., Chen, Y.J., 2012. Fluid inclusion study of the Nannihu giant porphyry Mo-W deposit, Henan Province, China: Implications for the nature of porphyry ore-fluid systems formed in a continental collision setting. Ore Geol. Rev. 46, 83–94.

Yang Y., Chen, Y.J., Zhang, J., Zhang, C., 2013a. Ore geology, fluid inclusions and four-stage hydrothermal mineralization of the Shangfanggou giant Mo-Fe deposit in Eastern Qinling, central China. Ore Geol. Rev. 55, 146–161.

Yang, Y.F., Chen, Y.J., Li, N., Mi, M., Xu, Y.L., Li, F.L., Wan, S.Q., 2013b. Fluid inclusion and isotope geochemistry

of the Qian'echong giant porphyry Mo deposit, Dabie Shan, China: A case of NaCl-poor, CO2-rich fluid systems. J. Geochem. Explor. 124, 1–13.

Yang, Y.Q., Li, B.L., Xu, Q.L., Zhang, B.S., 2013c. Zircon U-Pb ages and its geological significance of the monzonitic granite in the Aikengdelesite, Eastern Kunlun. Northwestern Geology 46(1), 56–62 (in Chinese with English abstract).

Yang, Z.M., Hou, Z.Q., Xu, J.F., Bian, X.F., Wang, G.R., Yang, Z.S., Tian, S.H., Liu, Y.C., Wang, Z.L., 2014a. Geology and origin of the post-collisional Narigongma porphyry Cu-Mo deposit, southern Qinghai, Tibet. Gondwana Res. 26, 536–556.

Yang, Y.Q., Li, B.L., Ma, Y.H., Zhu, M.X., 2014b. Fluid inclusion study on the Aikengdelesite Mo(Cu) ore deposit, Eastern Kunlun. Northwestern Geology 47(2), 109–118 (in Chinese with English abstract).

Yang, Y.F., Chen, Y.J., Pirajno, F., Li, N., 2015. Evolution of ore fluid in the Donggou giant porphyry Mo system, East Qinling, China. Ore Geol. Rev. 65, 148–164.

Yang, Y.F., Wang, P., Chen, Y.J., Li, Y., 2016a. Geochronology and geochemistry of the Tianmugou Mo deposit, Dabie Shan, eastern China: Implications for ore genesis and tectonic setting. Ore Geol. Rev. this issue.

Yang, L.Q., Deng, J., Dilek, Y., Meng, J.Y., Gao, X., Santosh, M., Wang, D., Yan, H., 2016b. Melt source and evolution of I-type granitoids in the SE Tibetan Plateau: Late Cretaceous magmatism and mineralization driven by collision-induced transtensional tectonics. Lithos 245, 258–273.

Yang, L.Q., Deng, J., Gao, X., He, W.Y., Meng, J.Y., Santosh, M., Yu, H.J., Yang, Z., Wang, D., 2016c. Timing of formation and origin of the Tongchanggou porphyry-skarn deposit: Implications for Late Cretaceous Mo-Cu metallogenesis in the southern Yidun Terrane, SE Tibetan Plateau. Ore Geol. Rev., http://554.rm.cglhub.com/10.1016/j.oregeorev.2016.03.015.

Yin, A., Nie, S.Y., 1996. A Phanerozoic palinspastic reconstruction of China and it s neighboring regions. Yin, A.,

Harrison, T.M., The Tectonic Evolution of Asia. Cambridge: Cambridge University Press, 442-485 .

Yin, A., Harrison, T.M., 2000. Geologic evolution of the Himalayan-Tibetan orogen. Annual Review of Earth and Planetary Sciences 28, 211–280.

Yin, A., Harrison, T.M., Ryerson, F.J., Chen, W.J., Kidd, W.S.F., Copeland, P., 1994. Tertiary structural evolution of the Gangdese thrust system, southeastern Tibet. J. Geophys. Res. 99, 18175–18201.

Yin, A., Rumelhart, P.E., Butler, R., Cowgill, E., Harrison, T.M., Foster, D.A., Ingersoll, R.V., Qing, Z., Xian-Qiang, Z., Xiao-Feng, W., Hanson, A., Raza, A., 2002. Tectonic history of the Altyn Tagh fault system in northern Tibet inferred from Cenozoic sedimentation. Geol. Soc. Am. Bull.114, 1257–1295.

Yin, J., Xu, J., Liu, C., Li, H., 1988. The Tibetan plateau: regional stratigraphic context and previous work. Philos. Trans. R. Soc. Lond., A 327, 5–52.

Ying, L.J., Wang, D.H., Tang, J.X., Chang, Z.S., Qu, W.J., Zheng, W.B., Wang, H., 2010. Re-Os dating of molybdenite from the Jiama copper polymetallic deposit in Tibet and its metallogenic significance. Acta Geol. Sin. 84(8), 1165–1174 (in Chinese with English abstract).

Ying, L.J., Tang, J.X., Wang, D.H., Zheng, W.B., Qin, Z.P., Zhang, L., 2011. Zircon SHRIMP U-Pb dating of porphyry vein from the Jiama copper polymetallic deposit in Tibet and its significance. Acta Petrol. Sin. 27(7), 2095–2102 (in Chinese with English abstract).

Ying, L.J., Wang, C.H., Tang, J.X., Wang, D.H., Qu, W.J., Li, C., 2014. Re-Os systematics of sulfides (chalcopyrite, bornite, pyrite and pyrrhotite) from the Jiama Cu-Mo deposit of Tibet, China. J Asian Earth Sci 79, 497–506.

Zaw, K., Peters, S.G., Cromie, P., Burrett, C, Hou, Z.Q., 2007. Nature, deposit types and metallogenic relations of South China. Ore Geol. Rev. 31, 3–47.

Zhang, Y.Q., Xie, Y.W., Qiu, H.N., Li, X.H., Zhong, S.L., 1998. Shoshonitic series: Sr, Nd, and Pb isotopic compositions of ore-bearing porphyry for Yulong copper ore belt in the eastern Tibet. Scientia Geologica Sinica

33(3), 359–366 (in Chinese with English abstract).

Zhang, S., Zheng, Y.C., Huang, K.X., Li, W., Sun, Q.Z., Li Q.Y., Fu Q., Liang, W., 2012. Re-Os dating of molybdenite from Nuri Cu-W-Mo deposit and its geological significance. Mineral Deposits 31(2), 337–346 (in Chinese with English abstract).

Zhao, J.X., Qin, K.Z., Li, G.M., Li, J.X., Xiao, B., Chen, L., 2012. Geochemistry and petrogenesis of granitoids at Sharang Eocene porphyry Mo deposit in the main-stage of India-Asia continental collision, Northern Gangdese, Tibet. Res. Geol. 62(1), 84-98.

Zhao, J.X., Qin, K.Z., Li, G.M., Li, J.X., Xiao, B., Chen, L., Yang Y.C., Li, C., Liu, Y.S., 2014. Collision-related genesis of the Sharang porphyry molybdenum deposit, Tibet: Evidence from zircon U−Pb ages, Re-Os ages and Lu-Hf isotopes. Ore Geol. Rev. 56, 312–326.

Zhao, X.Y., Yang, Z.S., Zheng, Y.C., Liu, Y.C., Tian, S.H., Fu, Q., 2015a. Geology and genesis of the post-collisional porphyry-skarn deposit at Bangpu, Tibet. Ore Geol. Rev. 70 (2015) 486–509.

Zhao, X.Y., Yang, Z.S., Liu, Y.C., Pei, Y., 2015b. Sr-Nd-Pb-Hf isotope compositions of porphyry monzogranite and Rb-Sr isochron age of sphalerite-pyrite at the Bangpu porphyry-skarn deposit. Acta Geol. Sin. 89(3), 522–533 (in Chinese with English abstract).

Zheng, Z., Deng, X.H., Chen, H.J., Yue, S.W., Dong, L.H., Qu, X., Chen, Y.J., 2016. Fluid sources and metallogenesis in the Baiganhu W–Sn deposit, East Kunlun, NW China: Insights from chemical and boron isotopic compositions of tourmaline. Ore Geol. Rev., http://dx.doi.org/10.1016/j.oregeorev.2015.09.006.

Zhong, J., Chen, Y.J., Pirajno, F., 2016. Geology, geochemistry and tectonic settings of the molybdenum deposits in South China: A review. Ore Geol. Rev., http://554.rm.cglhub.com/10.1016/j.oregeorev.2016.04. 012 .

Zhou, X., Wen, C.Q., Wen, Q., Wu, P.Y., Cao, S.Y., Fei, G.C., Huo, Y., Zhou, Yu., 2010. Zircon U-Pb SHRIMP dating of the monzonite granite-porphyry from the Bangpu large porphyry molybdenum-copper deposits ,Tibet ,

and its geological significance. Bull. Mineral. Petrol. Geochem. 29, 373–379 (in Chinese with English abstract).

Zhou, X., Wen, C.Q., Wen, Q., Fei, G.C., Cao, S.Y., Zhou, Y., Wu, P.Y., 2011b. Laser Microprobe 40Ar/39Ar dating on vein quartz containing Mo and Cu in the Bangpu porphyry-type Mo-Cu polymetallic deposit, Tibet. J. Minera. L. Petrol. 31(1), 43–48 (in Chinese with English abstract).

Zhou, Y., Wang, X.W., Tang, J.X., Qin, Z.P., Peng, H.J., Li, A.G., Yang, K, Wang, H., Li, J., Zhang, J.C., 2011a. Origin and evolution of ore-forming fluids from Jiama copper polymetallic deposit in Tibet. Mineral Deposits 30(2), 231–248 (in Chinese with English abstract).

Zhou, X., Wen, C.Q., Zhang, Y., Zhou, Y., Fei, G.C., Zhang, X.Q., 2013. Re-Os dating of molybdenite from the Bangpu polymetallic deposit of Tibet, and its geological significance. J. Minera. L. Petrol. 31(2), 48–53 (in Chinese with English abstract).

Zu, B., Xue, C.J., Zhao, Y., Qu, W.J., Li, C., Symons, D.T.A., Du, A.D., 2015. Late Cretaceous metallogeny in the Zhongdian area: Constraints from Re–Os dating of molybdenite and pyrrhotite from the Hongshan Cu deposit, Yunnan, China. Ore Geol. Rev. 64, 1–12.

Zu, B., Xue, C.J., Chi, G.X., Zhao, X.B., Li, C., Zaho, Y., Yalikun, Y., Zhang, G.Z., Zhao, Y., 2016. Geology, geochronology and geochemistry of granitic intrusions and the related ores at the Hongshan Cu-polymetallic deposit: Insights into the Late Cretaceous post-collisional porphyry-related mineralization systems in the southern Yidun arc, SW China. Ore Geol. Rev. 77, 25–42.

Figure captions

Fig. 1. Simplified geologic map of the Tibetan Plateau and its surrounding region, showing the distribution of major Mo deposits (modified after Qin, 2012). Abbrev: MBT, Main Boundary Thrust; MCT, Main Central Thrust; LHM, Lesser Himalayan Metasedimentary series; HHM, Higher Himalayan Metasedimentary series; STDS, South Tibet Detachment System; THS, Tethyan Himalayan Sequences; IYS, Indus–Yarlung suture; BNS, Bangong–Nujiang suture; JS, Jinshajiang suture; GLS, Ganzi–Litang suture; AKMS, Ayimaqin–Kunlun–Mutztagh suture.

Fig. 2. Compilation of isotopic ages of the major Mo deposits and causative magmatism in SW China.

Fig. 3. (a) Simplified geologic map and (b) cross-section A-A' of the Qulong porphyry Cu-Mo deposit (modified after Yang et al., 2008, 2009a).

Fig. 4. (a) Simplified geological map and (b) cross-section A-A' of the Sharang porphyry Mo deposit (modified after Zhao et al., 2014).

Fig. 5. (a) Simplified geological map and (b) cross-section A-A' of the Narigongma porphyry Mo-Cu deposit (modified after Yang et al., 2014a).

Fig. 6. (a) Simplified geological map and (b) cross-section A-A' of the Yulong porphyry Cu-Mo deposit (modified after Hou et al., 2007b).

Fig. 7. (a) Simplified geological map and (b) cross-section A-A' of the Tongchanggou porphyry Cu-Mo deposit (modified after Yang et al., 2016c).

Fig. 8. Simplified geological map of the Lalingzaohuo porphyry Mo deposit (modified after Wang et al., 2013).

Fig. 9. Petrochemical discriminations of the ore-related intrusions for the major Mo deposits in SW China.

Fig. 10. (A, C, E, G) Chondrite-normalized REE patterns and (B, D, F, H) primitive mantle-normalized trace element patterns of the ore-related intrusions for the major Mo deposits in SW China (chondrite and primitive mantle normalization values are from Sun and McDonough, 1989).

Fig. 11. (A) Correlative diagrams of $^{207}Pb/^{204}Pb$ vs. $^{206}Pb/^{204}Pb$ and (B) $^{208}Pb/^{204}Pb$ vs. $^{206}Pb/^{204}Pb$ for the ore-associated intrusions from the major Mo deposits in SW China.

Fig. 12. δD–$\delta^{18}O$ systematics for the major Mo deposits in SW China (base map after Taylor, 1974).

Fig. 13. Compilation of sulfur isotope compositions of sulfides from the major Mo deposits in SW China.

Fig. 14. Molybdenite Re-Os ages vs. Re diagram for the major Mo deposits in SW China.

Tables

Table 1. List of major Mo deposits in SW China.

Deposit type: P, porphyry type; S, skarn type; PS, porphyry-skarn type; QV, quartz vein type.
Texture: Diss, disseminated; Sw, stockwork; Br, breccia; V, veined.
Ore and alteration mineral abbreviations: Act, actinolite; An, anhydrite; Asp, arsenopyrite; Bi, biotite; Bo, Bornite; Cc, calcite; Chl, chlorite; Cp, chalcopyrite; Di, diopside; Do, dolomite; Ep, epidote; Fl, fluorite; Ga, galena; Gr, garnet; Kao, kaolinite; Kf, K-feldspar; Mb, molybdenite; Mt, magnetite; Py, pyrite; Pyr, pyrrhotite ; Qz, quartz; Sch, scheelite; Ser, sericite; Sph, sphalerite; Sb, stibnite; Wol, wollastonite

Table 2. Isotopic ages of the major Mo deposits in SW China.

Table 3. Whole-rock Sr-Nd-Pb isotopic compositions of the ore-related granites for the major Mo deposits in SW China.

Table 4. Fluid inclusion types and microthermometric results of several Mo deposits in SW China.

FIs types: WV-vapor-rich H_2O-NaCl solution; WL-liquid-rich H_2O-NaCl solution; S-daughter mineral-bearing FIs; C-carbonic-aqueous FIs.

Table 5. H-O isotopic compositions of the major Mo deposits in SW China.

Table 6. $\delta^{34}S$ values of sulfides from the major Mo deposits in SW China.

Table 7. Lead-isotopic compositions of sulfides from the major Mo deposits in SW China.

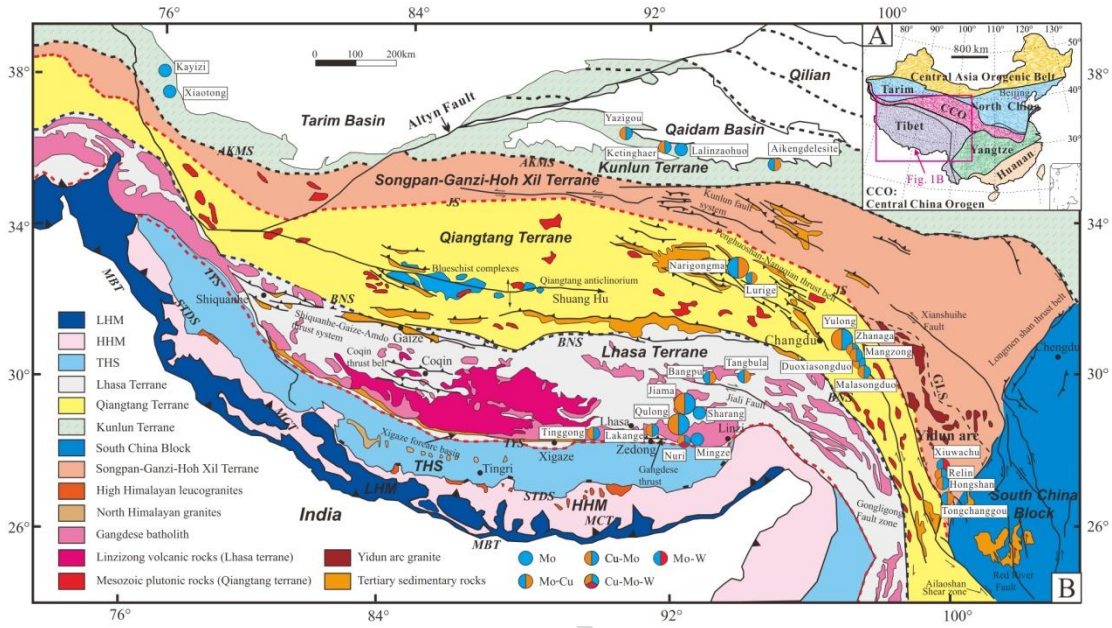

Fig. 1

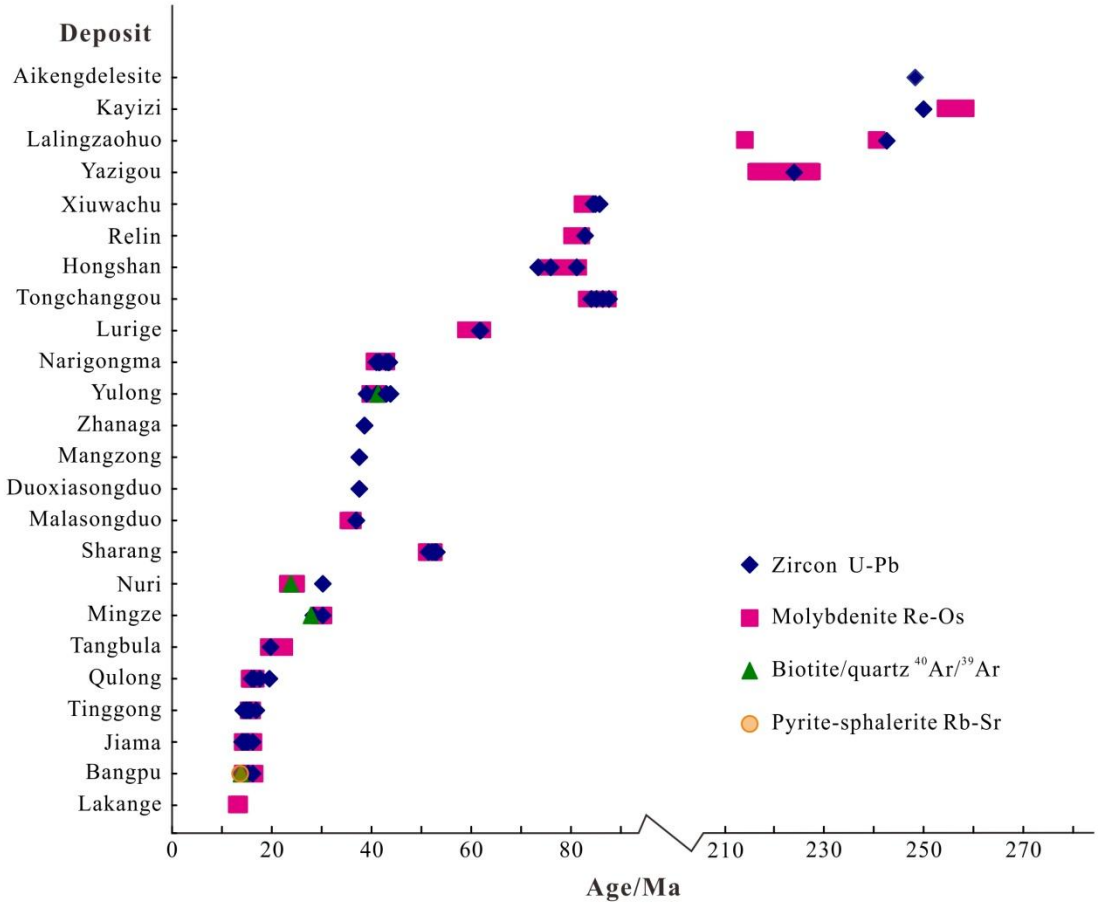

Fig. 2

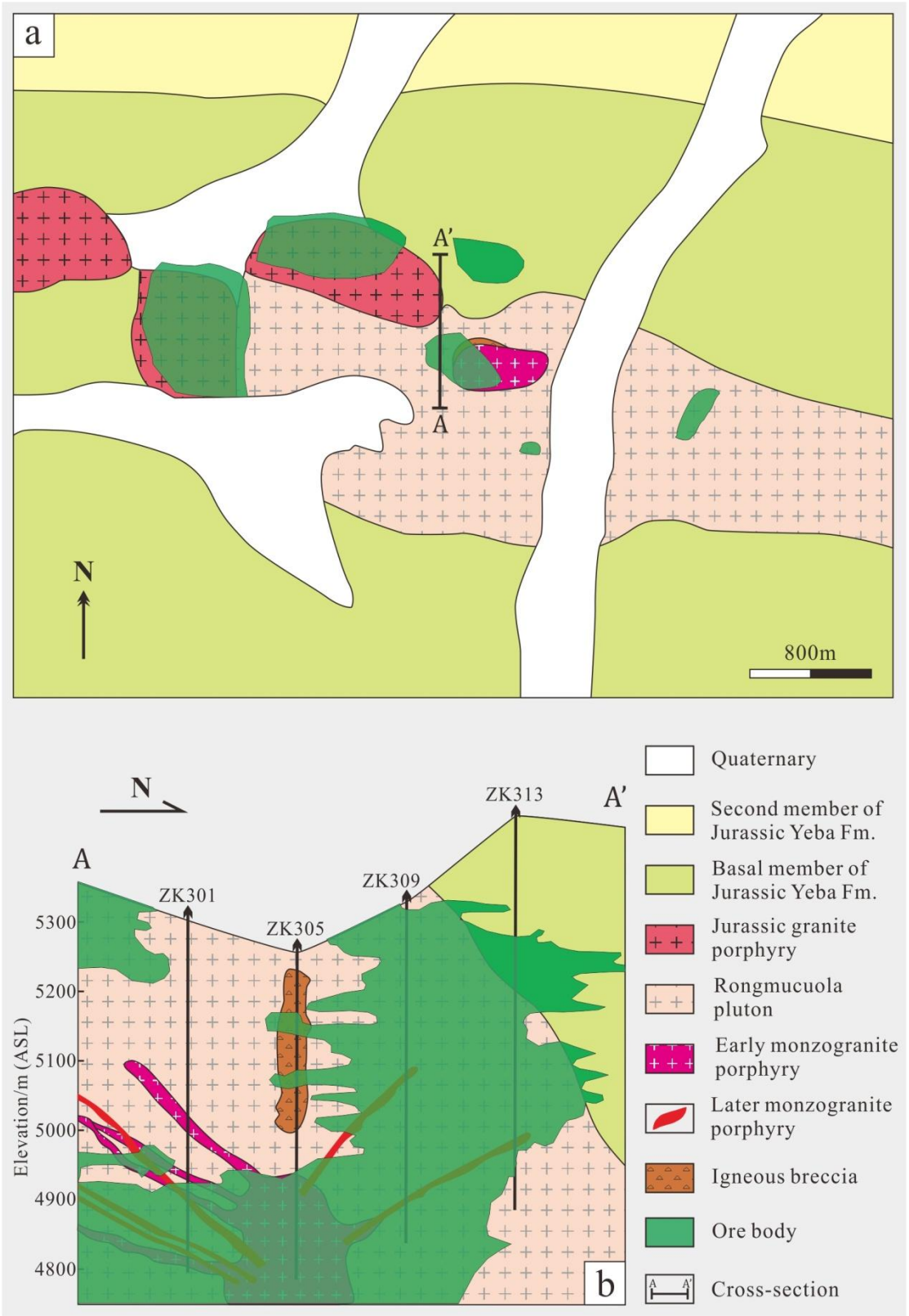

Fig. 3

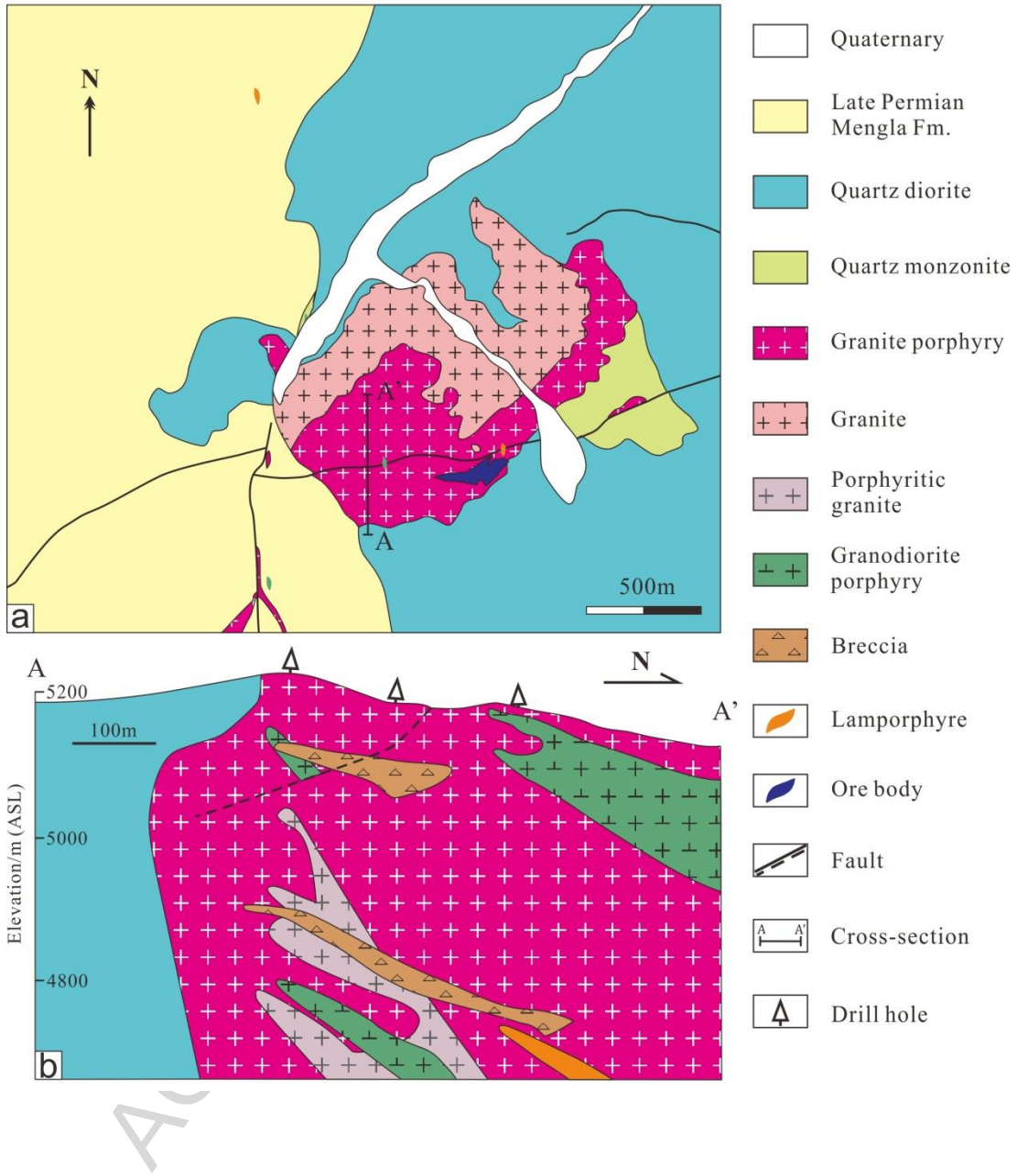

Fig. 4

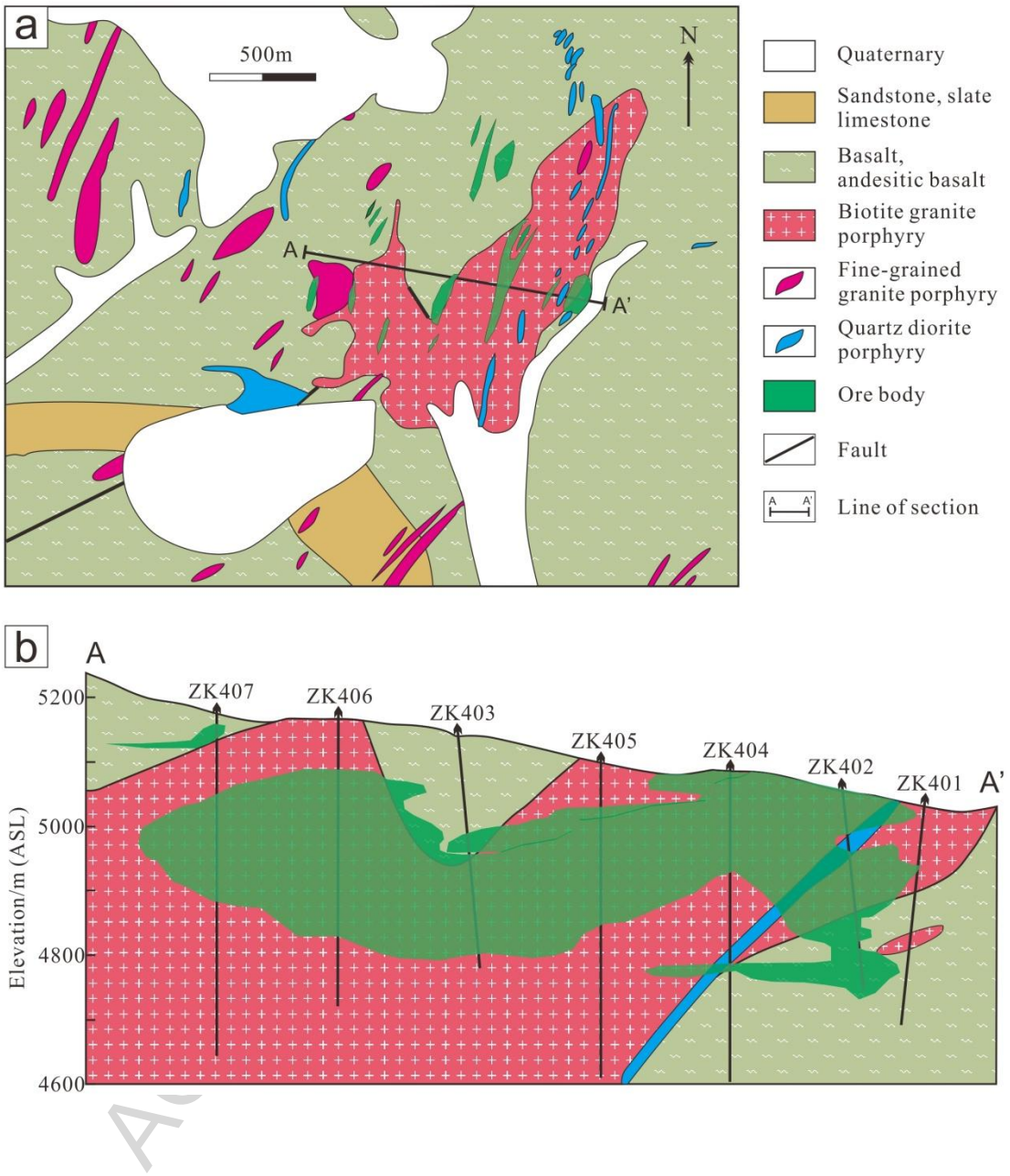

Fig. 5

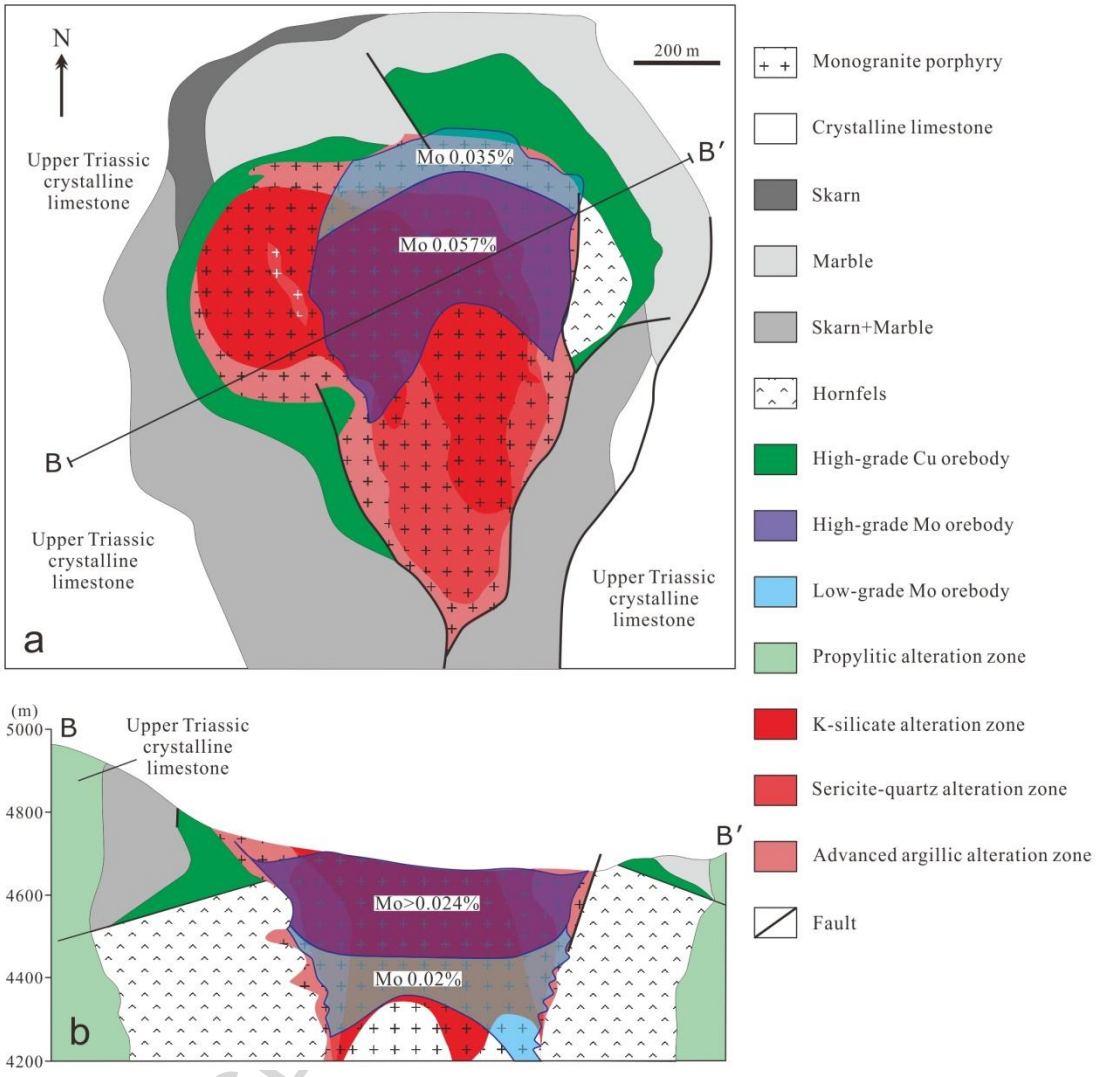

Fig. 6

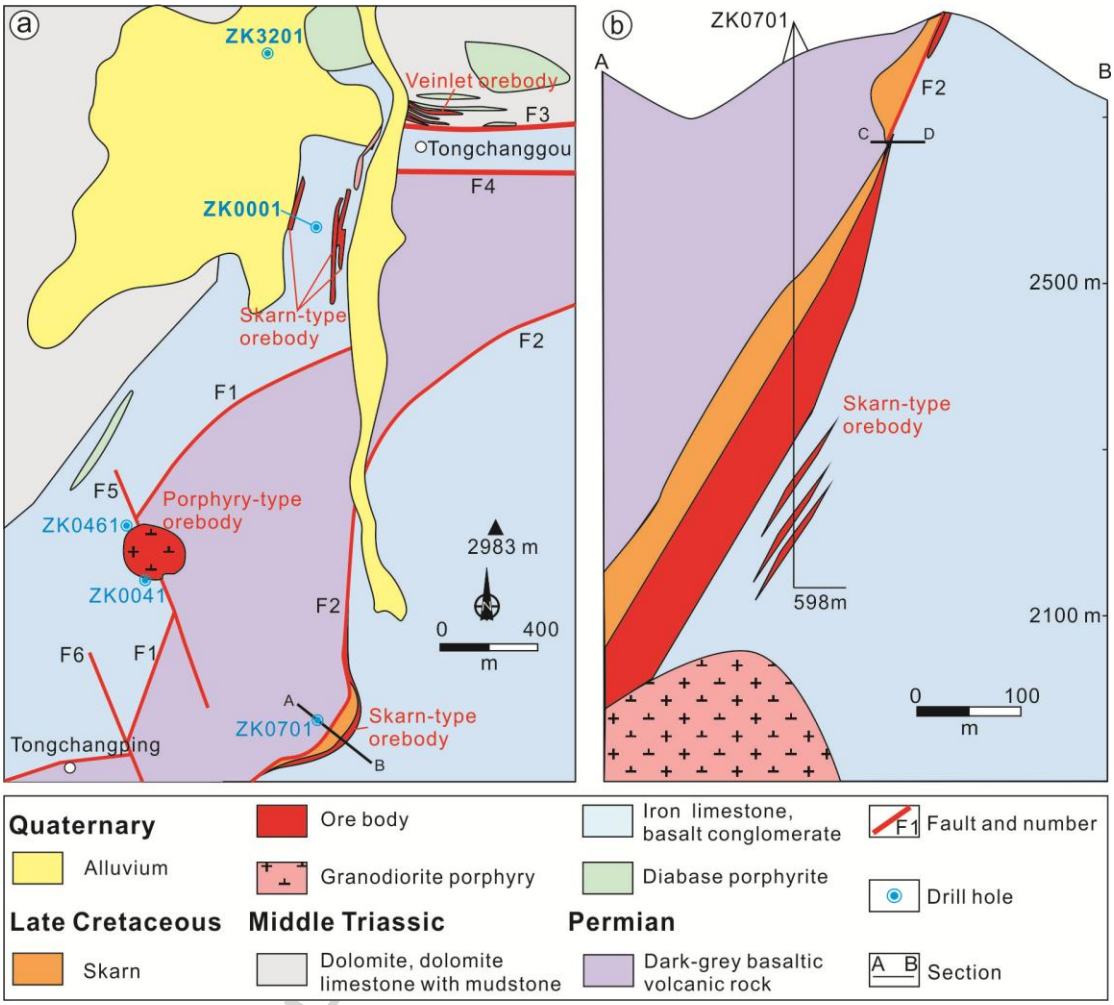

Fig. 7

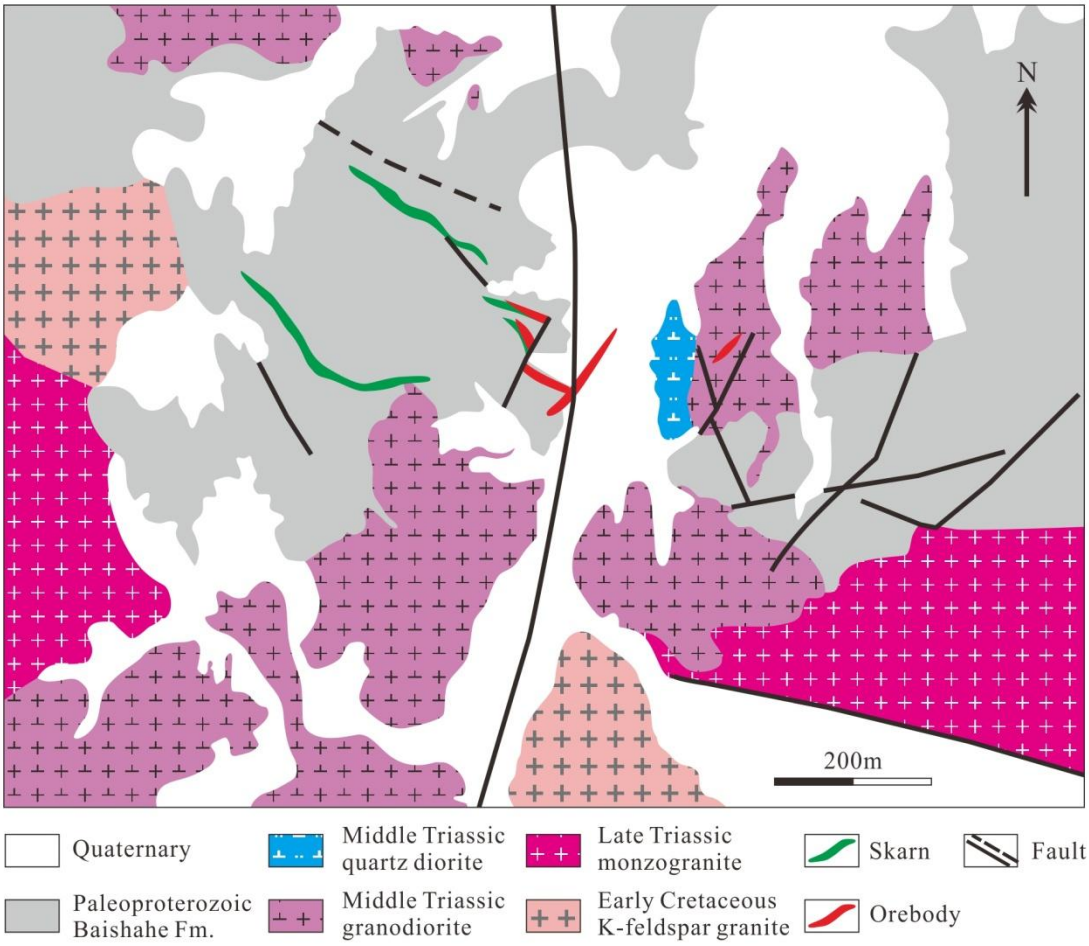

Fig. 8

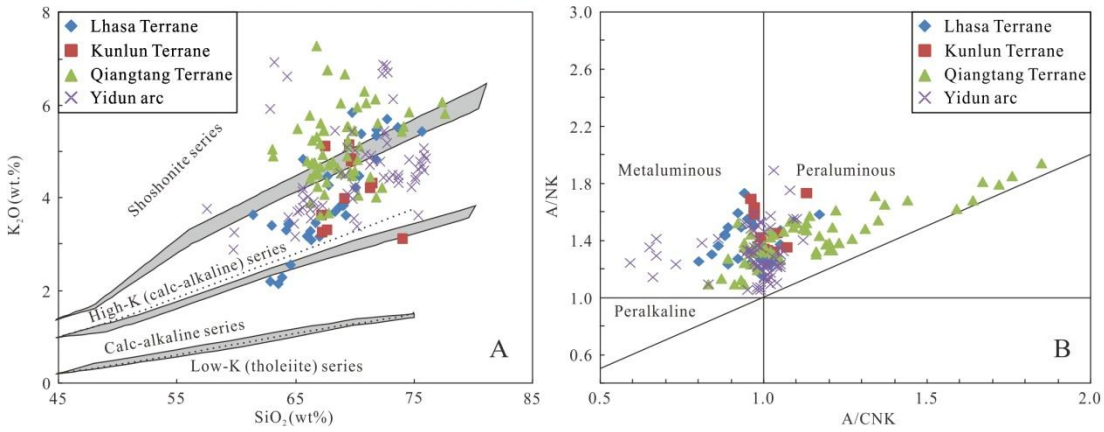

Fig. 9

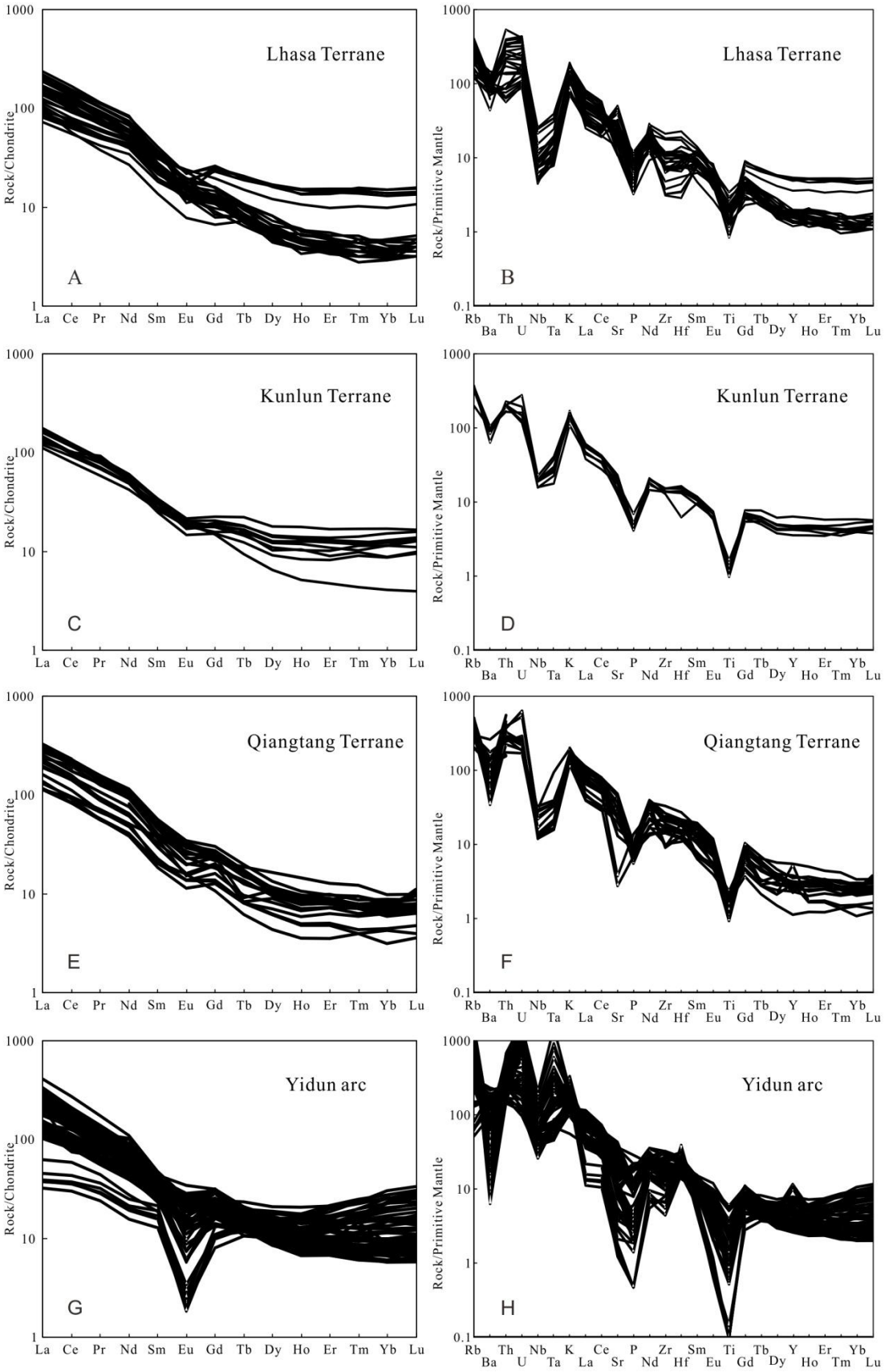

Fig. 10

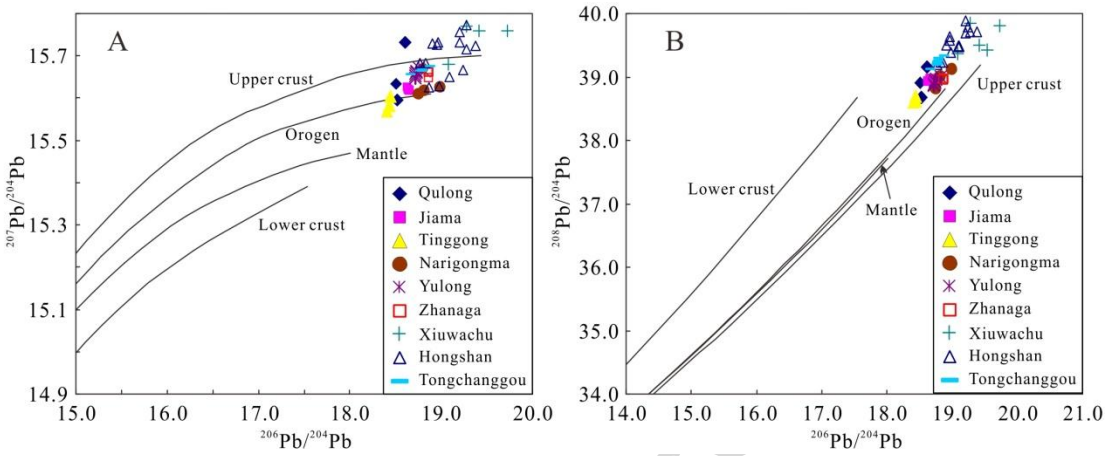

Fig. 11

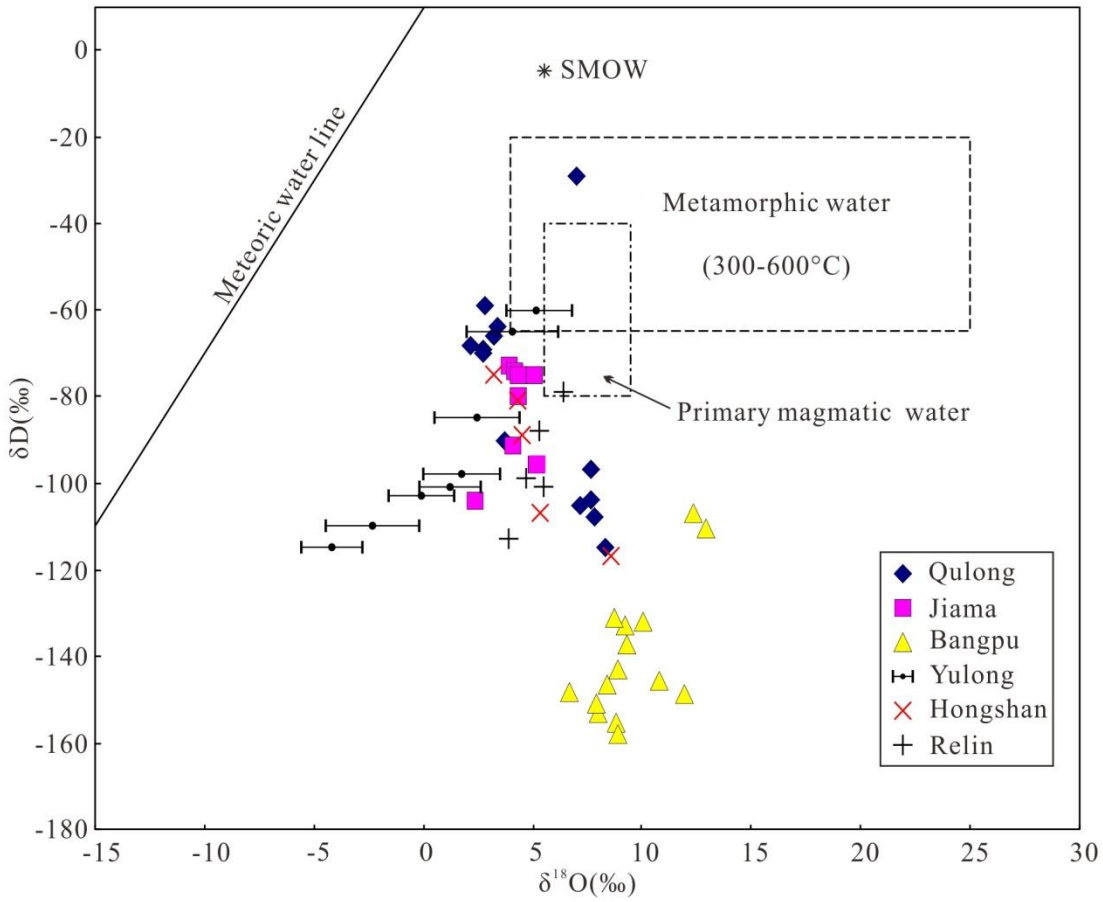

Fig. 12

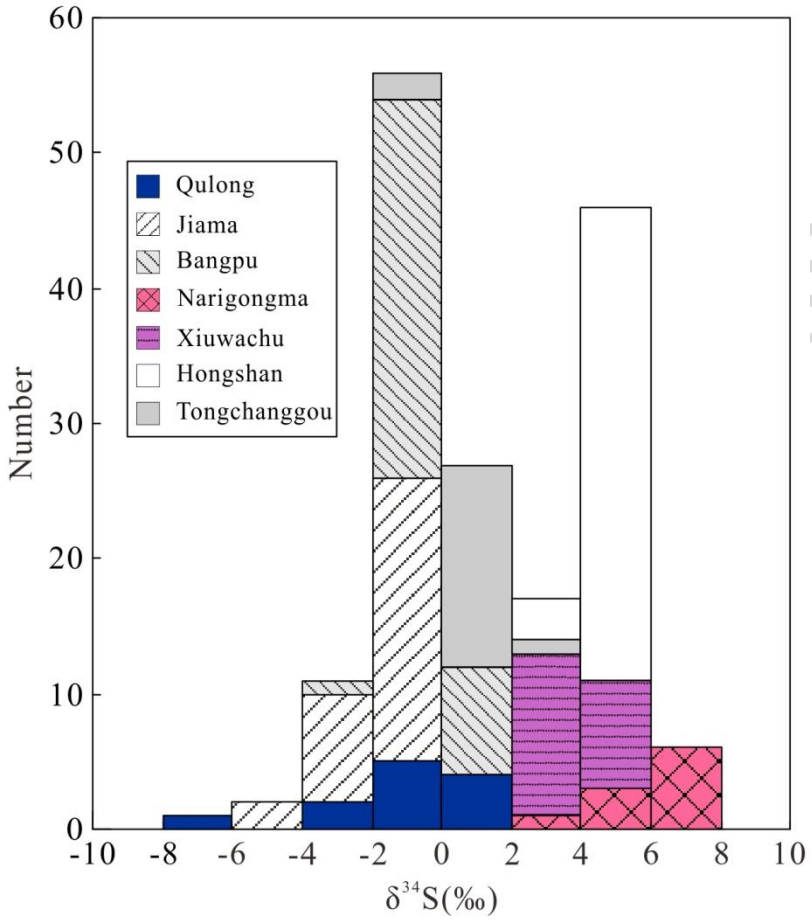

Fig. 13

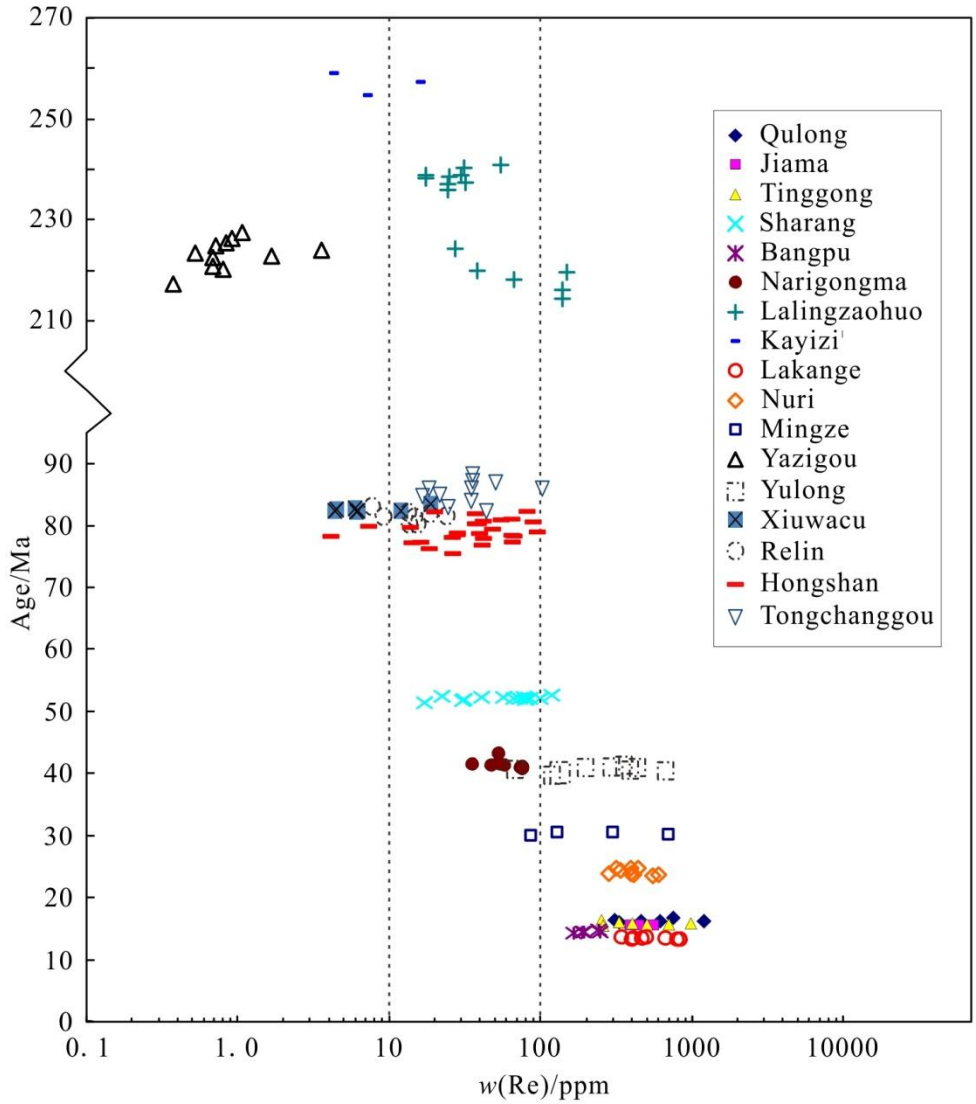

Fig. 14

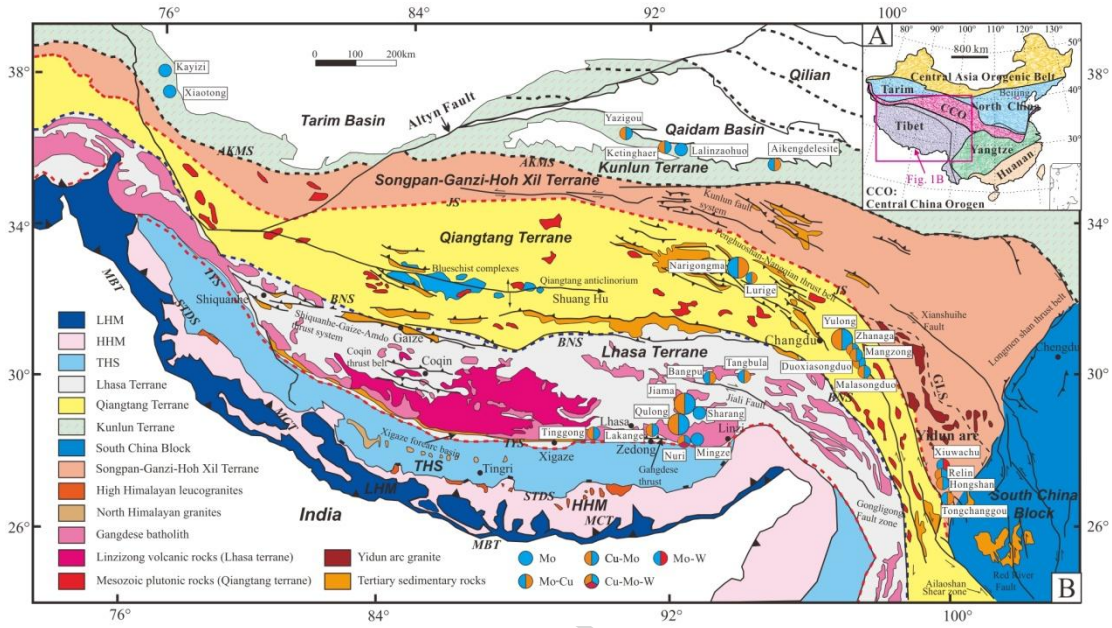

Graphical abstract

Table 1 List of major Mo deposits in SW China.

Deposit	Type	Commodity	Ore-causative intrusion	Host strata	Reserves (kt)	Grade (%)	Texture	Major ore minerals	Alteration minerals	Reference
Kayizi, Xinjiang	P	Mo	Granodiorite	Meso-proterozoic slate, quartz schist, tuff, marble, limestone		0.04-1.53	Diss, Sw	Mb, Py	Qz, Ser, Chl, Cc	Liu et al. (2010a)
Xiaotong, Xinjiang	PS	Mo	Granodiorite	Meso-proterozoic crystalline schist, quartzite, marble, gneisses			Diss, Sw	Mb, Py, Cp	Qz, Gr, Di, Ep, Act, Chl, Cc	Liu et al. (2010b)
Aikengdelesite, Qinghai	P	Mo-Cu	Granite porphyry	Triassic andesite, andesitic tuff lava;		0.037	Diss, Sw	Mb, Cp, Py	Qz, Ser, An, Chl, Cc	Yang et al. (2013c, 2014b)
Lalingzaohuo, Qinghai	PS	Mo	Granodiorite, quartz diorite	Paleo-proterozoic biotite-bearing plagioclase gneisses, siltstone, dolomite marble, migmatite		0.05-0.09	Diss, Sw	Mb, Py, Cp, Mt	Gr, Di, Qz, Cc, Ser, Kf, Chl	Wang et al. (2013); Chen et al. (2013); Ma et al. (2014)
Ketinghaer, Qinghai	P	Cu-Mo	Granite porphyry	Paleo-proterozoic gneisses, marble, schist; Devonian basalt, andesite		0.062	Diss, Sw, Br	Mb, Py, Cp	Qz, Ser, Bi, Kf, Chl, Cc	Su et al. (2014)
Yazigou, Qinghai	PS	Cu-Mo-Pb-Zn	K-feldspar granite porphyry; granodiorite porphyry	Cambrian-Ordovician andesite, basalt, marble; Triassic tuff, andesite, rhyolite		0.028	Diss, Sw	Mb, Py, Cp, Ga, Sph	Qz, Ser, Bi, Kf, Chl, Cc	Li et al. (2008); He et al. (2009)
Narigongma, Qinghai	P	Mo-Cu	Biotite granite porphyry;	Permian basalt, basaltic andesite, sandstone, slate	Mo: 675; Cu: 251.6	Mo: 0.08; Cu: 0.33	Diss, Sw	Mb, Cp, Py	Kf, Bi, Qz, Ser	Wang et al. (2008); Yang et al. (2014a)

			fine-grained granite porphyry	and muddy limestone						
Lurige, Qinghai	P	Mo-Cu	Biotite mozongranite porphyry	Carboniferous clastic rocks, carbonate; Permian clastic rocks, volcanic rocks, carbonate		Mo: 0.01-0.1 Cu: 0.45-6.19	Diss, Sw	Mb, Cp, Py, Ga, Sph	Qz, Kf, Ep, Ser, Chl, Cc	Hao et al. (2013)
Qulong, Tibet	P	Cu-Mo	Monzogranite porphyry	Jurassic felsic lava, volcanoclastic rocks, limestone, sandstone and slate	Cu:10600 Mo: 510	Cu: 0.50; Mo: 0.03	Sw, Diss	Cp, Py, Mb, Bo	Qz, Ser, Kf, An	Hou et al. (2003); Xiao et al. (2009, 2012)
Jiama, Tibet	PS	Cu-Mo-Pb-Zn	Felsic-intermediate porphyries	Jurassic limestone; Cretaceous sandstone, siltstone, shale	Cu: 4640 Mo: 380	Cu: 0.44 Mo: 0.036	Diss, Sw	Cp, Mb, Bo, Py, Ga, Sph	Gr, Di, Ep, Qz, Cc, Fl, Chl, Ep, An	Tang et al. (2010); Qin et al. (2011); Ying et al. (2010, 2014);
Sharang, Tibet	P	Mo	Granite porphyry; porphyritic granite; granite; fine-grained granite porphyry	Late Permian quartz sandstone	61	Mo: 0.061	Sw, Diss, Br	Mb, Py	Ser, Qz, Kao	Zhao et al. (2014); Tang et al. (2009a)
Mingze, Tibet	PS	Mo	Granite porphyry	Cretaceous metamorphic siltstone, tuff, and slate; Triassic sandslate, sandstone		Mo: 0.1	Diss	Cp, Py, Bo, Mb	Qz, Ser, Bi, Kf, Do, Gr, Di, Wol, Ep, Cc	Fan et al. (2011)

Tangbula, Tibet	P	Mo-Cu	Granite porphyry, monzogranite porphyry, etc.	Cretaceous biotite monzogranite, biotite granite	Mo: 100; Cu: 10	Mo: 0.1; Cu: 0.21	Sw, Diss	Mb, Cp, Py, Mt	Qz, Ser, Kf, Chl	Xia et al. (2010); Wang et al. (2010)
Tinggong, Tibet	P	Cu-Mo	Granite porphyry	Eocene volcanic tuff, tuffaceous sandstone		Mo: 0.04-0.08 Cu: 0.55-1.47	Diss, Sw	Py, Cp, Mb, Bo	Qz, Kf, Ser, Chl	Chen et al. (2014); Yang et al. (2005)
Bangpu, Tibet	P	Mo-Cu	Porphyritic monzogranite	Palaeogene tuff, tuff breccia; Permian volcanic breccia, tuff, sandstone, limestone	Mo: 210; Cu: 500	Mo: 0.09; Cu: 0.33	Diss, Sw, Br	Mb, Cp, Py, Bo, Ga, Sph	Qz, Kf, Ser, Chl, Fl	Wang et al. (2012b); Zhao et al. (2015b)
Lakange, Tibet	P	Cu-Mo	Granodiorite porphyry	Jurassic andesite, volcanic breccia, quartz schist, tuff, limestone, marble			Diss, Sw	Mb, Cp, Py	Qz, Kf, Bi, Ser, Chl, Kao	Leng et al. (2015)
Nuri, Tibet	S	Cu-W-Mo	Granite porphyry	Early Cretaceous marble, argillceous limestone, siltstone, hornfels, tuff	Cu: 500	Cu: 0.71 WO_3: 0.22 Mo: 0.067	Diss, Sw	Cp, Mb, Sch, Py	Qz, Gr, Di, Ep, Act, Chl, Cc	Chen et al. (2015); Wu et al. (2015); Wang et al. (2014b)
Yulong, Tibet	PS	Cu-Mo	Monzogranite porphyry; quartz monzogranite	Triassic limestone, marble, sand-shale, slate	Cu: 6500; Mo: 150	Cu: 0.52 Mo: 0.028	Diss, Sw	Cp, Mb, Py, Bo, Sph, Ga	Kf, Qz, Ser, Kao, Chl, Ep	Hou et al. (2007); Liang et al. (2008, 2009a)
Zhanaga, Tibet	P	Cu-Mo	Monzogranite porphyry, syenogranite porphyry	Permian volcanic rocks; Triassic sandstone, mudstone	Cu: 300	Cu: 0.36 Mo: 0.03	Diss, Sw	Cp, Mb, Py, Mt	Kf, Qz, Ser, Kao, Chl, Ep	He et al. (2014)
Mangzong	P	Cu-Mo	Monzogranite porphyry, syenogranite	Permian volcanic rocks; Triassic sandstone, mudstone	Cu: 250	Cu: 0.34 Mo: 0.01-0.02	Sw	Cp, Mb, Py	Kf, Qz, Ser, Kao, Chl, Ep	Wu et al. (2011)

			porphyry							
Duoxiasongduo Tibet	P	Cu-Mo	Monzogranite porphyry, alkali-feldspar granite porphyry	Triassic sandstone, mudstone, shale	Cu: 500	Cu: 0.38 Mo: 0.04	Diss, Sw	Cp, Mb, Py, Mt, Ga, Sph, Bo	Kf, Qz, Ser, Chl, Ep	Hou et al. (2003) Wu et al. (2013)
Malasongduo, Tibet	P	Cu-Mo	Monzogranite porphyry, syenogranite porphyry	Triassic siltstone, mudstone, rhyolite, tuff	Cu: 1000; Mo: >100	Cu: 0.44 Mo: 0.14	Diss, Sw	Cp, Mb, Py, Mt, Ga, Sph, Bo	Kf, Qz, Ser, Chl, Ep, Kao	Hou et al. (2003); Liang et al. (2009b)
Xiuwacu, Yunnan	P-QV	Mo-W	Biotite monzogranite, alkali-feldspar granite	Triassic sandstone, slate	Mo: 13.6 WO_3: 8.4	Mo: 0.38 WO_3: 0.28	Sw, V	Mb, Sch, Cp, Py, Pyr, Sb, Asp	Kf, Qz, Ser, Kao	Wang et al. (2014c, 2015)
Relin, Yunnan	P	Cu-Mo	Monzogranite, granite porphyry	Upper Triassic sandstone and slate		Mo: 0.049	Sw, V	Mb, Sch, Cp, Py, Pyr	Kf, Qz, Ser, Kao	Wang et al. (2014c, 2015); Wan et al. (2012)
Hongshan, Yunnan	PS	Cu-Mo	Quartz monzonite porphyry	Upper Triassic sandy-slate, limestone, marble	Cu: 650 Mo: 5.8	Cu: 1.23 Mo: 0.14	Diss, Sw	Mb, Cp, Py, Pyr, Sph	Qz, Gr, Di, Ep, Act, Chl, Cc	Wang et al. (2014c, 2015); Zu et al. (2015)
Tongchanggou Yunnan	PS	Mo-Cu	Granodiorite porphyry	Triassic limestone and marble; Permian basalt interbedded with volcanic breccia.	Mo: 300 Cu: 3.4	Mo: 0.3 Cu: 0.8	Diss, Sw, V	Mb, Cp, Py, Pyr	Qz, Gr, Di, Ep, Act, Chl, Cc	Li et al. (2012b); Yang et al. (2016c)

Deposit type: P, porphyry type; S, skarn type; PS, porphyry-skarn type; QV, quartz vein type.

Texture: Diss, disseminated; Sw, stockwork; Br, breccia; V, veined.

Ore and alteration mineral abbreviations: Act, actinolite; An, anhydrite; Asp, arsenopyrite; Bi, biotite; Bo, Bornite; Cc, calcite; Chl, chlorite; Cp, chalcopyrite; Di, diopside; Do, dolomite; Ep, epidote; Fl, fluorite; Ga, galena; Gr, garnet; Kao, kaolinite; Kf, K-feldspar; Mb, molybdenite; Mt, magnetite; Py, pyrite; Pyr, pyrrhotite ; Qz, quartz; Sch, scheelite; Ser, sericite; Sph, sphalerite; Sb, stibnite; Wol, wollastonite

Table 2 Isotopic ages of Mo deposits in SW China.

Deposits	Porphyry/ores	N	Method	Age (Ma)	Reference
Kayizi	Granodiorite	1	LA-ICPMS zircon U-Pb weighted average	250.0 ± 4.6	Liu et al. (2010a)
	Ores	3	Molybdenite Re-Os	254.4 ± 1.9 – 258.5 ± 2.0	Liu et al. (2010a)
Aikengdelesite	Granite porphyry	1	LA-ICPMS zircon U-Pb weighted average	248.3 ± 1.5	Xu (2014)
Lalingzaohuo	Granodiorite porphyry	1	LA-ICPMS zircon U-Pb weighted average	242.6 ± 3.4	Chen et al. (2013)
	Ores	15	Molybdenite Re-Os	214.1 ± 1.2–240.6 ± 1.6	Wang et al. (2013)
Yazigou	K-feldspar granite porphyry	1	SHRIMP zircon U-Pb weighted average	224.0 ± 1.6	Li et al. (2008)
	Ores	11	Molybdenite Re-Os	217.0 ± 3.2–227.1 ± 4.0	He et al. (2009)
Narigongma	Biotite granite porphyry	1	SHRIMP zircon U-Pb weighted average	43.3 ± 0.5	Yang et al. (2008)
	Biotite granite porphyry	2	LA-ICPMS zircon U-Pb weighted average	43.4 ± 0.4, 42.9 ± 0.3	Hao et al. (2012)
	Biotite granite porphyry	1	LA-ICPMS zircon U-Pb weighted average	41.53 ± 0.24	Song et al. (2012)
	Granodiorite porphyry	1	LA-ICPMS zircon U-Pb weighted average	41.44 ± 0.23	Song et al. (2012)
	Granite porphyry	1	SHRIMP zircon U-Pb weighted average	43.6 ± 0.5	Yang et al. (2014a)
	Quartz diorite porphyryr	1	SHRIMP zircon U-Pb weighted average	41.7 ± 0.5	Yang et al. (2014a)
	Ores	6	Molybdenite Re-Os	40.91 ± 0.57–43.05 ± 0.57	Wang et al. (2008)
	Ores	1	Molybdenite Re-Os	40.8 ± 0.4	Hao et al. (2012)
Lurige	Biotite granite porphyry	1	LA-ICPMS zircon U-Pb weighted average	62.1 ± 0.4	Hao et al. (2013)
	Fine-grained granite porphyry	1	LA-ICPMS zircon U-Pb weighted average	61.7 ± 0.3	Hao et al. (2013)
	Ores	5	Molybdenite Re-Os	59.2 ± 0.6 – 62.8 ± 0.6	Hao et al. (2013)
Qulong	Monzogranite porphyry	1	SHRIMP zircon U-Pb weighted average	17.6 ± 0.7	Hou et al. (2004)
	Granite porphyry	1	SHRIMP zircon U-Pb weighted average	17.7 ± 0.3	Yang (2008)
	Diorite porphyry	1	LA-ICPMS zircon U-Pb weighted average	15.9 ± 0.3	Yang (2008)
	Granodiorite	1	SHRIMP zircon U-Pb weighted average	19.5 ± 0.4	Yang (2008)

	Biotite granodiorite	2	SHRIMP zircon U-Pb weighted average	16.35 ± 0.40, 16.38 ± 0.46	Wang et al.(2006)
	Ores	6	Molybdenite Re-Os	15.99 ± 0.31–16.74 ± 0.28	Meng et al. (2003)
	Ores	4	Molybdenite Re-Os	15.82 ± 0.19–16.85 ± 0.19	Wang et al.(2006)
	Ores	4	Molybdenite Re-Os	15.8 ± 0.4–16.2 ± 0.9	Hou et al.(2009)
	Ores	4	Molybdenite Re-Os	15.69 ± 1.98–16.23 ± 0.9	Li et al. (2005a)
Jiama	Granite porphyry	3	LA-ICPMS zircon U-Pb weighted average	15.31 ± 0.24 – 16.27 ± 0.31	Qin et al. (2011)
	Monzogranite porphyry	1	LA-ICPMS zircon U-Pb weighted average	14.81 ± 0.16	Qin et al. (2011)
	Granite porphyry	1	SHRIMP zircon U-Pb weighted average	14.2 ± 0.2	Ying et al. (2011)
	Granodiorite porphyry	1	SHRIMP zircon U-Pb weighted average	14.1 ± 0.3	Ying et al. (2011)
	Ores	27	Molybdenite Re-Os	14.20 ± 0.20 – 16.50 ± 0.20	Ying et al. (2010)
	Ores	7	Molybdenite Re-Os	15.4 ± 0.2 – 15.5 ± 0.3	Li et al. (2005b)
Tinggong	Adamellite porphyry	1	SHRIMP zircon U-Pb weighted average	17.0 ± 0.6	Rui et al. (2004)
	Adamellite porphyry	1	LA-ICPMS zircon U-Pb weighted average	15.54 ± 0.28	Chen et al. (2014)
	Diorite porphyry	1	LA-ICPMS zircon U-Pb weighted average	15.02 ± 0.25	Chen et al. (2014)
	Diorite porphyry	1	LA-ICPMS zircon U-Pb weighted average	15.74 ± 0.22	Chen et al. (2014)
	Diorite porphyry	1	Biotite $^{40}Ar/^{39}Ar$ plateau	14.9 ± 0.2	Li et al. (2007b)
	Granodiorite porphyry	1	Biotite $^{40}Ar/^{39}Ar$ plateau	14.2 ± 0.2	Li et al. (2007b)
	Ores	7	Molybdenite Re-Os	15.5 ± 0.3 – 16.3 ± 0.3	Hou et al.(2009)
Bangpu	Monzogranite porphyry	1	SHRIMP zircon U-Pb weighted average	13.9 ± 0.3	Zhou et al. (2010)
	Granite porphyry	1	SHRIMP zircon U-Pb weighted average	14.2 ± 0.2	Wen et al. (2011)
	Monzogranite porphyry	1	SHRIMP zircon U-Pb weighted average	13.9 ± 0.3	Wen et al. (2011)
	Monzogranite porphyry	5	Whole-rock Rb-Sr isochron	13.88 ± 0.38	Wen et al. (2011)
	Monzogranite porphyry	1	LA-ICPMS zircon U-Pb weighted average	16.23 ± 0.19	Wang et al. (2012b)
	Diorite porphyry	1	LA-ICPMS zircon U-Pb weighted average	15.16 ± 0.09	Wang et al. (2012b)
	Adamellite porphyry	2	LA-ICPMS zircon U-Pb weighted average	14.07 ± 0.08, 14.96 ± 0.16	Wang et al. (2012c)

	Diorite porphyry	1	LA-ICPMS zircon U-Pb weighted average	15.30 ± 0.25	Wang et al. (2012c)
	Ores	5	Molybdenite Re-Os	14.3 ± 0.3 – 14.8 ± 0.3	Hou et al.(2009)
	Ores	1	Quartz $^{40}Ar/^{39}Ar$ isochron	13.9 ± 0.9	Zhou et al. (2011b)
	Ores	3	Molybdenite Re-Os	14.96 ± 0.23 – 16.61 ± 0.23	Wang et al. (2012c)
	Ores	4	Molybdenite Re-Os	14.43 ± 0.08 – 14.67 ± 0.09	Zhou et al. (2013)
	Ores	10	Pyrite-sphalerite Rb-Sr isochron	13.9 ± 0.9	Zhao et al. (2015)
Sharang	Pre-ore quartz monzonite	1	LA-ICPMS zircon U-Pb weighted average	53.1 ± 0.6	Zhao et al. (2014)
	Granite	1	LA-ICPMS zircon U-Pb weighted average	52.9 ± 0.5	Zhao et al. (2014)
	Granite porphyry	2	LA-ICPMS zircon U-Pb weighted average	52.9 ± 0.4, 52.6 ± 0.5	Zhao et al. (2014)
	Porphyritic granite	1	LA-ICPMS zircon U-Pb weighted average	52.3 ± 0.4	Zhao et al. (2014)
	Fine-grained granite porphyry	1	LA-ICPMS zircon U-Pb weighted average	51.6 ± 0.4	Zhao et al. (2014)
	Ores	7	Molybdenite Re-Os	51.57 ± 0.81 – 52.69 ± 0.77	Tang et al. (2009a)
	Ores	13	Molybdenite Re-Os	51.37 ± 0.75 – 52.45 ± 0.75	Zhao et al. (2014)
Mingze	Granodiorite	1	SHRIMP zircon U-Pb weighted average	28.4 ± 0.4	Sun et al. (2013)
	Monzonlite	1	SHRIMP zircon U-Pb weighted average	30.4 ± 0.6	Sun et al. (2013)
	Ores	4	Molybdenite Re-Os	29.90 ± 0.44 – 30.44 ± 0.44	Sun et al. (2013)
	Ores	1	Biotite $^{40}Ar/^{39}Ar$ plateau	28.02 ± 0.33	Fan et al. (2011)
Tangbula	Granite porphyry	1	LA-ICPMS zircon U-Pb weighted average	19.72 ± 0.20	Wang et al.(2010)
	Granodioritic porphyry	1	LA-ICPMS zircon U-Pb weighted average	19.88 ± 0.38	Xia et al. (2010)
	Ores	5	Molybdenite Re-Os	19.5 ± 0.2 – 22.6 ± 0.3	Wang et al.(2010)
Lakange	Ores	8	Molybdenite Re-Os	13.20 ± 0.20 – 13.62 ± 0.26	Leng et al.(2015)
Nuri	Granite porphyry	1	MC-ICPMS zircon U-Pb weighted average	30.3 ± 0.5	Chen et al.(2015)
	Ores	9	Molybdenite Re-Os	23.46 ± 0.38 – 24.77 ± 0.36	Zhang et al. (2012)
	Ores	2	Chalcopyrite Re-Os	24.94 ± 0.35, 23.53 ± 0.37	Wang et al. (2014b)

	Ores	1	Biotite $^{40}Ar/^{39}Ar$ plateau	23.75 ± 0.18	Wu et al. (2015)
Yulong	Monzogranite porphyry	1	SHRIMP zircon U-Pb weighted average	41.0 ± 1.0	Guo et al. (2006)
	Monzogranite porphyry	1	SHRIMP zircon U-Pb weighted average	38.86 ± 0.8	Jiang et al. (2006)
	Monzogranite porphyry	1	LA-ICPMS zircon U-Pb weighted average	41.2 ± 0.2	Liang et al. (2006)
	Quartz monzonite-porphyry	1	LA-ICPMS zircon U-Pb weighted average	41.3 ± 0.3	Liang et al. (2008)
	Syenogranite porphyry	1	LA-ICPMS zircon U-Pb weighted average	41.2 ± 0.3	Liang et al. (2008)
	Monzogranite porphyry	1	SHRIMP zircon U-Pb weighted average	43.0 ± 0.5	Wang et al. (2009)
	Monzogranite porphyry	1	SHRIMP zircon U-Pb weighted average	43.8 ± 0.7	Wang et al. (2009)
	Potassic alteration	1	Biotite $^{40}Ar/^{39}Ar$ plateau	41.3 ± 0.8	Liang et al. (2008)
	Ores	4	Molybdenite Re-Os	40.9 ± 0.7 – 41.0 ± 0.8	Hou et al. (2006a)
	Ores	5	Molybdenite Re-Os	39.69 ± 0.57 – 41.29 ± 0.57	Tang et al. (2009b)
Zhanaga	Monzogranite porphyry	1	LA-ICPMS zircon U-Pb weighted average	38.5 ± 0.2	Liang et al. (2006)
	Monzogranite porphyry	1	LA-ICPMS zircon U-Pb weighted average	38.5 ± 0.2	He et al. (2014)
	Syenogranite porphyry	1	LA-ICPMS zircon U-Pb weighted average	38.5 ± 0.2	He et al. (2014)
Mangzong	Syenogranite porphyry	1	LA-ICPMS zircon U-Pb weighted average	37.6 ± 0.2	Liang et al. (2006)
Duoxiasongduo	Syenogranite porphyry	1	LA-ICPMS zircon U-Pb weighted average	37.5 ± 0.2	Liang et al. (2006)
	Ores	1	Molybdenite Re-Os	36.0 ± 0.4	Du et al. (1994)
Malasongduo	Alkali-feldspar granite porphyry	1	LA-ICPMS zircon U-Pb weighted average	36.9 ± 0.2	Liang et al. (2006)
	Quartz monzogranite porphyry	1	LA-ICPMS zircon U-Pb weighted average	36.9 ± 0.4	Liang et al. (2009b)
	Alkali-feldspar granite porphyry	1	LA-ICPMS zircon U-Pb weighted average	36.9 ± 0.3	Liang et al. (2009b)
	Ores	3	Molybdenite Re-Os	35.4 ± 1.3 – 36.2 ± 1.1	Tang and Luo (1995)
	Ores	1	Molybdenite Re-Os	35.8 ± 0.4	Du et al. (1994)
Xiuwacu	Biotite granitic porphyry	1	LA-ICPMS zircon U-Pb weighted average	85.6 ± 0.5	Wang et al. (2014c)
	Biotite monzogranite	1	LA-ICPMS zircon U-Pb weighted average	84.8 ± 0.6	Wang et al. (2014c)

	Alkali-feldspar leucogranite	1	LA-ICPMS zircon U-Pb weighted average	84.4 ± 1.4	Wang et al. (2014c)
	Ores	7	Molybdenite Re-Os	82.3 ± 1.1 – 83.5 ± 0.3	Li et al. (2007c)
Relin	Monzogranitic porphyry	1	LA-ICPMS zircon U-Pb weighted average	82.7 ± 0.5	Wang et al. (2014c)
	Ores	8	Molybdenite Re-Os	80.3 ± 1.1 – 82.9 ± 1.1	Li et al. (2007c)
Hongshan	Granitic porphyry	1	LA-ICPMS zircon U-Pb weighted average	81.1 ± 0.5	Wang et al. (2011)
	Granitic porphyry	1	LA-ICPMS zircon U-Pb weighted average	75.8 ± 1.3	Huang et al. (2012)
	Quartz monzonite porphyry	1	SHRIMP zircon U-Pb weighted average	73.4 ± 0.7	Zu et al. (2016)
	Monzonite porphyry	4	LA-ICPMS zircon U-Pb weighted average	76 ± 0.8 –79 ± 0.7	Yang et al. (2016b)
	Ores	7	Pyrite Re-Os isochron	75 ± 18	Li et al. (2007c)
	Ores	8	Pyrrhotite Re-Os isochron	79 ± 16	Zu et al. (2015)
	Ores	6	Molybdenite Re-Os	75.46 ± 0.89 – 78.10 ± 2.26	Xu et al. (2006)
	Ores	8	Molybdenite Re-Os	77.90 ± 1.10 – 81.05 ± 1.17	Meng et al. (2013)
	Ores	5	Molybdenite Re-Os	78.3 ± 0.6 – 82.3 ± 0.8	Wang et al. (2014c)
	Ores	8	Molybdenite Re-Os	77.2 ± 1.6 – 81.9 ± 1.1	Zu et al. (2015)
Tongchanggou	Biotite monzogranite	2	LA-ICPMS zircon U-Pb weighted average	87.4 ± 0.6, 86.3 ± 0.6	Wang et al. (2014c)
	Granodiorite	2	LA-ICPMS zircon U-Pb weighted average	85 ± 0.4, 84 ± 0.4	Yang et al. (2016c)
	Ore	4	Molybdenite Re-Os	86 ± 0.4 – 87 ± 0.6	Yang et al. (2016c)
	Ore	6	Molybdenite Re-Os	82.34 ± 1.28 – 88.27 ± 1.23	Li et al. (2012b)

Table 3 Whole-rock Sr-Nd-Pb isotopic compositions of the ore-associated granites from Mo deposits in SW China.

Deposit	Sample	$^{87}Rb/^{86}Sr$	$^{87}Sr/^{86}Sr$	$(^{87}Sr/^{86}Sr)i$	$^{147}Sm/^{144}Nd$	$^{143}Nd/^{144}Nd$	$\varepsilon Nd(t)$	$^{206}Pb/^{204}Pb$	$^{207}Pb/^{204}Pb$	$^{208}Pb/^{204}Pb$	Reference
Qulong	Monzogranite porphyry	1.792	0.70649	0.70610	0.1019	0.512601	−0.53	18.510	15.634	38.899	Wang (2007)
	Monzogranite porphyry	1.647	0.70627	0.70590	0.0962	0.512605	−0.44	18.608	15.733	39.153	Wang (2007)
	Monzogranite porphyry	1.057	0.70745	0.70720	0.1043	0.512603	−0.49	18.521	15.595	38.682	Wang (2007)
Jiama	Granodiorite porphyry	4.206	0.70792	0.70690	0.0942	0.512559	−1.50	18.628	15.626	38.930	Wang (2007)
	Granodiorite porphyry	2.238	0.70736	0.70680	0.0912	0.512511	−2.28	18.639	15.620	38.924	Wang (2007)
	Granodiorite porphyry	4.403	0.70754	0.70650	0.0923	0.512313	−6.18	18.661	15.618	38.960	Wang (2007)
Tinggong	Granodiorite porphyry							18.408	15.567	38.609	Qu et al. (2004)
	Granodiorite porphyry							18.437	15.581	38.620	Qu et al. (2004)
	Granodiorite porphyry							18.446	15.605	38.695	Qu et al. (2004)
Tangbula	Granite porphyry	1.218	0.70706	0.70671	0.0914	0.512457	−3.27				Wang et al. (2010)
	Granite porphyry	0.523	0.70617	0.70603	0.0864	0.512534	−1.75				Wang et al. (2010)
	Granodiorite	0.342	0.70621	0.70611	0.1043	0.512492	−2.61				Wang et al. (2010)
	Granodiorite	0.529	0.70691	0.70676	0.0857	0.512514	−2.14				Wang et al. (2010)
	Granodiorite	0.306	0.70622	0.70613	0.1038	0.512527	−1.93				Wang et al. (2010)
	Granite porphyry	0.355	0.70608	0.70598	0.0927	0.512535	−1.75				Wang et al. (2010)
Sharang	Granite porphyry	1.570	0.70741	0.70623	0.1071	0.512434	−3.37				Wang (2007)
	Granite porphyry	2.279	0.70833	0.70661	0.1076	0.512382	−4.40				Wang (2007)
	Granite porphyry	1.917	0.70796	0.70652	0.1054	0.512399	−4.05				Wang (2007)
	Granite porphyry	2.371	0.70857	0.70679	0.1082	0.512372	−4.59				Wang (2007)
Narigongma	Biotite granite porphyry	0.536	0.70535	0.70502	0.1000	0.512635	0.50	18.808	15.669	39.009	Yang et al. (2008)
	Biotite granite porphyry	0.600	0.70536	0.70500	0.0993	0.512642	0.60	18.755	15.609	38.809	Yang et al. (2008)
	Biotite granite porphyry	1.017	0.70562	0.70499	0.0992	0.512642	0.60	18.995	15.625	39.121	Yang et al. (2008)
	Biotite granite porphyry	2.271	0.70664	0.70524	0.0987	0.512564	−0.90	18.818	15.616	38.999	Yang et al. (2008)

Yulong	Monzogranite porphyry	0.4451	0.70677	0.70651	0.1051	0.512482	−2.6	18.714	15.658	38.895	Jiang et al. (2006)
	Monzogranite porphyry	0.5208	0.70686	0.70656	0.1010	0.512487	−2.4	18.751	15.673	38.963	Jiang et al. (2006)
	Monzogranite porphyry	0.6122	0.70731	0.70695	0.0965	0.512486	−2.4	18.736	15.662	38.937	Jiang et al. (2006)
	Syenogranite porphyry	0.7398	0.70696	0.70653	0.0837	0.512478	−2.5	18.713	15.646	38.867	Jiang et al. (2006)
	Alkali-feldspar granite porphyry	1.359	0.70708	0.70629	0.0945	0.512486	−2.4	18.824	15.665	38.999	Jiang et al. (2006)
	Monzogranite porphyry	1.054	0.70746	0.70685	0.0980	0.512478	−2.6	18.731	15.661	38.924	Jiang et al. (2006)
	Quartz monzogranite porphyry	0.9713	0.70726	0.70670	0.1140	0.512513	−2.0	18.718	15.652	38.895	Jiang et al. (2006)
	Monzogranite porphyry	0.8419	0.70720	0.70671	0.1019	0.512465	−2.9	18.719	15.654	38.894	Jiang et al. (2006)
	Monzogranite porphyry	0.7382	0.70688	0.70645	0.0997	0.512482	−2.5	18.718	15.646	38.874	Jiang et al. (2006)
	Monzogranite porphyry	0.9272	0.70710	0.70656	0.1000	0.512461	−3.0	18.735	15.663	38.933	Jiang et al. (2006)
Zhanaga	Monzogranite porphyry		0.70582			0.512509	−2.5	18.867	15.661	38.963	Zhang et al. (1998)
	Syenogranite porphyry		0.70600			0.512485	−3.0	18.870	15.648	38.955	Zhang et al. (1998)
Duoxiasongduo	Monzogranite porphyry		0.70545			0.512532	−2.1	18.852	15.634	38.915	Zhang et al. (1998)
	Alkali-feldspar granite porphyry		0.70658			0.512492	−2.8				Zhang et al. (1998)
Mangzong	Monzogranite porphyry		0.70633			0.512522	−2.3	18.883	15.629	38.921	Zhang et al. (1998)
Malasongduo	Alkali-feldspar granite porphyry		0.70683			0.512473	−3.2				Zhang et al. (1998)
Xiuwacu	Biotite granitic porphyry	11.719	0.721695	0.7075	0.1127	0.512237	− 6.9				Wang et al. (2014d)
	Biotite granitic porphyry	4.425	0.713422	0.7081	0.0982	0.512205	− 7.4				Wang et al. (2014d)
	Monzogranite	4.312	0.712908	0.7077	0.0980	0.512205	− 7.4				Wang et al. (2014d)
	Monzogranite	12.449	0.722964	0.7079	0.1033	0.512205	− 7.4				Wang et al. (2014d)
	Monzogranite	10.666	0.721374	0.7085	0.1313	0.512210	− 7.6				Wang et al. (2014d)
	Monzogranite	4.578	0.713064	0.7075	0.1015	0.512215	−7.2				Wang et al. (2014d)
	Alkali-feldspar leucogranite	18.025	0.729223	0.7075	0.1238	0.512220	−7.4				Wang et al. (2014d)
	Alkali-feldspar leucogranite	79.546	0.804946	0.7089	0.2029	0.512231	−8.0				Wang et al. (2014d)
	Alkali-feldspar leucogranite	156.688	0.899085	0.7098	0.1260	0.512210	−7.6				Wang et al. (2014d)
	Biotite granite porphyry							19.280	15.770	39.850	Wang et al. (2015)

	Monzogranite							19.530	16.650	39.420	Wang et al. (2015)
	Monzogranite							19.730	15.760	39.810	Wang et al. (2015)
	Alkali-feldspar leucogranite							19.080	15.680	39.370	Wang et al. (2015)
	Alkali-feldspar leucogranite							19.410	15.758	39.498	Wang et al. (2015)
Relin	Monzogranite	2.196	0.710371	0.7078	0.1460	0.512227	−7.5				Wang et al. (2014d)
	Monzogranite	1.729	0.709790	0.7078	0.1489	0.512219	−7.7				Wang et al. (2014d)
Hongshan	Granitic porphyry	1.252	0.709670	0.7082	0.1375	0.512197	−8.0				Wang et al. (2014d)
	Monzogranite porphyry	1.5766	0.710126	0.708423	0.0946	0.512292	−5.8	19.0941	15.6498	39.4892	Yang et al. (2016b)
	Monzogranite porphyry	2.2172	0.710765	0.708257	0.0907	0.51226	−6.3	19.2458	15.6657	39.7894	Yang et al. (2016b)
	Monzogranite porphyry	1.7545	0.710215	0.708321	0.0893	0.512247	−6.6	18.9833	15.6293	39.3865	Yang et al. (2016b)
	Monzogranite porphyry	1.3286	0.709465	0.707993	0.0839	0.512195	−7.5	19.2037	15.756	39.701	Yang et al. (2016b)
	Monzogranite porphyry	1.3115	0.709766	0.708313	0.0906	0.512209	−7.3	19.3771	15.7236	39.7156	Yang et al. (2016b)
	Monzogranite porphyry	1.1735	0.709418	0.708117	0.0846	0.512216	−7.1	19.2839	15.7161	39.7043	Yang et al. (2016b)
	Monzogranite porphyry	1.8274	0.710659	0.708686	0.0926	0.512193	−7.7	18.8646	15.6245	39.2281	Yang et al. (2016b)
	Monzogranite porphyry	1.3705	0.709935	0.708416	0.0891	0.512222	−7.0	18.7673	15.6816	39.2038	Yang et al. (2016b)
	Monzogranite porphyry	1.191	0.709892	0.708572	0.0908	0.512210	−7.3	18.8286	15.6839	39.2276	Yang et al. (2016b)
	Quartz monzonite porphyry	7.042	0.71498	0.7076	0.0984	0.512281	−6.0	18.970	15.732	39.630	Zu et al. (2016)
	Quartz monzonite porphyry	2.314	0.71097	0.7086	0.0942	0.512287	−5.9	18.958	15.726	39.571	Zu et al. (2016)
	Quartz monzonite porphyry	4.210	0.71449	0.7101	0.1070	0.512293	−5.9	18.903	15.729	39.508	Zu et al. (2016)
	Quartz monzonite porphyry	2.390	0.71052	0.7080	0.0957	0.512280	−6.1	19.204	15.731	39.892	Zu et al. (2016)
	Quartz monzonite porphyry	1.986	0.71035	0.7083	0.0921	0.512280	−6.0	19.283	15.774	40.065	Zu et al. (2016)
Tongchanggou	Biotite granitic porphyry	0.606	0.707640	0.7069	0.1360	0.512333	−5.3				Wang et al. (2014d)
	Biotite granitic porphyry	0.582	0.707624	0.7069	0.1442	0.512323	−5.6				Wang et al. (2014d)
	Granodiorite porphyry	0.3399	0.707176	0.706770	0.0885	0.512312	−5.2				Wang et al. (2014d)
	Granodiorite porphyry	0.3624	0.707176	0.706743	0.0975	0.512312	−5.3	18.7748	15.6625	39.2006	Yang et al. (2016c)
	Granodiorite porphyry	0.3789	0.706937	0.706485	0.0973	0.512347	−4.6	18.7721	15.6631	39.2416	Yang et al. (2016c)

	Granodiorite porphyry	0.3799	0.706739	0.706286	0.0889	0.512352	−4.4	18.7939	15.6656	39.2837	Yang et al. (2016c)
	Granodiorite porphyry	0.3214	0.706728	0.706344	0.0988	0.512347	−4.6	18.7943	15.6648	39.2525	Yang et al. (2016c)
	Granodiorite porphyry	0.2553	0.706803	0.706498	0.0945	0.512365	−4.2	18.8811	15.6747	39.3318	Yang et al. (2016c)
	Granodiorite porphyry	0.4667	0.706811	0.706254	0.0862	0.512343	−4.6	18.6746	15.6567	39.1140	Yang et al. (2016c)

Table 4 Fluid inclusions Types and microthermometric results of several Mo deposits in SW China.

Deposit	FIs types	T_h (°C)	*Salinity (wt% NaCl)*	*Density (g/cm3)*	Pressure (Mpa)	Reference
Qulong	WV, WL, S	232–550	2.4–55.7		30–105	Yang et al. (2009a)
Tinggong	WV, WL, S	195–474	1.7–48.2		1.4–140	Hou et al. (2009); Yang et al. (2005)
Bangpu	WV, WL, S	119–550	0.9–50.6	0.59–1.25	20–120	Luo et al. (2012); Zhao et al. (2015a)
Jiama	WV, WL, S	102–540	3.2–60.6	0.92–1.08	11–59.1	Zhou et al. (2011)
Nuri	W, C, S	140–386	1.2–55.8		5–25	Chen et al. (2010)
Narigongma	WV, WL, S	208–361	8.3–42.2	0.98–1.15		Nan et al. (2005)
Lalingzaohuo	W, C	146–410	2.7–17	0.55–0.97	13–45	Ma et al. (2014)
Yulong	WL, WV, S, C	115–590	2.6–54.8			Hou et al. (2007)
Xiuwacu	W, C	152–550	3.2–12.5			Wang et al. (2015)
Hongshan	WV, WL, S, C	205–414	3.1–41.1	0.56–1.17		Li et al. (2013c)
Relin	WV, WL, S, C	160–380	2.1–42.0	0.65–1.12		Wan et al. (2012)

Pressure means the minimum trapping pressures of the fluid inclusions.

FIs types: WV-vapor-rich H_2O-NaCl solution; WL-liquid-rich H_2O-NaCl solution; S-daughter mineral-bearing FIs; C-carbonic-aqueous FIs.

Table 5 The H−O istopic compositions of the Mo deposits in SW China.

Dreposit	Mineral	T(°C)	$\delta^{18}O_{mineral}$ (‰)	$\delta^{18}O_{H2O}$ (‰)	δD_{H2O} (‰)	Reference
Qulong	Quartz	575	9.0	7.7	−104	Yang and Hou (2009)
	Quartz	575	9.0	7.7	−97	Yang and Hou (2009)
	Quartz	575	8.5	7.2	−105	Yang and Hou (2009)
	Quartz	575	9.6	8.3	−115	Yang and Hou (2009)
	Quartz	575	9.1	7.8	−108	Yang and Hou (2009)
	Epidote	400	2.3	2.7	−69	Yang and Hou (2009)
	Epidote	400	1.8	2.2	−68	Yang and Hou (2009)
	Epidote	400	2.4	2.8	−59	Yang and Hou (2009)
	Epidote	400	2.8	3.2	−66	Yang and Hou (2009)
	Epidote	400	2.3	2.7	−70	Yang and Hou (2009)
	Epidote	400	3.0	3.4	−64	Yang and Hou (2009)
	Epidote	400	6.6	7.0	−29	Yang and Hou (2009)
	Sericite	350	5.5	3.7	−90	Yang and Hou (2009)
Jiama	Quartz	361	9.4	4.4	−80	Li et al. (2012c)
	Quartz	367	10.0	5.2	−96	Li et al. (2012c)
	Quartz	336	9.8	4.1	−91	Li et al. (2012c)
	Quartz	322	8.7	2.4	−104	Li et al. (2012c)
	Quartz	325	10.3	4.0	−73	Li et al. (2012c)
	Quartz	318	10.5	4.2	−74	Li et al. (2012c)
	Quartz	315	10.6	4.4	−75	Li et al. (2012c)
	Quartz	358	10.2	5.1	−75	Li et al. (2012c)
Bangpu	Quartz	550	12.4	10.8	−146	Zhao et al. (2015a)
	Quartz	550	10.4	8.8	−155	Zhao et al. (2015a)
	Quartz	550	9.6	8.0	−153	Zhao et al. (2015a)
	Quartz	550	13.9	12.3	−107	Zhao et al. (2015a)
	Quartz	550	9.5	7.9	−151	Zhao et al. (2015a)
	Quartz	550	14.5	12.9	−110	Zhao et al. (2015a)
	Quartz	550	10.9	9.3	−137	Zhao et al. (2015a)
	Quartz	550	13.5	11.9	−149	Zhao et al. (2015a)
	Quartz	550	10.8	9.2	−133	Zhao et al. (2015a)
	Quartz	550	10.5	8.9	−158	Zhao et al. (2015a)
	Quartz	550	10.0	8.4	−146	Zhao et al. (2015a)
	Quartz	420	13.7	10.1	−132	Zhao et al. (2015a)
	Quartz	420	12.5	8.9	−143	Zhao et al. (2015a)
	Quartz	420	10.3	6.7	−149	Zhao et al. (2015a)
	Quartz	420	12.4	8.8	−131	Zhao et al. (2015a)
Yulong	Quartz	420–520	10.4	5.7–7.4		Hou et al. (2007)
	Quartz	380–540	9.5	3.8–6.8	−60	Hou et al. (2007)
	Quartz	340–550	8.8	2.0–6.2	−65	Hou et al. (2007)

	Quartz	280–400	9.5	0.5–4.4	−85	Hou et al. (2007)
	Quartz	251–340	10.3	0.0–3.5	−98	Hou et al. (2007)
	Quartz	280–360	8.8	−0.2–2.6	−101	Hou et al. (2007)
	Quartz	260–340	8.2	−1.6–1.4	−103	Hou et al. (2007)
	Quartz	200–290	8.7	−4.5–−0.2	−110	Hou et al. (2007)
	Quartz	201–250	7.5	−5.6–−2.8	−115	Hou et al. (2007)
Hongshan	Quartz	340	11.7	4.32	−81	Li et al. (2013c)
	Quartz	340	11.9	4.52	−89	Li et al. (2013c)
	Quartz	320	15.3	8.59	−117	Li et al. (2013c)
	Quartz	300	12.2	3.21	−75	Li et al. (2013c)
	Calcite	280	13.0	5.34	−107	Li et al. (2013c)
Relin	Quartz	330	11.7	5.3	−88	Wan et al. (2012)
	Quartz	330	12.8	6.4	−79	Wan et al. (2012)
	Quartz	300	11.1	4.7	−99	Wan et al. (2012)
	Quartz	300	12.9	5.5	−101	Wan et al. (2012)
	Quartz	260	12.0	3.9	−113	Wan et al. (2012)

Table 6 $\delta^{34}S$ values of sulfides from the major Mo deposits in SW China.

Deposit	Sample	$\delta^{34}S$ (‰)	Reference	Deposit	Sample	$\delta^{34}S$ (‰)	Reference
Qulong	Pyrite	0.3	She et al. (2005)	Narigongma	Pyrite	4.7	Li et al. (2015b)
	Chalcopyrite	−0.3	She et al. (2005)		Molybdenite	4.2	Li et al. (2015b)
	Pyrite	0.1	She et al. (2005)		Pyrite	6.6	Li et al. (2015b)
	Anhydrite	14.1	Meng et al. (2006)		Molybdenite	4.1	Li et al. (2015b)
	Anhydrite	14.4	Meng et al. (2006)		Pyrite	8.0	Li et al. (2015b)
	Anhydrite	12.5	Meng et al. (2006)		Chalcopyrite	3.9	Li et al. (2015b)
	Anhydrite	12.6	Meng et al. (2006)		Pyrite	7.5	Li et al. (2015b)
	Chalcopyrite	−1.2	She et al. (2005)		Pyrite	7.5	Li et al. (2015b)
	Pyrite	−0.3	She et al. (2005)		Pyrite	7.2	Li et al. (2015b)
	Pyrite	1.1	She et al. (2005)		Pyrite	7.2	Li et al. (2015b)
	Pyrite	0.8	She et al. (2005)	Bangpu	Pyrite	−1.1	Zhao et al. (2015a)
	Chalcopyrite	−1.5	Meng et al. (2006)		Galena	1.1	Zhao et al. (2015a)
	Chalcopyrite	−2.7	Meng et al. (2006)		Pyrite	−1.1	Zhao et al. (2015a)
	Chalcopyrite	−1.0	Meng et al. (2006)		Pyrite	−0.4	Zhao et al. (2015a)
	Chalcopyrite	−2.3	Meng et al. (2006)		Pyrite	−1.5	Zhao et al. (2015a)
	Chalcopyrite	−6.3	Meng et al. (2006)		Galena	−0.6	Zhao et al. (2015a)
Jiama	Bornite	−0.5	Li et al. (2012c)		Galena	−0.8	Zhao et al. (2015a)
	Bornite	−0.3	Li et al. (2012c)		Sphalerite	−0.4	Zhao et al. (2015a)
	Bornite	−1.2	Li et al. (2012c)		Sphalerite	0.3	Zhao et al. (2015a)
	Bornite	−0.6	Li et al. (2012c)		Pyrite	0.1	Zhao et al. (2015a)
	Bornite	−1.1	Li et al. (2012c)		Pyrite	0.2	Zhao et al. (2015a)
	Bornite	−1.2	Li et al. (2012c)		Pyrite	1.1	Zhao et al. (2015a)
	Galena	−2.2	Li et al. (2012c)		Pyrite	−1.0	Zhao et al. (2015a)
	Galena	−2.3	Li et al. (2012c)		Pyrite	−0.9	Zhao et al. (2015a)
	Galena	−2.5	Li et al. (2012c)		Pyrite	−0.6	Zhao et al. (2015a)
	Galena	−2.2	Li et al. (2012c)		Pyrite	−0.4	Zhao et al. (2015a)
	Galena	−1.6	Li et al. (2012c)		Pyrite	−0.5	Zhao et al. (2015a)
	Galena	−2.1	Li et al. (2012c)		Pyrite	−1.2	Zhao et al. (2015a)
	Galena	−2.7	Li et al. (2012c)		Pyrite	−1.0	Zhao et al. (2015a)
	Galena	−2.4	Li et al. (2012c)		Pyrite	−1.3	Zhao et al. (2015a)
	Galena	−3.7	Li et al. (2012c)		Pyrite	−0.6	Zhao et al. (2015a)
	Galena	−4.4	Li et al. (2012c)		Pyrite	0.2	Zhao et al. (2015a)
	Pyrite	−1.6	Li et al. (2012c)		Pyrite	−0.9	Zhao et al. (2015a)
	Pyrite	−1.5	Li et al. (2012c)		Pyrite	−1.3	Zhao et al. (2015a)
	Pyrite	−4.9	Li et al. (2012c)		Pyrite	−0.6	Zhao et al. (2015a)
	Pyrite	−1.1	Li et al. (2012c)		Pyrite	−1.6	Zhao et al. (2015a)
	Pyrite	−1.0	Li et al. (2012c)		Pyrite	−0.1	Zhao et al. (2015a)
	Pyrite	−1.9	Li et al. (2012c)		Molybdenite	−0.3	Zhao et al. (2015a)
	Chalcopyrite	−0.2	Li et al. (2012c)		Molybdenite	0.3	Zhao et al. (2015a)
	Chalcopyrite	−1.2	Li et al. (2012c)		Molybdenite	0.7	Zhao et al. (2015a)

	Chalcopyrite	−0.1	Li et al. (2012c)		Molybdenite	−0.3	Zhao et al. (2015a)
	Chalcopyrite	−0.4	Li et al. (2012c)		Molybdenite	−1.0	Zhao et al. (2015a)
	Chalcopyrite	−0.3	Li et al. (2012c)		Molybdenite	−0.1	Zhao et al. (2015a)
	Chalcopyrite	−0.9	Li et al. (2012c)		Chalcopyrite	−2.3	Zhao et al. (2015a)
	Chalcopyrite	−1.0	Li et al. (2012c)		Chalcopyrite	−1.2	Zhao et al. (2015a)
	Chalcopyrite	−1.0	Li et al. (2012c)		Chalcopyrite	−1.0	Zhao et al. (2015a)
	Molybdenite	−1.6	Li et al. (2012c)		Chalcopyrite	−1.3	Zhao et al. (2015a)
Xiuwacu	Chalcopyrite	2.7	Wang et al. (2015)	Hongshan	Pyrrhotite	5.2	Zu et al. (2016)
	Chalcopyrite	2.4	Wang et al. (2015)		Pyrrhotite	4.8	Zu et al. (2016)
	Molybdenite	3.6	Wang et al. (2015)		Pyrrhotite	5.2	Zu et al. (2016)
	Molybdenite	3.3	Wang et al. (2015)		Pyrrhotite	4.6	Zu et al. (2016)
	Molybdenite	2.8	Wang et al. (2015)		Pyrrhotite	4.3	Zu et al. (2016)
	Molybdenite	2.8	Wang et al. (2015)		Pyrrhotite	4.7	Zu et al. (2016)
	Molybdenite	2.1	Wang et al. (2015)		Pyrrhotite	4.2	Zu et al. (2016)
	Molybdenite	2.7	Wang et al. (2015)		Pyrrhotite	4.3	Zu et al. (2016)
	Molybdenite	2.1	Wang et al. (2015)		Pyrrhotite	4.6	Zu et al. (2016)
	Molybdenite	3.0	Wang et al. (2015)		Pyrrhotite	4.6	Zu et al. (2016)
	Molybdenite	2.1	Wang et al. (2015)		Pyrrhotite	4.7	Zu et al. (2016)
	Pyrite	4.3	Wang et al. (2015)		Pyrrhotite	3.9	Zu et al. (2016)
	Pyrite	4.1	Wang et al. (2015)		Pyrrhotite	4.1	Zu et al. (2016)
	Pyrite	4.2	Wang et al. (2015)		Pyrrhotite	3.8	Zu et al. (2016)
	Pyrite	3.8	Wang et al. (2015)		Pyrrhotite	4.7	Zu et al. (2016)
	Pyrite	4.2	Wang et al. (2015)		Pyrrhotite	4.8	Zu et al. (2016)
	Pyrite	4.2	Wang et al. (2015)		Pyrite	5.2	Zu et al. (2016)
	Pyrite	4.3	Wang et al. (2015)		Pyrite	5.2	Zu et al. (2016)
	Sphalerite	4.2	Wang et al. (2015)		Pyrite	5.2	Zu et al. (2016)
	Sphalerite	4.1	Wang et al. (2015)		Pyrite	4.3	Zu et al. (2016)
Tongchanggou	Pyrite	−0.1	Liu et al. (2016)		Pyrite	4.5	Zu et al. (2016)
	Pyrite	−0.7	Liu et al. (2016)		Pyrite	4.7	Zu et al. (2016)
	Pyrite	0.6	Liu et al. (2016)		Pyrite	4.5	Zu et al. (2016)
	Pyrite	1.0	Liu et al. (2016)		Pyrite	4.8	Zu et al. (2016)
	Pyrite	0.2	Liu et al. (2016)		Pyrite	4.5	Zu et al. (2016)
	Pyrite	0.5	Liu et al. (2016)		Pyrite	3.9	Zu et al. (2016)
	Molybdenite	0.1	Liu et al. (2016)		Chalcopyrite	4.8	Zu et al. (2016)
	Chalcopyrite	0.4	Liu et al. (2016)		Chalcopyrite	5.1	Zu et al. (2016)
	Molybdenite	0.7	Liu et al. (2016)		Chalcopyrite	4.8	Zu et al. (2016)
	Molybdenite	1.1	Liu et al. (2016)		Chalcopyrite	4.2	Zu et al. (2016)
	Pyrite	1.4	Liu et al. (2016)		Chalcopyrite	5.4	Zu et al. (2016)
	Pyrite	0.7	Liu et al. (2016)		Chalcopyrite	4.4	Zu et al. (2016)
	Pyrite	0.7	Liu et al. (2016)		Chalcopyrite	4.7	Zu et al. (2016)
	Molybdenite	1.1	Liu et al. (2016)		Chalcopyrite	4.4	Zu et al. (2016)
	Pyrite	1.4	Liu et al. (2016)		Chalcopyrite	4.8	Zu et al. (2016)
	Pyrite	1.2	Liu et al. (2016)		Chalcopyrite	4.3	Zu et al. (2016)
	Molybdenite	3.8	Liu et al. (2016)		Chalcopyrite	5.8	Zu et al. (2016)

Molybdenite	0.1	Liu et al. (2016)	Chalcopyrite	4.9	Zu et al. (2016)

Table 7 The Pb istopic compositions of sulfides from the Mo deposits in SW China

Deposit	Sample	$^{206}Pb/^{204}Pb$	$^{207}Pb/^{204}Pb$	$^{208}Pb/^{204}Pb$	Reference
Qulong	Pyrite	18.471	15.580	38.611	She et al. (2005)
	Pyrite	18.445	15.569	38.539	She et al. (2005)
	Chalcopyrite	18.453	15.572	38.565	She et al. (2005)
	Pyrite	18.488	15.586	38.649	She et al. (2005)
	Pyrite	18.479	15.588	38.658	She et al. (2005)
	Pyrite	18.483	15.598	38.673	She et al. (2005)
	Chalcopyrite	18.542	15.598	38.745	Meng et al. (2006)
	Chalcopyrite	18.493	15.577	38.647	Meng et al. (2006)
	Chalcopyrite	18.537	15.615	38.783	Meng et al. (2006)
	Chalcopyrite	18.591	15.605	38.857	Meng et al. (2006)
	Chalcopyrite	18.443	15.576	38.557	Meng et al. (2006)
Bangpu	Galena	19.080	15.820	40.140	Zhao et al. (2015a)
	Galena	19.080	15.850	39.870	Zhao et al. (2015a)
	Pyrite	19.280	15.850	40.340	Zhao et al. (2015a)
	Pyrite	19.220	15.890	40.140	Zhao et al. (2015a)
	Pyrite	18.810	15.640	39.160	Zhao et al. (2015a)
	Pyrite	19.130	15.890	40.880	Zhao et al. (2015a)
	Pyrite	18.990	15.930	39.730	Zhao et al. (2015a)
	Pyrite	19.050	15.910	40.170	Zhao et al. (2015a)
	Pyrite	18.990	15.820	40.450	Zhao et al. (2015a)
	Pyrite	18.850	15.650	39.810	Zhao et al. (2015a)
	Pyrite	19.110	15.730	39.470	Zhao et al. (2015a)
	Pyrite	18.910	15.770	39.990	Zhao et al. (2015a)
	Pyrite	18.790	15.730	39.770	Zhao et al. (2015a)
	Pyrite	18.790	15.650	39.350	Zhao et al. (2015a)
	Pyrite	18.890	15.840	40.120	Zhao et al. (2015a)
Jiama	Galena	18.728	15.608	38.961	Li et al. (2012c)
	Galena	18.752	15.633	39.047	Li et al. (2012c)
	Galena	18.150	15.480	38.850	Li et al. (2012c)
	Galena	18.661	15.686	39.135	Li et al. (2012c)
	Galena	18.603	15.643	39.001	Li et al. (2012c)
	Galena	18.640	15.669	39.086	Li et al. (2012c)
	Galena	18.728	15.608	38.961	Li et al. (2012c)
	Galena	18.752	15.633	39.074	Li et al. (2012c)
	Galena	18.588	15.634	39.010	Li et al. (2012c)
	Pyrite	18.557	15.597	38.939	Li et al. (2012c)
	Pyrite	18.600	15.628	38.952	Li et al. (2012c)
	Chalcopyrite	18.725	15.615	38.987	Li et al. (2012c)
	Chalcopyrite	18.752	15.638	39.058	Li et al. (2012c)
	Chalcopyrite	18.725	15.615	38.987	Li et al. (2012c)

	Chalcopyrite	18.752	15.638	39.058	Li et al. (2012c)
	Chalcopyrite	18.607	15.625	38.944	Li et al. (2012c)
	Chalcopyrite	18.584	15.620	38.956	Li et al. (2012c)
	Molybdenite	18.484	15.547	39.740	Li et al. (2012c)
Narigongma	Pyrite	18.481	15.526	38.602	Li et al. (2015)
	Pyrite	18.586	15.574	38.726	Li et al. (2015)
	Galena	18.749	15.602	38.829	Li et al. (2015)
	Galena	18.764	15.622	38.860	Li et al. (2015)
Xiuwacu	Pyrrhotite	18.646	15.650	38.857	Wang et al. (2015)
	Pyrite	18.911	15.700	39.349	Wang et al. (2015)
	Pyrite	18.884	15.697	39.297	Wang et al. (2015)
	Sphalerite	18.878	15.690	39.296	Wang et al. (2015)
	Bismuthinite	18.936	15.710	39.404	Wang et al. (2015)
	Molybdenite	18.909	15.700	39.350	Wang et al. (2015)
	Molybdenite	18.905	15.697	39.334	Wang et al. (2015)
Hongshan	Pyrrhotite	18.101	15.696	38.452	Zu et al. (2016)
	Chalcopyrite	18.055	15.550	38.057	Zu et al. (2016)
	Pyrite	18.625	15.631	38.860	Zu et al. (2016)
	Pyrrhotite	18.453	15.673	38.744	Zu et al. (2016)
	Chalcopyrite	18.433	15.633	38.624	Zu et al. (2016)
	Pyrrhotite	18.058	15.644	38.285	Zu et al. (2016)
	Chalcopyrite	18.014	15.583	38.080	Zu et al. (2016)
	Pyrite	18.678	15.621	38.991	Zu et al. (2016)
	Chalcopyrite	18.809	15.785	39.538	Zu et al. (2016)
	Galena	18.744	15.708	39.290	Zu et al. (2016)
	Sphalerite	18.799	15.755	39.468	Zu et al. (2016)
	Pyrite	18.670	15.615	38.975	Zu et al. (2016)
	Pyrite	18.703	15.646	39.081	Zu et al. (2016)
	Galena	18.701	15.661	39.126	Zu et al. (2016)
	Chalcopyrite	18.712	15.651	39.114	Zu et al. (2016)
	Galena	18.701	15.661	39.048	Zu et al. (2016)
	Chalcopyrite	18.712	15.651	39.067	Zu et al. (2016)
	Pyrite	18.665	15.625	37.884	Zu et al. (2016)
	Pyrite	18.605	15.628	37.816	Zu et al. (2016)
Tongchanggou	Pyrite	18.494	15.634	38.876	Liu et al. (2016)
	Molybdenite	18.332	15.594	38.619	Liu et al. (2016)
	Chalcopyrite	18.463	15.588	38.454	Liu et al. (2016)
	Molybdenite	18.515	15.599	38.864	Liu et al. (2016)
	Molybdenite	18.694	15.624	39.076	Liu et al. (2016)
	Pyrite	18.665	15.619	39.047	Liu et al. (2016)
	Molybdenite	18.576	15.625	39.008	Liu et al. (2016)
	Molybdenite	18.554	15.663	39.088	Liu et al. (2016)
	Molybdenite	18.550	15.609	38.862	Liu et al. (2016)
	Pyrite	18.620	15.630	39.023	Liu et al. (2016)

Research Highlights

- Southwest China host more than 26 Mo deposits with total reserve of more than 2.5 Mt Mo
- Ore ages cluster mainly in 63–14 Ma and 73–88 Ma, minor in 258–214 Ma
- Ore types are porphyry, porphyry-skarn, skarn and porphyry-vein
- Mo mineralization formed in various tectonic setting with various Re contents